Title
Dopaminergic Modulation in Medial Prefrontal Cortex and its Dysfunction in Psychiatric Disease

Author
Robinson Schwartz, Sarah Elizabeth

Publication Date
2017

Peer reviewed|Thesis/dissertation

Dopaminergic Modulation in Medial Prefrontal Cortex and its Dysfunction in Psychiatric Disease

by

Sarah Elizabeth Robinson Schwartz

DISSERTATION

Submitted in partial satisfaction of the requirements for the degree of

DOCTOR OF PHILOSOPHY

in

Neuroscience

in the

GRADUATE DIVISION

of the

UNIVERSITY OF CALIFORNIA, SAN FRANCISCO

Acknowledgements

First and foremost, I need to thank my family - my wonderful husband, Michael Schwartz, my mother Susan Russell-Robinson, and my father Gilpin Robinson - for their guidance, encouragement, and loving support. I will be forever grateful to my parents for introducing me to science at a very early age. My own curiosity and interest in science grew out of the many hours of my childhood spent hiking throughout New England and in their offices being exposed to their own geology research. My mother, disappointed by the opportunities for young minds to have real hands-on science experience, collaborated to start a summer science camp in my home town providing me with the early opportunity to meet scientists and try my own experiments in biology, chemistry, physics, and geology. I appreciate their unending support for me throughout everything and their remarkable patience to endure my whirlwind of activity. Michael, I am incredibly fortunate to have had you by my side all throughout graduate school. Thank you for listening to my practice talks, making me coffee when I am up working at 2am, and supporting me throughout my scientific endeavors, health and family struggles, and wedding planning while writing this dissertation. I cannot imagine graduate school without you.

I am pleased to acknowledge Dr. Nancy Simon for nearly two decades of inspiration and mentorship. Thank you for welcoming a high schooler into your laboratory to conduct biochemical research and for bringing me along on adventurous field expeditions. Thank you also for the many years of conversations about science, career opportunities, philosophy, and life as a whole. Your advice has been invaluable for shaping me as a scientist. I would also like to thank Dr. Milos Dolnik and Dr. Irving Epstein for giving me the opportunity to participate in nonlinear chemical dynamics research as an undergraduate.

Their guidance was formative for training me in experimental design and thinking critically about my own research.

In addition, I would especially like to thank the many smart and talented classmates, colleagues, and friends here at UCSF. It is my privilege to have gotten to know you and to count you among my friends. Special thanks to Laura Devault, for many awesome dinners and fun nights, to Rebecca Clarkson for afternoon coffee runs and useful advice, and to Peter Chisnell and Mihir Vohra, for always welcoming us into your home. Thank you all.

I have also been fortunate to have the support of many people outside of the UCSF community. I am incredibly grateful to all of the Mixed Masters team at Lake Merritt Rowing Club. Thank you for many wonderful rows, some impressive medals, and frequent evening escapades. I am also fortunate that several of my Tanzania Returned Peace Corps Volunteers also live here in the Bay Area. Thank you for the continual support, deep conversations, and fun times we've shared both here and abroad. Special thanks to Kate Yusi, for her continued friendship, support, advice, and for literally saving my life.

I will be forever grateful for the UCSF faculty members who have advised, taught, and mentored me through the years. My thesis committee members, Dr. Anatol Kreitzer, Dr. Kevin Bender, and Dr. Jennifer Whistler, have been ready with valuable advice and deep probing questions. Thank you also to Dr. Louis Reichardt, Dr. Roger Nicoll, and Dr. Anatol Kreitzer, the program directors for the Neuroscience Graduate Program, as well as, Pat Veitch, the Neuroscience Graduate Program coordinator, and Lucita Nacionales, the Neuroscience Program assistant. They have had all of our best interests at heart and worked tirelessly to ensure that the UCSF Neuroscience Graduate Program support all of its students.

I also owe a great many thanks to the members of the Sohal lab with whom I have worked and collaborated. My research is better for having you as my colleagues and friends. Dr. Ian Ellwood trained me in my very first animal research and most importantly taught me how to perform whole-cell patch clamp electrophysiology. I am indebted to Dr. Audrey Brumback, Dr. Celia Kjaerby, Dr. Kathleen Cho, Dr. Nicholas Frost, Dr. Jillian Iafrati, Dr. Scott Wilke, and Dr. Ruchi Malik for their expertise, kindness, and support these past four years. I also need to thank Tosha Patel, Helia Seifikar, and Varun Wadia for their consistent high-quality work and seamless running of the lab. And a special thanks to my fellow graduate students in the Sohal lab, Karuna Meda, Jegath Athilingam, and Margaret Cunniff, it has been a long-haul but also a sincere pleasure learning and working alongside you.

Finally, I owe a great debt of gratitude to Dr. Vikaas Sohal, my thesis mentor. Dr. Sohal first welcomed me into his lab as a rotation student my first semester in graduate school. He then welcomed me back into his lab early in 2014 after a very turbulent period in my life. I am extremely grateful to Dr. Sohal for seeing potential in me and for dedicating his time and efforts into guiding me toward success. It has been an absolute pleasure working in his lab. I feel very fortunate to have been trained by such a brilliant and insightful scientist. I could not thank him enough.

This work was supported by the National Science Foundation (Graduate Research Fellowship 1144247 to S.E.R) and the National Institutes of Health (Grant R01 MH100292 to V.S.S).

Author Contributions

The text of Chapter II of this dissertation is a reprint of the material as it originally appeared in The Journal of Neuroscience (Robinson et al., 2017). Sarah Robinson performed all experiments and analysis. Vikaas Sohal directed and supervised the research. Sarah Robinson and Vikaas Sohal co-wrote the paper.

The text of Chapter IV of this dissertation contains excerpts from two manuscripts in preparation. Sarah E. Robinson Schwartz performed all electrophysiology and behavior experiments as well as viral injections for the histology experiments. Bin Chen collaborated on generating the *Tbr1* conditional mutant mouse. Siavash Fazel Darbandi generated the *Tbr1* layer 5 and layer 6 mutant mice, performed ChIP-Seq, FACS RNA-Seq and in situ hybridization transcriptome analyses, as well as synaptic staining and all histology experiments. Jeremy Willsey, Jeff Mandell, and Qihao Qi performed bioinformatics analysis of the *Tbr1* RNA-Seq data. Alex Nord and Rinaldo Catta-Preta conducted bioinformatics analysis of *Tbr1* ChIP-Seq data. Vikaas Sohal, John Rubenstein, and Matthew State directed and supervised the research. S.E.R.S, S.F.D., V.S.S., J.L.R., and M.W.S. contributed to the text.

Abstract

The prefrontal cortex (PFC) mediates many executive functions including working memory, behavioral flexibility, decision making, and social cognition. The normal functioning of the PFC depends strongly on regulation by neuromodulators. Dysfunction of the PFC leads to deficits in these abilities and is a major factor in many neuropsychiatric disorders including schizophrenia and autism. Layer 5 (L5) of the PFC, a major site of dopaminergic modulation, is thought to play an important role in regulating these higher order processes. Indeed, many neurological disorders such as schizophrenia have been associated with imbalances in dopamine neurotransmission.

Prefrontal dopamine D2 receptors (D2Rs), the primary target for first generation antipsychotic drugs, specifically play a major role in tasks that are disrupted in schizophrenia. One major hypothesis is that excessive D2R activation within the PFC contributes to many of the cognitive impairments associated with schizophrenia. This dissertation investigates the mechanisms of D2R-mediated neuromodulation within the PFC and abnormalities within PFC circuitry and neuromodulation in mouse models of schizophrenia and autism.

We have previously described a phenomenon whereby D2R activation elicits afterdepolarization (ADPs) in subcortically-projecting (SC) pyramidal neurons within L5 of the PFC. Results presented in Chapter II of this dissertation show that this unusual physiological phenomenon, in which D2Rs enhance cellular excitability dependent on synaptic input, is mediated at the cellular level through the recruitment of signaling pathways associated with G_s, rather than G_i-associated mechanisms that have classically been ascribed to D2Rs.

In Chapter III, I discuss differences in D2R neuromodulation in mice with a dominant-negative mutation in disrupted in schizophrenia 1 (DISC1). DISC1 dysfunction has been associated with schizophrenia and causes deficits in working memory. Current studies, it has been shown that there is an upregulation of D2R expression and/or activity in DISC1 mouse models. Interestingly, DISC1 is also implicated in the regulation of cAMP. Here, I will show that these mice lack the quinpirole-induced G_i-independent ADP.

The medial prefrontal cortex (mPFC), particularly deep layer projection neurons, has also been implicated as a potential locus for Autism Spectrum Disorder (ASD) pathology. Previous work from our lab has shown that social exploration preferentially recruits mPFC D2R positive pyramidal neurons and that this recruitment is attenuated in three etiologically distinct mouse models of autism. In Chapter IV of this dissertation, we investigate the affects of *T-brain-1 (Tbr1)* selectively within layer 5 and layer 6 cortical neurons. We found that *Tbr1* function is required to maintain many aspects of layer 6 identity, $Tbr1^{layer6}$ mutant neurons transform towards the identity of L5 neurons, including their transcriptome, dendritic pattern, and physiological properties. $Tbr1^{layer5}$ mutant neurons become a more homogeneous population transforming towards the identity of D2R expressing pyramidal neurons. Both $Tbr1^{layer6}$ and $Tbr1^{layer5}$ mutants have reduced excitatory and inhibitory synaptic density as well as reduced spontaneous EPSCs and IPSCs. We also present data suggesting that loss of *Tbr1* function in layer 6 leads to increased anxiety and aggressive behavior whereas loss of *Tbr1* function in layer 5 leads to decreased social behaviors, phenotypes consistent with different aspects of observed ASD patient behavioral characteristics.

Table of Contents

List of Figures

Chapter II Figures

Chapter III Figures

Chapter IV Figures

CHAPTER I

General Introduction

Normal and pathological roles of the PFC

The ability to appropriately make decisions which guide our subsequent goal-directed behaviors requires integration of previously learned action-outcome relationships and accurate environmental assessment. This ability is thought to be primarily mediated by the prefrontal cortex (PFC), which also plays a critical role in high-order executive tasks such as attention, behavioral flexibility, working memory, and social cognition (Druzin *et al.*, 2000; Dalley *et al.*, 2004; Floresco *et al.*, 2006). Neuromodulation via dopamine plays a critical role in mediating these prefrontal functions. Dopamine dysfunction is strongly implicated in neuropsychiatric diseases (Roberts and Bruton, 1990; Kalivas and Volkow, 2005; Durstewitz and Seamans, 2008). This dissertation focuses on understanding the mechanisms of D2R-mediated neuromodulation within the PFC and abnormalities within the PFC circuitry in mouse models of schizophrenia and autism. By understanding these mechanisms, we hope to advance our understanding of how these mechanisms contribute to prefrontal dysfunction in psychiatric disease.

The effects of dopamine on the PFC

In order for the PFC to provide flexible top-down control of complex cognitive and behavioral processes it is heavily connected, sending and receiving inputs to and from numerous brain regions including sensory cortices, contralateral PFC, and subcortical regions (Wernicke, 1906; Carr and Sesack, 2000; Hoover and Vertes, 2007). In addition to these long-range projections, pyramidal neurons within the PFC also form highly recurrent connections with other PFC pyramidal neurons (Morishima and Kawaguchi, 2006). Importantly, the PFC receives strong mesocortical dopaminergic inputs from the ventral tegmental area (VTA) (Björklund and Dunnett, 2007). Traditionally, activity of the dopamine neurons within the VTA is believed to encode reward-prediction error (RPE), driving

learning by indicating a discrepancy between expectation and outcome (Schultz, 2007). However, the VTA contains anatomically and functionally heterogeneous dopamine neuron subpopulations with distinct axonal projections and input sources (Lammel *et al.*, 2014). Recently, dopamine neuron activity has been associated with a variety of additional brain functions including aversion, salience, uncertainty, and novelty (Schultz, 2007; Bromberg-Martin *et al.*, 2010; Ungless *et al.*, 2010). For example, dopaminergic cells projecting to the nucleus accumbens respond to rewarding stimuli whereas dopaminergic cells projecting to the medial prefrontal cortex (mPFC) respond to aversive stimuli (Lammel *et al.*, 2012). However, optogenetic stimulation of VTA terminals within the VTA rather than being positively or negatively reinforcing, instead shifts an animal between flexible or preservative behavior modalities (Ellwood *et al.*, 2017). Neuromodulation by prefrontal dopamine is a topic of extensive research due to its critical role in higher cognitive processes and neuropsychiatric pathology (Seamans and Yang, 2004).

Different effects of dopamine by D1R and D2R receptors in the PFC

Dopamine modulates neuronal functioning by acting at five distinct G protein-coupled receptors (GPCRs). These dopamine receptors are canonically subdivided into two families: “D1-like” (D1 and D5) which tend to couple to the stimulatory G proteins G_s and G_q, and “D2-like” (D2, D3, and D4) which tend to couple to the inhibitory proteins $G_{i/o}$ (Bonci and Hopf, 2005). Interestingly, the dopamine D1 receptor (D1R) family and the dopamine D2 receptors (D2R) family are thought to have opposing effects on PFC-dependent cognitive function (Sawaguchi and Goldman-Rakic, 1994; Seamans *et al.*, 2001; Wang and Goldman-rakic, 2004; Tseng and O’Donnell, 2005). The “Dual-State Theory” of prefrontal function proposes that D1Rs within the PFC stabilize network activity, decreasing the

influence of weaker inputs thereby maintaining patterns of activity supporting previously learned behavioral strategies (Durstewitz and Seamans, 2008). Contrastingly, D2Rs are thought to destabilize the prefrontal network, shifting it toward promoting a more flexible behavioral state. Successful behavioral adaptation in the face of uncertainty therefore depends on a balance between these "exploit" and "explore" modalities (Daw *et al.*, 2006).

D1Rs and D2Rs within the basal ganglia are expressed on non-overlapping populations of medium spiny neurons (MSNs) with distinct projection targets. "Direct pathway" MSNs in the striatum express D1Rs and project to the internal segment globus pallidus/sustantia nigra pars reticulate. Dopamine acting on these MSNs via D1Rs, acts through canonical GPCR signaling pathways, increasing intercellular levels of cAMP and cellular excitability (Surmeier *et al.*, 2007). Activity in this pathway has been shown to facilitate movement whereas activity in the "indirect pathway" is thought to inhibit movement (Lalonde and Botez-Marquard, 2010). Indirect pathways MSNs project to the external segment of the globus pallidus and express D2Rs coupled to $G_{i/o}$, inhibiting cAMP production in response to dopamine. While this model is likely an oversimplification, it does provide a useful framework for testing the role of specific circuits and cell populations in basal ganglia function (DeLong and Wichmann, 2009; Kravitz *et al.*, 2012). A similar detailed framework for dopaminergic modulation within the PFC is largely lacking.

The mechanisms by which D1Rs modulate excitability in the PFC have been extensively studied whereas the mechanisms through which D2Rs exert their influence remain mostly unclear. Neuromodulation by prefrontal dopamine D2 receptors (D2Rs) is of particular interest because of their implications in many neuropsychiatric disease pathologies. The infusion of D2R agonists and antagonists into the PFC modulates working memory and set-shifting in rodents (Druzin *et al.*, 2000; Floresco *et al.*, 2006; St Onge, Abhari and Floresco, 2011a). Selective photostimulation of mPFC pyramidal neurons

expressing D2Rs disrupts normal social behavior in mice whereas inhibition of these neurons improves social interaction in mouse models of autism (Brumback *et al.*, 2017). Prefrontal D2Rs have also been shown to be necessary for neural activity associated with memory-guided saccades in non-human primates (Wang and Goldman-Rakic, 2004). In humans, genetic variation in D2Rs modulates prefrontal activity and working memory (Zhang *et al.*, 2007). Interestingly, all known antipsychotics block prefrontal D2Rs supporting a major hypothesis that aberrant D2R activation contributes to prefrontal dysfunction in schizophrenia (Winterer and Weinberger, 2004; Durstewitz and Seamans, 2008). Thus, D2Rs play a major role in both normal and pathological prefrontal function. It is therefore crucial to reveal the underlying mechanisms of dopaminergic modulation in the prefrontal cortex.

Recent studies have classified separate populations of PFC pyramidal neurons with distinct morphology, physiological properties and dopamine receptor expression (Gee *et al.*, 2012). D2Rs are selectively expressed in a subpopulation of layer 5 pyramidal subcortical-projection (SC) neurons, which have thick apical tufts and prominent h-current. A recent study by Clarkson et al. confirmed that D2R expressing pyramidal neurons within the mPFC exhibit prominent voltage sag during hyperpolarizing current steps and have a voltage rebound that depolarizes past resting membrane potential after the current step (Clarkson *et al.*, 2017). This electrophysiological phenotype alone was enough to distinguish D2R expressing neurons from those lacking D2Rs with approximately 75% accuracy.

Within this D2R expressing SC-projecting population we found pharmacological activation of D2Rs by the agonist results in a pronounced afterdepolarization (ADP) (Gee *et al.*, 2012). This ADP was not observed in quiescent slices and only occurred when NMDA receptors were activated, via either optogenetic stimulation of excitatory synapses or bath application of low dose NMDA. D2Rs are classically assumed to couple to inhibitory G

proteins, reducing neuronal excitability by activating $G_{\alpha i/o}$ and inhibiting adenylate cyclase (Bonci and Hopf, 2005). The $G_{\beta\gamma}$ subunits also directly interact with several different types of ion channels and can facilitate release of Ca^{2+} from internal calcium stores. Prolonged activation of D2Rs leads to binding of β-arrestin which results in desensitization and internalization of the receptors. Recently it has been discovered that the D2R-β-arrestin complex can also initiate signal cascades which are temporally and spatially distinct from the D2R-G-protein signaling pathway (Beaulieu *et al.*, 2009; Beaulieu and Gainetdinov, 2011). In Chapter II, we explore two different aspects of the intercellular signaling pathways through which activation of D2Rs elicits ADPs in prefrontal SC-projecting neurons using a combination of electrophysiological, transgenic, pharmacological, and chemogenic approaches. We find that the prolonged ability of synaptic stimulation to facilitate D2R-dependent ADPs depends on voltage-dependent (likely Ca^{2+}) currents. Furthermore, we show that the D2R-dependent ADP persists following disruptions to G_i or β-arrestin signaling. The ADP can also be mimicked by chemogenetic activation of G_s signaling suggesting that this phenomenon reflects novel intracellular signaling downstream of D2Rs via stimulatory G proteins.

The role of dopamine in disease

Many neurological disorders have been associated with imbalances in dopamine neurotransmission. Prefrontal D2Rs have also been postulated to contribute to schizophrenia (Winterer and Weinberger, 2004; Durstewitz and Seamans, 2008), Tourette syndrome (Simonic *et al.*, 1998; Minzer *et al.*, 2004; Yoon *et al.*, 2007; Steeves *et al.*, 2010), and bipolar disorder (Minton *et al.*, 2009). Thus, D2Rs play a major role in both normal and pathological prefrontal function. One major hypothesis regarding the role of D2Rs in

psychiatric disease postulates that D2Rs increase the variability of PFC, under normal conditions facilitating adaptation to a changing environment (Durstewitz *et al.*, 2010;). However, excessive or imbalanced D2R activation could produce pathological variability that contributes to “prefrontal noise” and cognitive dysfunction in schizophrenia (Winterer and Weinberger, 2004; Durstewitz and Seamans, 2008).

Schizophrenia is a devastating psychiatric disorder affecting approximately 1% of the population (Cloutier *et al.*, 2016). The majority of patients suffer lifelong symptoms as the age of onset is in late adolescence to young adulthood. While symptoms vary from patient to patient, typical symptoms can be grouped into three main categories: ‘positive’ symptoms include hallucinations and delusions, ‘negative’ symptoms include emotional blunting, reduced motivation, and a lack of social interactions, and cognitive impairments including deficits in executive function, attention, and working memory (Meltzer, 1997; Evans *et al.*, 2004). D2Rs are the main target of antipsychotic medications and the clinical potency of antipsychotic drugs is correlated with D2R binding affinity (Seeman *et al.*, 1976). However, current antipsychotics are ineffective at controlling symptoms in many patients and cause serious side effect. Thus understanding the specific mechanisms of D2R signaling and its dysfunction in schizophrenia is critical for developing novel more effective therapies.

Disrupted in schizophrenia 1 (DISC1) dysfunction is associated with an increased risk for schizophrenia and other psychiatric disorders (Pletnikov *et al.*, 2008). The DISC1 gene was originally discovered in a Scottish family with high rates of schizophrenia (Jacobs *et al.*, 1970). DISC1 is a scaffold protein which interacts with several other proteins in the dopamine system, including serine/threonine protein kinase Akt and glycogen synthase kinase-3 (GSK-3). It plays an important role in regulating the cAMP pathway and mGluR activation (El-Hassar *et al.*, 2014). In DISC1 mouse models there is an upregulation of D2R expression in the mPFC and striatum (Niwa *et al.*, 2013). DISC1 mutant mice exhibit

spontaneous hyperactivity in the open field, alterations in social interaction, and deficiency in spatial memory which a behavioral deficits similar to some features of schizophrenia.

In Chapter III of this dissertation, we investigate abnormalities in D2R-mediated modulation of PFC pyramidal cell excitability in transgenic mice with inducible expression of mutant human DISC1 (hDISC1) via the Tet-off system under regulation of the CAMKII promoter (Pletnikov *et al.*, 2008). I will present results showing that SC-projecting pyramidal neurons within the mPFC lack the quinpirole-induced afterdepolarization.

Throughout my dissertation we focus on layer 5 pyramidal neurons because these neurons contain most prefrontal D2Rs (Lidow *et al.*, 1998; Santana, Mengod and Artigas, 2009; Clarkson *et al.*, 2017). Specific mechanisms for D2R-modualtion of L5 pyramidal neurons in PFC remains elusive with several contradictory studies describing ways that D2Rs enhance (Wang and Goldman-rakic, 2004) and suppress (Gulledge and Jaffe, 1998; Tseng and O'Donnell, 2004) excitability in these neurons. Understanding how mechanisms of dopaminergic modulation are perturbed in various psychiatric disorders is critical for the development of safer and more efficient drug therapies.

Autism spectrum disorder (ASD) is a neurodevelopmental disorder clinically characterized by social communication and interaction impairments which causes lifelong disability in millions of people (Baio, 2012). Individuals with ASD have impaired social behaviors often accompanied by abnormalities in language development. Many genes have been implicated in ASDs but specific cellular abnormalities that link genes with behavior remain elusive. Several of the genes strongly linked to autism are convergently co-expressed within deep layer (L5 & L6) projection neurons in the PFC (Willsey *et al.*, 2013). In humans, functional imaging studies reveal abnormally decreased activation of the mPFC during social tasks (Pierce *et al.*, 2004). The mPFC has been specifically implicated in deficits associated with ASD: lesions cause impairments in emotional learning and loss of

social skills (Bachevalier et al., 1986; Morgan et al., 1993). Optogenetic manipulation of the excitatory/inhibitory balance within rodent mPFC disrupts normal social exploration (Yizhar *et al.*, 2011). Another recent study from our lab found that social exploration preferentially recruits mPFC D2R+ neurons and is disrupted in valproic acid (VPA) *in utero* exposure, a mouse model of autism (Brumback *et al.*, 2017). Additionally, optogenetic stimulation of D2Rs+ mPFC neurons disrupts normal social behavior in mice whereas inhibition of these neurons improves social interaction in three etiologically distinct mouse models of autism (Brumback *et al.*, 2017)

T-brain-1 (Tbr1), a T-box transcription factor strongly expressed in deep cortical layers, has been identified as a high-confidence ASD gene. Together with the John Rubenstein Lab, we focused on Tbr1 function in deep neocortical neurons using Cre-lox conditional mutagenesis. Siavash Fazel Darbandi created both $Tbr1^{layer6}$ and $Tbr1^{layer5}$ mutant mice. Results presented in Chapter IV of this dissertation show that late gestation/neonatal *Tbr1* function is required to maintain many aspects layer 6 (L6) identity. $Tbr1^{layer6}$ mutant neurons transformed towards identity of L5 neurons, including their transcriptome, their dendritic pattern and electrophysiological properties (h-current). Similarly, $Tbr1^{layer5}$ mutant neurons have enhanced h-current typical of D2R expressing SC-projection pyramidal neurons. The $Tbr1^{layer6}$ and $Tbr1^{layer5}$ mutant neurons also have reduced excitatory and inhibitory synaptic density. We found that this reduction in excitatory and inhibitory synapse density functionally translates into reduced spontaneous EPSCs and IPSCs in mouse brain slices. We have also discovered that loss of *Tbr1* function in layer 6 leads to increased anxiety and aggressive behavior, a phenotype that is also observed in ASD patients. Contrastingly we show that loss of *Tbr1* function in layer 5 leads to a pronounced decrease in social behaviors, reminiscent of the main phenotype associated with Autism Spectrum Disorders.

References

Bachevalier, J. and Mishkin, M. (1986) 'Visual recognition impairment follows ventromedial but not dorsolateral prefrontal lesions in monkeys.', *Behavioural brain research*, 20(3), pp. 249–61.

Baio, J. (2012) 'Prevalence of Autism Spectrum Disorders — Autism and Developmental Disabilities Monitoring Network, 14 Sites, United States, 2008', *Morb Mortal Wkly Rep*, 61, pp. 1–19.

Beaulieu, J.-M. and Gainetdinov, R. R. (2011) 'The physiology, signaling, and pharmacology of dopamine receptors.', *Pharmacological reviews*. American Society for Pharmacology and Experimental Therapeutics, 63(1), pp. 182–217.

Beaulieu, J.-M., Gainetdinov, R. R. and Caron, M. G. (2009) 'Akt/GSK3 signaling in the action of psychotropic drugs.', *Annual review of pharmacology and toxicology*, 49, pp. 327–47.

Björklund, A. and Dunnett, S. B. (2007) 'Fifty years of dopamine research', *Trends in Neurosciences*, 30(5), pp. 185–187.

Bonci, A. and Hopf, F. W. (2005) 'The dopamine D2 receptor: new surprises from an old friend.', *Neuron*, 47(3), pp. 335–8.

Bromberg-Martin, ES; Matsumoto, M; Hikosaka, O. (2010) 'Dopamine in Motivational Control: Rewarding, Aversive, and Alerting', *Neuron*. Cell Press, 68(5), pp. 815–834.

Brumback, A. C. *et al.* (2017) 'Identifying specific prefrontal neurons that contribute to autism-associated abnormalities in physiology and social behavior', *Molecular Psychiatry*.

Carr, D. B. and Sesack, S. R. (2000) 'Projections from the rat prefrontal cortex to the ventral tegmental area: target specificity in the synaptic associations with mesoaccumbens and mesocortical neurons.', *The Journal of neuroscience : the official journal of the Society for Neuroscience*, 20(10), pp. 3864–73.

Clarkson, R. L. *et al.* (2017) 'D3 Receptors Regulate Excitability in a Unique Class of Prefrontal Pyramidal Cells.', *The Journal of neuroscience : the official journal of the Society for Neuroscience*, 37(24), pp. 5846–5860.

Cloutier, M. *et al.* (2016) 'The Economic Burden of Schizophrenia in the United States in 2013', *The Journal of Clinical Psychiatry*, 77(6), pp. 764–771.

Dalley, J. W., Cardinal, R. N. and Robbins, T. W. (2004) 'Prefrontal executive and cognitive functions in rodents: neural and neurochemical substrates', *Neuroscience & Biobehavioral Reviews*, 28(7), pp. 771–784.

Daw, N. D. *et al.* (2006) 'Cortical substrates for exploratory decisions in humans.', *Nature*, 441(7095), pp. 876–9.

DeLong, M. and Wichmann, T. (2009) 'Update on models of basal ganglia function and dysfunction', *Parkinsonism & Related Disorders*, 15, pp. S237–S240.

Dembrow, N. C., Chitwood, R. a and Johnston, D. (2010) 'Projection-specific neuromodulation of medial prefrontal cortex neurons.', *The Journal of neuroscience : the official journal of the Society for Neuroscience*, 30(50), pp. 16922–37.

Druzin, M. Y. *et al.* (2000) 'The effects of local application of D2 selective dopaminergic drugs into the medial prefrontal cortex of rats in a delayed spatial choice task.', *Behavioural brain research*, 109(1), pp. 99–111.

Durstewitz, D. *et al.* (2010) 'Abrupt Transitions between Prefrontal Neural Ensemble States Accompany Behavioral Transitions during Rule Learning', *Neuron*, 66(3), pp. 438–448.

Durstewitz, D. and Seamans, J. K. (2008) 'The Dual-State Theory of Prefrontal Cortex Dopamine Function with Relevance to Catechol-O-Methyltransferase Genotypes and Schizophrenia', *Biological Psychiatry*, 64(9), pp. 739–749.

El-Hassar, L. *et al.* (2014) 'Disrupted in schizophrenia 1 modulates medial prefrontal cortex pyramidal neuron activity through cAMP regulation of transient receptor potential C and small-conductance k(+) channels.', *Biological psychiatry*. Elsevier, 76(6), pp. 476–85.

Ellwood, I. T. *et al.* (2017) 'Tonic or phasic stimulation of dopaminergic projections to prefrontal cortex causes mice to maintain or deviate from previously learned behavioral strategies', *The Journal of Neuroscience*, 37(35), pp. 1221–17.

Evans, J. D. *et al.* (2004) 'Cognitive and clinical predictors of success in vocational rehabilitation in schizophrenia.', *Schizophrenia research*, 70(2–3), pp. 331–42.

Floresco, S. B. *et al.* (2006) 'Multiple dopamine receptor subtypes in the medial prefrontal cortex of the rat regulate set-shifting.', *Neuropsychopharmacology : official publication of the American College of Neuropsychopharmacology*, 31(2), pp. 297–309.

Gee, S. *et al.* (2012) 'Synaptic activity unmasks dopamine D2 receptor modulation of a specific class of layer V pyramidal neurons in prefrontal cortex.', *The Journal of neuroscience*, 32(14), pp. 4959–71.

Gulledge, A. T. and Jaffe, D. B. (1998) 'Dopamine decreases the excitability of layer V pyramidal cells in the rat prefrontal cortex.', *The Journal of neuroscience : the official journal of the Society for Neuroscience*, 18(21), pp. 9139–51.

Hoover, W. B. and Vertes, R. P. (2007) 'Anatomical analysis of afferent projections to the medial prefrontal cortex in the rat', *Brain Structure and Function*, 212(2), pp. 149–179.

Jacobs, PA; Brunton, M; Frackiewicz, A; Newton, M; Cook, PJL; Robson, E. (1970) 'Studies on a family with three cytogenetic markers.', *Annals of Human Genetics*, 33, pp. 325–336.

Kalivas, P. W. and Volkow, N. D. (2005) 'The Neural Basis of Addiction: A Pathology of Motivation and Choice', *American Journal of Psychiatry*, 162(8), pp. 1403–1413.

Kravitz, Alexxai V.; Tye, Lynne D.; Kreitzer, A. C. (2012) 'Distinct roles for direct and indirect pathway striatal neurons in reinforcement', *Nature neuroscience*, 15(6), pp. 816–818.

Lalonde, R. and Botez-Marquard, T. (2010) 'The neurobiological basis of movement initiation.', *Reviews in the neurosciences*, 8(1), pp. 35–54.

Lammel, S. *et al.* (2012) 'Input-specific control of reward and aversion in the ventral tegmental area.', *Nature*, 491(7423), pp. 212–7.

Lammel, S., Lim, B. K. and Malenka, R. C. (2014) 'Reward and aversion in a heterogeneous midbrain dopamine system', *Neuropharmacology*, 76, pp. 351–359.

Lidow, M. S. *et al.* (1998) 'Layer V neurons bear the majority of mRNAs encoding the five distinct dopamine receptor subtypes in the primate prefrontal cortex', *Synapse*, 28(1), pp. 10–20.

Meltzer, H. Y. (1997) 'Treatment-Resistant Schizophrenia - The Role of Clozapine', *Current Medical Research and Opinion*, 14(1), pp. 1–20.

Minton, G. O. *et al.* (2009) 'Profound Changes in Dopaminergic Neurotransmission in the Prefrontal Cortex in Response to Flattening of the Diurnal Glucocorticoid Rhythm: Implications for Bipolar Disorder', *Neuropsychopharmacology*, 34(10), pp. 2265–2274.

Minzer, K. *et al.* (2004) 'Increased prefrontal D2 protein in Tourette syndrome: a postmortem analysis of frontal cortex and striatum', *Journal of the Neurological Sciences*, 219(1–2), pp. 55–61.

Morgan, M. A., Romanski, L. M. and LeDoux, J. E. (1993) 'Extinction of emotional learning: contribution of medial prefrontal cortex.', *Neuroscience letters*, 163(1), pp. 109–13.

Morishima, M. and Kawaguchi, Y. (2006) 'Recurrent Connection Patterns of Corticostriatal Pyramidal Cells in Frontal Cortex', *Journal of Neuroscience*, 26(16), pp. 4394–4405.

Niwa, M. *et al.* (2013) 'Adolescent Stress-Induced Epigenetic Control of Dopaminergic Neurons via Glucocorticoids', *Science*, 339(6117), pp. 335–339.

Pierce, K. *et al.* (2004) 'The brain response to personally familiar faces in autism: findings of fusiform activity and beyond', *Brain*, 127(12), pp. 2703–2716.

Pletnikov, M. V *et al.* (2008) 'Inducible expression of mutant human DISC1 in mice is associated with brain and behavioral abnormalities reminiscent of schizophrenia.', *Molecular psychiatry*, 13(2), pp. 173–86, 115.

Roberts, G. W. and Bruton, C. J. (1990) 'Notes from the graveyard: neuropathology and schizophrenia.', *Neuropathology and applied neurobiology*, 16(1), pp. 3–16.

Santana, N., Mengod, G. and Artigas, F. (2009) 'Quantitative analysis of the expression of dopamine D1 and D2 receptors in pyramidal and GABAergic neurons of the rat prefrontal cortex.', *Cerebral cortex (New York, N.Y. : 1991)*, 19(4), pp. 849–60.

Sawaguchi, T. and Goldman-Rakic, P. S. (1994) 'The role of D1-dopamine receptor in working memory: local injections of dopamine antagonists into the prefrontal cortex of rhesus monkeys performing an oculomotor delayed-response task.', *Journal of neurophysiology*, 71(2), pp. 515–28.

Schultz, W. (2007) 'Multiple dopamine functions at different time courses.', *Annual review of neuroscience*, 30, pp. 259–88.

Seamans, J. K. *et al.* (2001) 'Dopamine D1/D5 receptor modulation of excitatory synaptic inputs to layer V prefrontal cortex neurons', *Proceedings of the National Academy of Sciences*, 98(1), pp. 301–306.

Seamans, J. K. and Yang, C. R. (2004) 'The principal features and mechanisms of dopamine modulation in the prefrontal cortex.', *Progress in neurobiology*, 74(1), pp. 1–58.

Seeman, P. *et al.* (1976) 'Antipsychotic drug doses and neuroleptic/dopamine receptors.', *Nature*, 261(5562), pp. 717–9.

Seong, H. J. and Carter, A. G. (2012) 'D1 receptor modulation of action potential firing in a subpopulation of layer 5 pyramidal neurons in the prefrontal cortex.', *The Journal of neuroscience : the official journal of the Society for Neuroscience*, 32(31), pp. 10516–21.

Simonic, I. *et al.* (1998) 'Identification of Genetic Markers Associated with Gilles de la Tourette Syndrome in an Afrikaner Population', *The American Journal of Human Genetics*, 63(3), pp. 839–846.

St Onge, J. R., Abhari, H. and Floresco, S. B. (2011) 'Dissociable contributions by prefrontal d1 and d2 receptors to risk-based decision making.', *The Journal of neuroscience : the official journal of the Society for Neuroscience*, 31(23), pp. 8625–33.

Steeves, T. D. L. *et al.* (2010) 'Extrastriatal dopaminergic dysfunction in tourette syndrome', *Annals of Neurology*, 67(2), pp. 170–181.

Surmeier, D. J. *et al.* (2007) 'D1 and D2 dopamine-receptor modulation of striatal glutamatergic signaling in striatal medium spiny neurons.', *Trends in neurosciences*, 30(5), pp. 228–35.

Tseng, K. Y. and O'Donnell, P. (2004) 'Dopamine-glutamate interactions controlling prefrontal cortical pyramidal cell excitability involve multiple signaling mechanisms.', *The Journal of neuroscience : the official journal of the Society for Neuroscience*, 24(22), pp. 5131–9.

Tseng, K. Y. and O'Donnell, P. (2005) 'Post-pubertal emergence of prefrontal cortical up states induced by D1-NMDA co-activation.', *Cerebral Cortex*, 15(1), pp. 49–57.

Ungless, MA; Argilli, E; Bonci, A. (2010) 'Effects of stress and aversion on dopamine neurons: Implications for addiction', *Neuroscience & Biobehavioral Reviews*. Pergamon, 35(2), pp. 151–156.

Wang, Y. and Goldman-rakic, P. S. (2004) 'D2 receptor regulation of synaptic burst firing in prefrontal cortical pyramidal neurons', *PNAS*, 101(14), pp. 5093–50978.

Wernicke, C. (1906) 'No Title', *Grundrisse der Psychiatrie. Leipzig, Germany: Thieme*.

Willsey, A. J. *et al.* (2013) 'Coexpression networks implicate human midfetal deep cortical projection neurons in the pathogenesis of autism.', *Cell*, 155(5), pp. 997–1007.

Winterer, G. and Weinberger, D. R. (2004) 'Genes, dopamine and cortical signal-to-noise ratio in schizophrenia.', *Trends in neurosciences*, 27(11), pp. 683–90.

Yizhar, O. *et al.* (2011) 'Neocortical excitation/inhibition balance in information processing and social dysfunction.', *Nature*, 477(7363), pp. 171–8.

Yoon, D. Y. *et al.* (2007) 'Frontal dopaminergic abnormality in Tourette syndrome: A postmortem analysis', *Journal of the Neurological Sciences*, 255(1–2), pp. 50–56.

Zhang, Y. *et al.* (2007) 'Polymorphisms in human dopamine D2 receptor gene affect gene expression, splicing, and neuronal activity during working memory.', *Proceedings of the National Academy of Sciences of the United States of America*. National Academy of Sciences, 104(51), pp. 20552–7.

CHAPTER II

Dopamine D2 Receptors Modulate Pyramidal Neurons in Mouse Medial Prefrontal Cortex through a Stimulatory G-Protein Pathway

As published in *The Journal of Neuroscience* 2017, 37(42): 10063-10073.

ABSTRACT

Dopaminergic modulation of prefrontal cortex is believed to play key roles in many cognitive functions and to be disrupted in pathological conditions such as schizophrenia. We have previously described a phenomenon whereby dopamine D2 receptor (D2R) activation elicits afterdepolarizations (ADPs) in subcortically-projecting (SC) pyramidal neurons within L5 of the prefrontal cortex. These D2R-induced ADPs only occur following synaptic input which activates NMDA receptors (NMDARs) even when the delay between the synaptic input and afterdepolarizations is relatively long, e.g., several hundred milliseconds. Here we use a combination of electrophysiological, optogenetic, pharmacological, transgenic, and chemogenetic approaches to elucidate cellular mechanisms underlying this phenomenon in male and female mice. We find that knocking out D2Rs eliminates the ADP in a cell autonomous fashion, confirming that this ADP depends on D2Rs. Hyperpolarizing current injection, but not AMPA receptor blockade, prevents synaptic stimulation from facilitating D2R-induced ADPs, suggesting that this phenomenon depends on the recruitment of voltage dependent currents, e.g., NMDAR-mediated Ca^{2+} influx, by synaptic input. Finally, the D2R-induced ADP is blocked by inhibitors of cAMP / PKA signaling, insensitive to pertussis toxin or β-arrestin knockout, and mimicked by G_s-DREADD stimulation, suggesting that D2R activation elicits the ADP by stimulating cAMP / PKA signaling. These results show that this unusual physiological phenomenon, in which D2Rs enhance cellular excitability in a manner that depends on synaptic input, is mediated at the cellular level through the recruitment of signaling pathways associated with G_s, rather than the $G_{i/o}$-associated mechanisms that have classically been ascribed to D2Rs.

SIGNIFICANCE STATEMENT

Dopamine D2 receptors in the prefrontal cortex (PFC) are believed to play important roles in behaviors including working memory and cognitive flexibility. Variation in D2Rs has also been implicated in schizophrenia, Tourette syndrome, and bipolar disorder. Recently, we described a new mechanism through which D2R activation can enhance the excitability of pyramidal neurons in the PFC. Here we explore the underlying cellular mechanisms. Surprisingly, although D2Rs are classically assumed to signal through $G_{i/o}$-coupled G-proteins and/or scaffolding proteins such as β-arrestin, we find that the effects of D2Rs on prefrontal pyramidal neurons are actually mediated by pathways associated with G_s-mediated signaling. Furthermore, we show how, via this D2R-dependent phenomenon, synaptic input can enhance the excitability of prefrontal neurons over timescales on the order of seconds. These results elucidate cellular mechanisms underlying a novel signaling pathway downstream of D2Rs that may contribute to prefrontal function under normal and pathological conditions.

Introduction

Dopaminergic modulation plays a key role in the prefrontal cortex (PFC). Prefrontal neurons receive dopaminergic input from a specific subpopulation of ventral tegmental area neurons which are strongly activated by aversive stimuli and have unique physiological properties (Lammel et al., 2011; Lammel et al., 2014). The infusion of dopamine D2 receptor agonists and antagonists into the PFC modulates working memory and set-shifting in rodents (Druzin et al., 2000; Floresco et al., 2006; St Onge et al., 2011). In nonhuman primates, prefrontal D2Rs are specifically necessary for neural activity associated with memory-guided saccades (Wang et al., 2004). Consistent with these animal studies, genetic variation in D2Rs modulates prefrontal activity and working memory in humans (Zhang et al., 2007). Prefrontal D2Rs have also been hypothesized to contribute to schizophrenia (Winterer and Weinberger, 2004; Durstewitz and Seamans, 2008), Tourette syndrome (Simonic et al., 1998; Minzer et al., 2004; Yoon et al., 2007; Steeves et al., 2010), and bipolar disorder (Minton et al., 2009). Thus, D2Rs play a major role in both normal and pathological prefrontal function.

Recently, our laboratory and others have shown that in the mouse medial prefrontal cortex (mPFC), three major subtypes of dopamine receptors (D1Rs, D2Rs, and D3Rs) are differentially expressed by distinct subtypes of layer 5 (L5) pyramidal neurons (Gee et al., 2012; Seong and Carter, 2012; Clarkson et al., 2017). Specifically, we found that D2Rs are selectively expressed within thick-tufted, subcortically-projecting (SC) L5 pyramidal neurons which exhibit prominent hyperpolarization-activated cationic current (I_h) (Gee et al., 2012). We found that in this population, pharmacological activation of D2Rs by the agonist quinpirole elicits a profound afterdepolarization (ADP) following depolarizing current injection. This ADP was also associated with a progressive membrane depolarization and

reduction in action potential amplitude during the depolarizing current pulse. The ADP was not observed under baseline conditions, and only occurred when NMDA receptors were activated, via either optogenetic stimulation of excitatory synapses or bath application of low dose (4 μM) NMDA. Similar to plateau potentials previously described in L5 pyramidal neurons (Milojkovic et al., 2005; Major et al., 2008), this ADP seems to rely on the intracellular accumulation of Ca^{2+} following influx through a combination of NMDA receptors (NMDARs) and L-type Ca2+ channels (LTCCs). In particular, it could be blocked by the NMDAR antagonist AP5, the selective LTCC antagonist nimodipine, and the intracellular Ca^{2+} chelator BAPTA; however, additional mechanistic details of intracellular signaling pathways related to this phenomenon are not known.

D2Rs are classically assumed to couple to inhibitory G proteins, reducing neuronal excitability by activating $G_{\alpha i/o}$ and inhibiting adenylate cyclase (Bonci and Hopf, 2005). D2Rs are also known to signal through at least two other pathways: via the $G_{\beta\gamma}$ subunits, and β-arrestin. Here we explore two aspects of the intracellular signaling pathways through which the activation of D2Rs elicits ADPs in prefrontal SC-projecting neurons using a combination of electrophysiological, transgenic, pharmacological, and chemogenetic approaches. We find that the ability of synaptic stimulation to facilitate D2R-dependent ADPs several hundred milliseconds later depends on voltage-dependent (likely Ca^{2+}) currents. Furthermore, we show that the D2R-dependent ADP persists following disruptions to G_i or β-arrestin signaling, and can be mimicked by chemogenetic activation of G_s signaling, suggesting that this phenomenon reflects novel intracellular signaling downstream of D2Rs.

Materials and Methods

Electrophysiology

Coronal brain slices (250 µm) including medial prefrontal cortex were made from adult mice of either sex that were at least 8 weeks old. We used the following transgenic mouse lines: wild-type C57BL/6J mice (www.jax.org/strain/000664), Drd1-Cre$^{+/-}$ (line EY262; www.gensat.org), Drd2-Cre$^{+/-}$ (line ER44; www.gensat.org), Drd2$^{fl/fl}$ (https://www.jax.org/strain/020631), Rosa26^{PTX} (from Shaun Coughlin, University of California, San Francisco), and βarr2-KO (https://www.jax.org/strain/011130). Slicing solution was chilled to 4°C and contained (in mM): 234 sucrose, 26 $NaHCO_3$, 11 glucose, 10 $MgSO_4$, 2.5 KCl, 1.25 NaH_2PO_4, 0.5 $CaCl_2$, bubbled with 5% CO_2/ 95% O_2. Slices were incubated in artificial cerebrospinal fluid (aCSF) at 32°C for 30 minutes and then at room temperature until recording. aCSF contained (in mM): 123 NaCl, 26 $NaHCO_3$, 11 glucose, 3 KCl, 2 $CaCl_2$, 1.25 NaH_2PO_4, 1 $MgCl_2$, also bubbled with 5% CO_2/ 95% O_2.

Neurons were visualized using differential interference contrast or DODT contrast microscopy on an upright microscope (Olympus). Recordings were made using a Multiclamp 700B (Molecular Devices) amplifier and acquired with pClamp. Patch pipettes (2-5 MΩ tip resistance) were filled with the following (in mM): 130 KGluconate, 10 KCl, 10 HEPES, 10 EGTA, 2 $MgCl_2$, 2 MgATP, 0.3 Na_3GTP. In some experiments, the internal solution contained 1mM GDP-βS or 100µM Rp-cAMPs. All recordings were made at 32-34°C. Series resistance was compensated in all current clamp experiments and monitored throughout recordings. Recordings were discarded if Rs changed by >25%.

D2R expressing, subcortically-projecting neurons were often identified by fluorescent visualization of retrograde tracer Alexafluor-tagged cholera toxin subunit B (CTb) injected

into the MD thalamus. In some experiments, pyramidal neuron subtypes were identified based on characteristic firing patterns, specifically h-current-induced “sag” greater than 3mV in response to hyperpolarizing current pulses.

All bath-applied drugs were dissolved in water (4 µM NMDA, 10 µM (-)quinpirole, 10 µM CNQX, 10 µM H89, 1 µM CNO), DMSO (5 µM sulpiride, 5 Aripiprazole), or 1M HCl (200 µM baclofen) before being diluted in aCSF.

Viral injection for expression of ChR2, fluorescent reporter, or DREADDs.

Viral injections were performed using standard mouse stereotactical methods. Mice were anesthetized for the duration of the surgery using isofluorane gas. After cleaning, an incision was made in the scalp, the skull was leveled, and small burr holes were drilled over the brain region of interest using a dental drill. Virus was injected through the burr holes using a microinjector at a speed of 150 nL/minute and the scalp was closed using tissue adhesive (Vetbond).

For expression of ChR2 in CC neurons, we injected a Cre-dependent ChR2 virus (AAV5-Ef1-DIO-ChR2-eYFP, 0.5 µL) into the mPFC of Drd1-Cre$^{+/-}$ mice (>p28) and waited 3-4 weeks for trafficking of ChR2 to the axon terminals in mPFC.

For fluorescent reporters, we injected a Cre-dependent eYFP virus (AAV5-Ef1-DIO-eYFP, 1 µL) into mPFC of Drd2-Cre$^{+/-}$, Drd2$^{fl/fl}$, or Rosa26^{PTX} mice (>p28) and waited 3-4 weeks. For retrogradely labelling SC-projecting neurons, Alexafluor-tagged cholera toxin subunit B (CTb; ThermoFisher) was first dissolved in PBS to make a 1.0mg/mL solution. 350nL of CTb were then injected into the MD thalamus at a rate of 100nL/min and waited 3-5 days before electrophysiological experiments.

To selectively knockout D2Rs in SC-projecting cells, we injected canine adenovirus-2 encoding Cre virus (Cav2-Cre, 0.5 µL; Institut de Génétique Moléculaire de Montpellier) into the MD thalamus as well as 1.5 µL AAV5-Ef1-DIO-eYFP into mPFC of $Drd2^{fl/fl}$ mice (>p28) and patched from both fluorescent and non-fluorescent cells after waited 4-5 weeks.

For DREADD experiments in D2R-expressing pyramidal neurons, we injected a Cre-dependent virus expressing the Gq-DREADD (AAV5-hSyn-DIO-hM3D(Gq)-mCherry, 750 nL), Gs-DREADD (AAV5-hSyn-DIO-rM3D(Gs)-mCherry, 750 nL), or Gi-DREADD (AAV5-hSyn-DIO-hM4D(Gi)-mCherry, 750 nL) into the mPFC of Drd2-$Cre^{+/-}$ mice and patched from fluorescent cells after waiting 5 weeks for expression.

MD thalamus injection coordinates were A/P = -1.7, M/L = +/- 0.3, D/V = -3.45. mPFC injection coordinates were A/P = 1.7, M/L = +/- 0.3, D/V = -2.75

ChR2 stimulation

We stimulated ChR2 in projections from the contralateral PFC using 5ms flashes of light generated by a Lambda DG-4 (Sutter Instruments) high-speed optical switch with a 300 W Xenon lamp delivered through a 470 nm excitation filter. For stimulation of fibers, 5 different trains of random light flashes (intensity: ~2mW, total train duration: 2.5 sec, ~60 flashes/train, flash duration: 2 msec) were delivered at through a 40x objective every 13 seconds.

Experimental Design and Statistical Analysis

All data are shown as mean +/- 1 SEM. Statistical significance was accepted at the level $p < 0.05$. All statistical computations were performed using GraphPad Prism 7.0 software. We used student's t-test to compare pairs of groups if data were normally

distributed (verified using Lillie test). If more than two groups were compared, we used ANOVA with post-hoc tests between groups corrected for multiple comparisons (Holm-Sidak or Bonferroni). The specific post-hoc test as well as exact F and corrected p values can be found in the text.

Results

The quinpirole-induced ADP depends on D2Rs

First, to confirm the basic properties of the D2R-mediated ADP we had described previously (Gee et al., 2012), we labeled SC-projecting neurons by injecting a retrogradely transported fluorescent tracer (Alexafluor-tagged cholera toxin subunit B; CTb) into the mediodorsal (MD) thalamus (Figure 1A). Then, we patched from CTb+ L5 pyramidal neurons in mPFC, and measured their voltage responses to depolarizing current pulses (250 msec duration) (Figure 1B). We did not observe an ADP following depolarizing current pulses in the presence of just NMDA (4 μM), however, following the addition of the D2R agonist (-)quinpirole (10 μM) to the bath, we observed a robust ADP for ~100-300 msec after the end of each depolarizing current pulse (Figure 1C: n = 11/9/11/4, baseline/NMDA/QPL/SUL; One-way ANOVA, $F_{(3,31)}$ =16.36, $p < 0.0001$; t-test, Bonferroni correction, baseline vs NMDA: $t_{(18)} = 0.1408$, baseline vs QPL: $t_{(20)} = 6.178$, $p < 0.0001$, NMDA vs QPL: $t_{(18)} = 5.721$, $p < 0.0001$) . Subsequent wash-in of the selective D2/D3 antagonist sulpiride (5 μM) eliminated this quinpirole-induced ADP (t-test, Bonferroni correction, QPL vs SUL: $t_{(13)} = 3.723$, $p = 0.0031$).

To further confirm that this ADP was mediated by D2Rs, we injected canine adenovirus-2 encoding Cre (Cav2-Cre) (Hnasko et al., 2006) into MD thalamus to drive Cre expression within a subset of SC-projecting neurons in D2R conditional KO mice ($Drd2^{fl/fl}$, Jackson Labs) (Bello et al., 2011) (Figure 1D). We then injected AAV to drive Cre-dependent expression of EYFP into the mPFC to identify SC-projecting neurons which expressed Cre, and from which D2Rs should have been knocked out. Finally, we made simultaneous recordings from pairs of EYFP+ and EYFP- neurons in L5 of the mPFC. We identified EYFP-negative SC-projecting neurons based on the presence of prominent

voltage sag and rebound afterdepolarization during responses to hyperpolarizing current pulses (Gee et al., 2012). We confirmed that the quinpirole-induced ADP still occurred in EYFP-negative SC-projecting neurons , but was completely absent from simultaneously recorded EYFP+ SC-projecting neurons (Figure 1E-F: n = 8 cell pairs; Mixed-model two-way ANOVA, $F_{(1,14)} = 20.15$, $p = 0.0005$; t-test, Holm-Sidak correction, eYFP+ baseline vs QPL: $t_{(7)} = 6.461$, $p < 0.0001$, eYFP- baseline vs QPL: $t_{(7)} = 0.1137$). This confirms that the quinpirole-induced ADP can be eliminated in a cell autonomous fashion by knocking out D2Rs.

Hyperpolarizing current suppresses the ability of synaptic input to facilitate the ADP

Next, we investigated mechanisms through which optogenetic stimulation of callosal synapses can unmask the quinpirole induced ADP (Gee et al., 2012). Again, bath application of quinpirole alone does not elicit an ADP. The ADP is only observed when quinpirole application is combined with the optogenetic stimulation of synaptic inputs, e.g., from the contralateral mPFC, or by bath application of low-dose NMDA. Synaptic stimulation can facilitate a subsequent ADP even when this stimulation is relatively weak, i.e., insufficient to elicit spiking in the postsynaptic neuron, and occurs several hundred milliseconds before the current pulse. Synaptic stimulation appears to act by recruiting NMDARs, since the ADP is blocked in the presence of AP5. We hypothesized that there could be at least two distinct mechanisms through which synaptic stimulation activates NMDARs and facilitates the ADP. First, synaptic stimulation may recruit significant NMDAR-mediated currents; in particular, even though the resulting EPSPs may be relatively modest when measured at the soma (e.g., ~1 mV in amplitude), they may be substantially larger in the dendrites leading to significant NMDAR-mediated Ca^{2+} influx, which persists for several

hundred milliseconds contributing to the subsequent ADP. Alternatively, synaptic stimulation may trigger ongoing network activity which continues for several hundred milliseconds.

To distinguish between these two possibilities, we compared the magnitude of the quinpirole-induced ADP under various conditions (Figure 2B). In each case we elicited the ADP as follows: we injected AAV5-Ef1α-DIO-ChR2-EYFP into the mPFC in one hemisphere of Drd1-Cre (D1-Cre) mice (to label callosally-projecting D1+ neurons), then after waiting 3 to 4 weeks for ChR2 expression, we made recordings from L5 SC-projecting neurons in the contralateral hemisphere (Figure 2A). After delivering a train of irregularly occurring light flashes (total train duration: 2.5 sec, ~60 flashes/train, flash duration: 2 msec) to stimulate callosal terminals, we waited for 500 msec, then injected a depolarizing current pulse (+400 pA, 500 msec duration) to elicit the ADP. Each experiment consisted of four phases. First, we simply recorded the ADP following synaptic stimulation (control; Figure 2C). Second, we injected hyperpolarizing current (-200 pA) while delivering the train of light flashes in order to suppress voltage-dependent currents (e.g., NMDAR-mediated Ca2+ influx) associated with synaptic stimulation ("Exp 1"; Figure 2C). Third, we washed on CNQX (10 μM) to block AMPA receptors and eliminate recurrent network activity elicited by synaptic stimulation ("Exp 2"; Figure 2D). Fourth, we delivered hyperpolarizing current during the light trains while CNQX remained in the bath ("Exp 1 + 2"; Figure 2D). To quantify the ADP, we measured the amount of time required the membrane potential to return to baseline following the depolarizing current pulse (more precisely, the time for 90% decay).

The duration of the ADP was significantly reduced when we injected hyperpolarizing current during the delivery of light flashes (Figure 2E: n = 12; 46 ± 8% reduction in ADP duration; repeated-measures ANOVA, F = 8.659, p = 0.0024; t-test, Holm-Sidak correction, for ACSF vs. QPL without hyperpolarizing current: $t_{(22)}$ = 5.067, p = 0.0036; for QPL with vs.

without hyperpolarizing current: $t_{(22)} = 3.544$, $p = 0.0318$). By contrast, there was relatively little effect of CNQX application alone (t-test, QPL with vs. without CNQX, no hyperpolarizing current: $t_{(22)} = 0.051$). Notably, the combined effect of CNQX application and hyperpolarizing current injection was significantly larger than that of hyperpolarizing current injection alone – in fact the ADP was almost eliminated in this case (70 ± 5% reduction in ADP duration; t-test, QPL with vs. without CNQX *and* hyperpolarizing current: $t_{(22)} = 4.988$, $p = 0.0037$), suggesting that dendritic space clamp may be significantly improved in the presence of CNQX. Note: hyperpolarizing current delivered during the period of synaptic stimulation also seemed to attenuate other phenomena elicited by combined D2R activation + synaptic stimulation, e.g., the progressive membrane depolarization and reduction in spike amplitude during a current pulse.

Finally, we explored the timescales over which synaptic input could contribute to the quinpirole-induced ADP. For these experiments, we simply varied the delay between the trains of light flashes and the subsequent depolarizing current pulses. Remarkably, we could still observe an ADP lasting ~100 msec even when current injection occurred up to 10 seconds following synaptic stimulation (Figure 2F; n = 5; Repeated measures 2-way ANOVA: $F_{(10,40)} = 4.8$, $p = 0.0002$; t-test, Holm-Sidak correction, for individual time delays were as follows: p = 0.0071 (0.5s), 0.0007 (1s), < 0.0001 (1.5s), < 0.0001 (2.0s), 0.1190 (2.5s), 0.0338 (5.0s), 0.0003 (10s), 0.6671 (30s), 0.4942 (60s), 0.6671 (90s), 0.1248 (120s)).

Inhibiting adenylate cyclase / PKA-dependent signaling inhibits the quinpirole-induced ADP

Next, we turned our attention to the intracellular signaling pathways through which D2R activation recruits the ADP. First, to verify that the quinpirole-induced ADP depends on G-protein signaling, we performed experiments with 1mM GDP-βS in our intracellular pipette. GDP-βS is a non-hydrolyzable form of GDP that binds to G-proteins, and prevents the conformational changes which normally follow receptor ligand binding, depend on the hydrolysis of GTP to GDP, and trigger downstream signaling (Seong and Carter, 2012). Indeed, whereas in control experiments (without GDP-βS in the intracellular pipette), we observed robust ADPs following application of (-)quinpirole (10 μM) + NMDA (4 μM), we observed no ADPs when 1mM GDP-βS was included in the intracellular pipette (Figure 3A-B; n=7/6, K-gluconate/GDP-βs; two-way ANOVA: $F_{(2,27)} = 6.406$, $p = 0.0053$; t-test, Holm-Sidak correction, quinpirole+NMDA condition for K-gluconate vs GDP-βs: $t_{(11)} = 4.241$, $p = 0.0007$).

Next, since D2Rs canonically signal through inhibitory G-proteins, we decided to test how inhibiting adenylate cyclase / PKA signaling would affect the ADP. Since inhibitory G-proteins normally inhibit these pathways, we expected PKA inhibitors such as Rp-cAMPs or H89 to mimic or enhance the ADP. In fact we found that when we included Rp-cAMPs (100 μM) in the intracellular pipette, we could initially elicit a quinpirole-induced ADP in a perforated patch recording configuration, but that when we subsequently broke in, shifted to a whole cell recording, and dialyzed the cell with our intracellular solution, the quinpirole-induced ADP was abolished (Figure 3C & E; n = 4; ANOVA, $F_{(2,9)} = 7.154$, $p = 0.0138$; t-test, Bonferroni correction; ACSF vs QPL: $t_{(6)} = 3.271$, $p = 0.029$, QPL vs Rp-cAMPs: $t_{(6)} = 3.281$, $p = 0.0285$). This demonstrates that Rp-cAMPs is actually sufficient to abolish the quinpirole-induced ADP. Similarly, the presence of H89 (10 μM) in the bath prevented us from inducing an ADP with bath application of quinpirole and NMDA (Figure 3D-E; n = 6;

ANOVA, $F_{(1,17)} = 5.841$, $p = 0.0272$, t-test, Holm-Sidak correction, Control ACSF vs QPL: $t_{(10)} = 3.524$, $p = 0.0052$, H89 control vs H89 + QPL: $t_{(6)} = 0.2426$). These results suggest that inhibition of adenylate cyclase / PKA signaling is sufficient to block the quinpirole-induced ADP in a cell-autonomous fashion.

The quinpirole-induced ADP is independent of β-arrestin

Activation of D2Rs with relatively high doses of quinpirole (10 mM) and for somewhat prolonged periods of time (e.g., 15-20 min) may induce β-arrestin-mediated desensitization and internalization. Thus, the preceding observations could be explained by a model in which at baseline, D2Rs inhibit adenylate cyclase / PKA signaling, suppressing the ADP, but that quinpirole induces receptor internalization, terminating this suppression, and leading to the appearance of the ADP. To explore whether the ADP might depend on β-arrestin signaling via such a mechanism, we measured the ADP after disrupting β-arrestin signaling in two ways. First, we studied β-arrestin2 KO mice (βarr2-KO) (Bohn et al., 1999), and found that quinpirole and NMDA continued to elicit ADPs (Figure 4A-B; n = 18/11, β-arrestin2 KO/C57BL/6 ; two-way ANOVA, $F_{genotype(1,75)} = 0.517$, $F_{drug(3,75)} = 16.56$, $p < 0.0001$; t-test, Holm-Sidak correction, β-arrestin2 KO ACSF vs QPL: $t_{(34)} = 5.759$, $p < 0.0001$). Moreover, in βarr2 KO mice, this quinpirole-induced ADP was still eliminated by the subsequent wash-in of the selective D2R antagonist sulpiride (5 μM), confirming that it still depends on D2Rs (Figure 4A-B; t-test, Holm-Sidak correction, β-arrestin2 KO QPL vs SUL: $t_{(20)} = 2.595$, $p = 0.0448$). Second, we found that quinpirole and NMDA could still elicit an ADP even in the presence of Aripiprazole (ARP; 5 μM; Figure 4 C-D; n = 6; ANOVA, $F_{(1,52)} = 0.005$, $F_{drug(2,52)} = 16.34$, $p < 0.0001$, t-test, Holm-Sidak correction, ARP ACSF vs ARP QPL: $t_{(10)} = 3.329$, $p <0.0416$). ARP is a functionally selective D2R ligand that is a complete

antagonist with respect to β-arrestin signaling, but a partial agonist with respect to canonical G-protein signaling (Burris et al., 2002; Madhavan et al., 2013). Together, these two experiments show that D2Rs can elicit the ADP in the absence of β-arrestin.

Pertussis toxin does not block the quinpirole-induced ADP

Next, we wanted to examine whether the quinpirole-induced ADP depends on G_i signaling at all. For this, we expressed pertussis toxin, which selectively blocks all G_i-mediated signaling. We crossed Drd2-Cre (D2-Cre) mice to a transgenic line expressing the Cre-dependent S1 catalytic subunit of pertussis toxin (PTX S1) inserted into the Rosa26 (Rosa26-PTX) (Regard et al., 2007) such that PTX S1 would be expressed in D2R+ cells which normally exhibit the D2R-mediated ADP (Figure 5A). We verified that pertussis toxin blocked G_i-mediated signaling in D2R+ neurons by comparing baclofen-induced currents in D2R+ (SC-projecting) neurons and D2R-negative (IT-projecting) neurons (distinguished based on the Cre-dependent expression of EYFP) (Figure 5B). Baclofen is a GABABR agonist which normally recruits GIRK currents via G_i signaling. We found that in voltage clamp recordings in wild-type mice, bath application of baclofen (200 μM), elicits large outward currents in both D2R+ and D2R-negative neurons (n = 4 of each; Figure 5C). In D2-Cre / Rosa26-PTX mice, baclofen continued to elicit GIRK currents normally in D2R-negative neurons; however, baclofen-induced currents were completely abolished in D2R+ neurons (Figure 5C; n = 4/4, D2R+ and D2R- from each genotype; two-way ANOVA, $F_{(1,12)} = 620$, $p < 0.001$, t-test, Holm-Sidak correction, $t_{(6)} = 31.48$, $p < 0.0001$). We found that the quinpirole-induced ADP was intact in D2R+ neurons from D2-Cre / Rosa26-PTX mice (Figure 5D-E; n = 6/5, Drd2Cre::Rosa26-PTX/C57BL6; repeated-measures two-way ANOVA, $F_{genotype(1,9)} = 0.0002$, $F_{drug(2,18)} = 45.4$, $p < 0.0001$; t-test, Holm-Sidak correction,

C57BL/6 ACSF vs QPL: $t_{(8)} = 5.581$, $p < 0.0001$, Drd2Cre::Rosa26-PTX ACSF vs QPL: $t_{(10)} = 6.047$, $p < 0.0001$). These experiments show that D2Rs elicit the ADP even in the absence of G_i-signaling.

G_s but not G_i or G_q coupled DREADDs elicit a quinpirole-like ADP

The preceding results strongly suggest that D2Rs do not act through G_i or β-arrestin to elicit the ADP. Furthermore, the fact that the PKA inhibitors Rp-cAMPs and H89 can inhibit the quinpirole-induced ADP raise the possibility that signaling through G_s or a G_s-like pathway may actually elicit this phenomenon. To test this directly, we injected virus to drive Cre-dependent expression of G_s, G_i, or G_q-coupled DREADDs into the mPFC of D2-Cre mice. We found that the presence of low dose (4 μM) NMDA together with clozapine-N-oxide (1 μM; CNO), which activates each DREADD, could elicit an ADP identical to the sort normally induced by quinpirole in SC-projecting cells expressing G_i DREADDs (Figure 6A-B; n = 8 for each DREADD; Mixed-model two-way ANOVA, $F_{(2,21)} = 15.94$, $p < 0.0001$; t-test, Holm-Sidak correction, G_s-DREADD ACSF vs CNO+NMDA: $t_{(14)} = 7.01$, $p <0.0001$). Activation of the G_s-DREADD increases the number of action potential during and immediately following the current pulse (i.e. including the ADP). By contrast, we observed no effect of CNO in mice expressing the G_q DREADDs. Furthermore, in mice expressing the G_i DREADDs, bath application of 1 μM CNO decreased action potential firing in response to a depolarizing current step (Figure 6C; n = 8 for each DREADD ; Mixed-model two-way ANOVA, $F_{(2,21)} = 20.79$, $p < 0.0001$; t-test, Holm-Sidak correction, G_i-DREADD ACSF vs CNO: $t_{(14)} = 3.319$, $p = 0.0065$, G_s-DREADD ACSF vs CNO: $t_{(14)} = 5.621$, $p < 0.0001$), confirming functional Gi DREADD expression in these neurons, and consistent with a G_i-induced reduction of neuronal excitability (Bonci and Hopf, 2005).

Discussion

Here we follow up on our earlier work (Gee et al., 2012), which described a new mechanism through which D2R activation could elicit an increase in excitability, specifically an ADP, within subcortically-projecting L5 pyramidal neurons in the mPFC. Several aspects of this phenomenon were unusual. First, we observed the ADP using relatively high doses of quinpirole (5-20 μM). This was in contrast to other effects of quinpirole can sometimes be observed using doses ~1 μM (Tseng et al., 2007). Second, the ADP represents an increase in excitability, whereas D2R activation has classically (in the striatum) been assumed to inhibit neuronal excitability. Third, this phenomenon was not readily observed under baseline conditions in brain slices, but required synaptic stimulation. All of these relatively unique features raised several questions, e.g., is this phenomenon, which is elicited by quinpirole and blocked by sulpiride, really mediated by D2Rs;? If so, is this phenomenon mediated by canonical D2R signaling, the desensitization or internalization of D2Rs, or another pathway (e.g. β-arrestin-mediated signaling) altogether? And finally what is the mechanism through which synaptic input regulates the occurrence of an ADP several hundred milliseconds later?

This study answers those questions, at least in part. Knocking out D2Rs abolishes the quinpirole-induced ADP in a cell-autonomous manner, confirming that it is D2R-mediated. Hyperpolarizing current injection, but not CNQX, prevents synaptic stimulation from facilitating the quinpirole-induced ADP, showing that this effect depends on the ability of synaptic stimulation to recruit voltage-dependent currents, likely NMDAR-mediated Ca^{2+} influx. Finally, the quinpirole-induced depolarization is blocked by inhibitors of PKA signaling, insensitive to pertussis toxin, and mimicked by G_s-DREADD stimulation. Taken together, our observations, following numerous manipulations targeting multiple aspects of

G-protein coupled signaling, suggest that D2R activation elicits the ADP by stimulating cAMP / PKA signaling that is downstream of G_s (Figure 7).

Importantly, neither quinpirole nor sulpiride distinguishes between D2Rs and D3Rs. Thus, pharmacology alone could not rule out the possibility that D3Rs, along with D2Rs, contribute to the quinpirole-induced ADP. However, another recent study shows that D3Rs are expressed by a distinct population of prefrontal neurons, and not by the prefrontal SC-projecting neurons which are the subject of this study (Clarkson et al., 2017).

Limitations

Of course, our experiments have some important limitations. For example, H89 inhibits other kinases besides PKA, although Rp-cAMPs (which we delivered intracellularly) is more selective. Our experiments have not directly tested whether G_i-associated βγ subunits might contribute to the effects we have observed by stimulating PKA signaling, but we consider this possibility unlikely, because the D2R-induced afterdepolarization is not blocked by pertussis toxin. By preventing dissociation of the heterotrimeric G-protein complex, pertussis toxin should block signaling by both α and βγ subunits associated with G_i. Similarly, although our results do suggest that D2Rs elicit an afterdepolarization via signaling pathways that are classically downstream of G_s, we have not determined to what extent G_s-associated βγ subunits might contribute to or modulate these effects (Figure 7). Finally, although our experiments with pertussis toxin strongly argue against a role for Gi-mediated signaling in the D2R-induced ADP, and our DREADD experiments show that Gs-mediated signaling is sufficient to elicit this phenomenon, we cannot completely rule out the possibility that native G_q-signaling might contribute to this phenomenon in ways that are not captured by simply stimulating Gq DREADDs.

Relationship to other modes of D2R signaling

D2R mediated signaling is diverse. D2Rs have classically been assumed to inhibit neuronal excitability via G_i signaling, e.g., in indirect pathway medium spiny neurons and dopaminergic terminals (Bonci and Hopf, 2005). However other studies have described novel mechanisms whereby D2Rs can signal through $G_{\beta\gamma}$ subunits or interactions with β-arrestin (Beaulieu et al., 2005) including in prefrontal interneurons (Urs et al., 2016). These results enlarge the family of possible signaling pathways downstream of D2R activation. At the same time, this study, which has focused on cellular physiology, does not elucidate the molecular or biochemical details of this pathway.

Relationship to D2R heterogeneity and heteroreceptors

D2Rs comprise 6 introns and are known to undergo alternative splicing giving rise to at least 2 major isoforms (Usiello et al., 2000; De Mei et al., 2009). There has also been controversy about whether D2Rs might form heteroreceptors with D1Rs in the cortex (Beaulieu and Gainetdinov, 2011; Zhang et al., 2011). Findings like these suggest that D2Rs exist in heterogeneous forms, which may explain how D2Rs can couple to various intracellular signaling pathways, giving rise to distinct effects on neuronal excitability, in different neuronal populations. It will be interesting for future studies to characterize the specific forms of D2Rs that are expressed in prefrontal SC-projecting neurons. In particular, there may be specific domains present in D2R isoforms expressed in prefrontal SC-projecting neurons which enable coupling to the G_s pathways, D1Rs, or other effectors.

Functional implications

The phenomenon studied here is one whereby synaptic activity, even when subthreshold with respect to action potential generation in the post-synaptic neuron, can enhance neuronal excitability several hundreds of milliseconds or even up to 10 seconds later. This could enable post-synaptic neurons to integrate their inputs over relative long durations. An alternative interpretation of this mechanism is that one set of inputs could switch neurons into a “high gain” mode whereby responses to subsequent inputs are potentiated, relative to the neuron’s baseline state. These effects could help to generate patterns of prefrontal activity e.g., the sequential patterns observed during the delay period of working memory or cued rule switching tasks (Bolkan et al., 2017; Schmitt et al., 2017). In these tasks, inhibiting prefrontal activity during the early portion of a delay disrupts subsequent sequential activity – early activity, if paired with D2R activation, may serve to “prime” the responses of neurons that fire later during the delay via this mechanism.

In this and previous studies (Gee et al., 2012) we have shown that optogenetically stimulating callosal inputs is sufficient to facilitate the D2R-dependent ADP. It will be interesting to explore whether other sources of inputs to mPFC can generate similar effects. We also have used trains of light flashes to stimulate synapses over periods of 2.5 seconds – it will be interesting to determine how this phenomenon depends on the duration of synaptic input. Finally, we have generally used patterns of synaptic stimulation that elicit EPSPs which are subthreshold for action potential generation in the postsynaptic neuron. An outstanding question is whether stronger patterns of stimulation are more or less effective for eliciting this phenomenon.

Clinical implications

Dopaminergic innervation of the prefrontal cortex is disrupted in schizophrenia (Slifstein et al., 2015), mutations in D2Rs are associated with schizophrenia (Schizophrenia Working Group of the Psychiatric Genomics Consortium, 2014), and all known clinically effective antipsychotics block D2Rs (Seeman, 2002). Together these observations raise the possibility that prefrontal D2R function may be abnormal in schizophrenia, although the precise nature of such dysfunction and its relationship to symptoms, remain largely unknown. As better models for schizophrenia are developed, e.g., based on neurons derived from patient iPS cells or mice with mutations in genetic loci strongly implicated in schizophrenia, it will be interesting to study whether this unusual form of prefrontal D2R signaling is altered.

Conclusion

Dopamine D2 receptors can enhance the excitability of subcortically-projecting pyramidal neurons in layer 5 of medial prefrontal cortex through a pathway that depends on increased cAMP / PKA signaling. This increase in neuronal excitability also appears to require the activation of synaptic NMDARs and voltage-dependent Ca^{2+} influx during the preceding several seconds. Important next steps will be understanding how this phenomenon contributes to normal brain function and is disrupted in the setting of diseases such as schizophrenia.

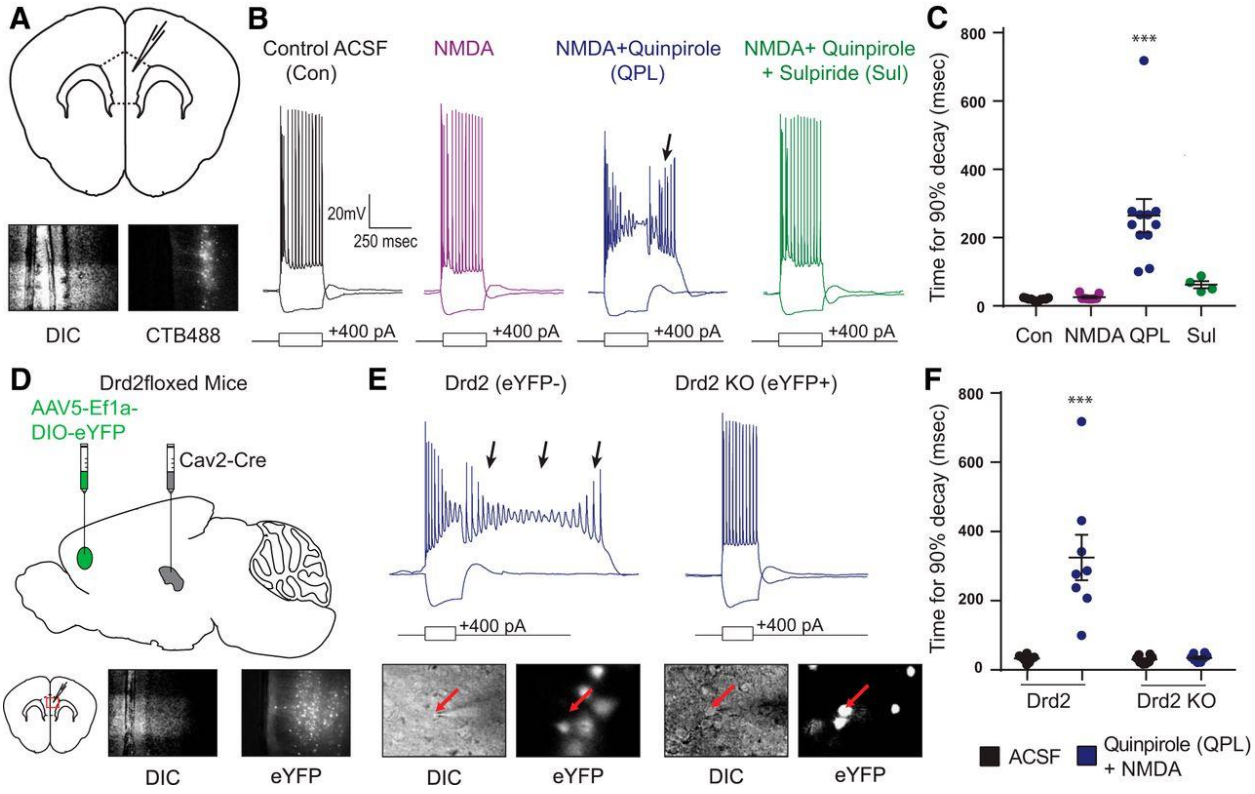

Figure 1. The quinpirole-induced afterdepolarization depends on D2Rs.

A) Schematic of coronal brain slice: we recorded from subcortically-projecting (SC) L5 pyramidal neurons labeled with CTB488 in the mouse mPFC (top). Images of a recorded neuron in DIC and exhibiting 488 fluorescence (bottom). **B)** Example pyramidal cell responses to hyperpolarizing and depolarizing current steps at baseline (black) and after application of drug (4 µM NMDA, purple; 4 µM NMDA + 10 µM Quinpirole, blue; 4 µM NMDA + 10 µM Quinpirole + 5µ Sulpiride, green). Arrow indicates the quinpirole-induced afterdepolarization (ADP). **C)** Changes in the ADP, quantified by the amount of time required for the membrane potential to return to baseline following the depolarizing current pulse (more precisely, the time for 90% decay), after pharmacological manipulations listed above. n = 11/9/11/4, baseline/NMDA/QPL/SUL. ***$p < 0.0001$. **D)** Experimental design: $Drd2^{fl/fl}$ mice were injected with Cav2-cre virus in the MD thalamus and DIO-EYFP virus in the mPFC 4-5 weeks prior to slice experiments. **E)** Example pyramidal cell responses to hyperpolarizing and depolarizing current steps in 4 µM NMDA + 10 µM Quinpirole for EYFP negative (control) and EFYP positive (Drd2 knockout) cells (top). Images of a recorded neuron in DIC showing EYFP fluorescence (bottom). **F)** The quinpirole-induced ADP (arrows) is absent in cells lacking Drd2. n = 8 cell pairs. ***$p < 0.0001$.

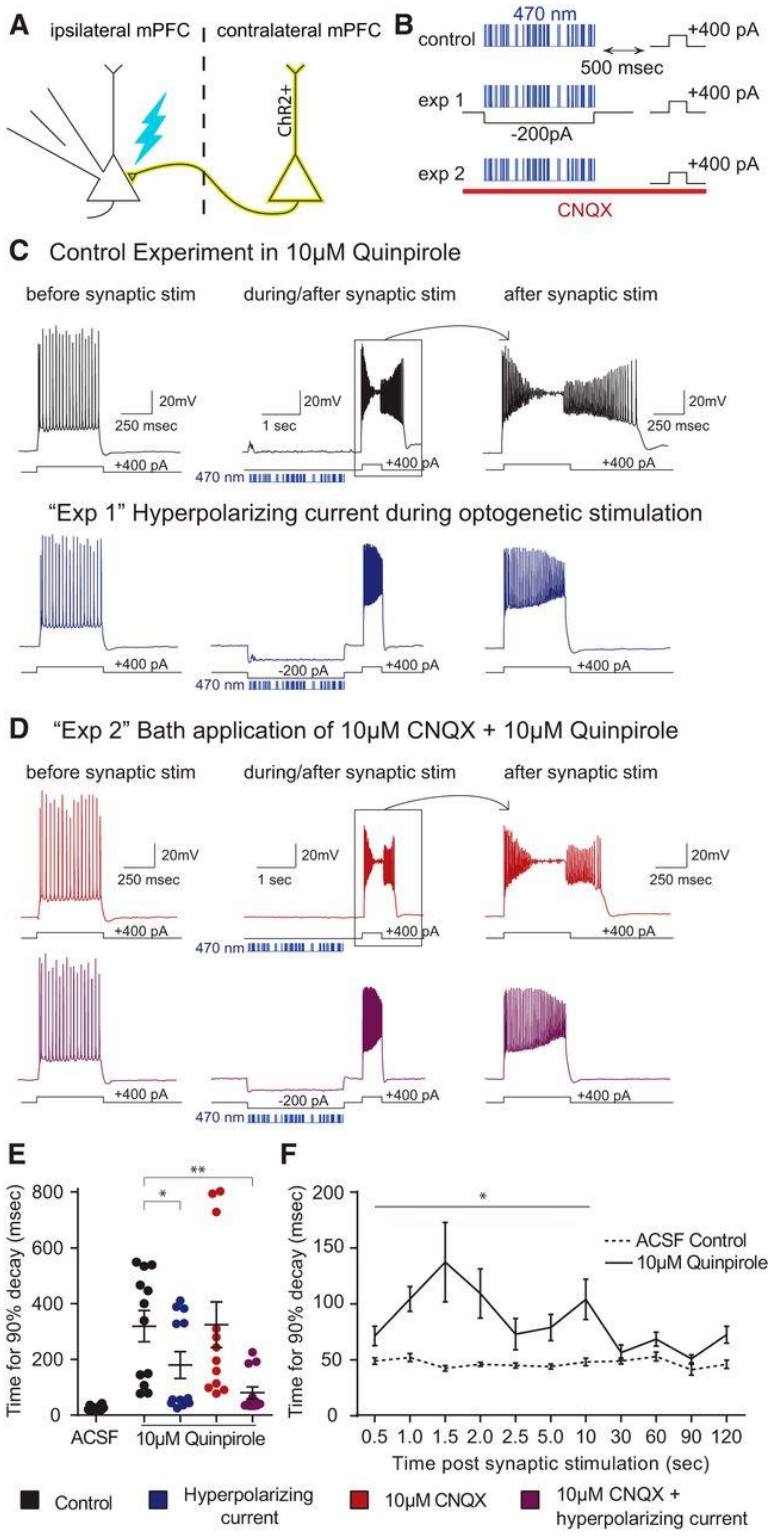

Figure 2. Hyperpolarizing current suppresses the ability of synaptic input to facilitate the quinpirole-induced ADP.

A) Experimental design: We recorded from ChR2-negative layer 5 neurons while stimulating ChR2-expressing axon terminals from the contralateral mPFC with trains of light flashes (470 nm, 2.5 msec, ~2 mW). **B)** For each cell with bath application of 10 μM quinpirole, we recorded the neuronal response under four different stimulation paradigms: synaptic stimulation (control, black); hyperpolarizing current (-200 pA) during the train of light flashes ("exp 1", blue); synaptic stimulation in 10 μM CNQX ("exp 2", red); hyperpolarizing current during light flashes while in 10 μM CNQX (purple). **C-D)** Responses of a layer 5 SC-projecting pyramidal neuron to current injection before (left panel) and immediately following (middle and right panels) optogenetic stimulation of synaptic inputs. Blue bars indicate the times of light flashes. **E)** Quinpirole-induced ADP is reduced by injection of hyperpolarizing current. n = 12. *p = 0.0318, **p = 0.0037. **F)** The quinpirole-induced ADP persists up to 10 seconds after the synaptic stimulation. n = 5. *p < 0.0001-0.0338 .

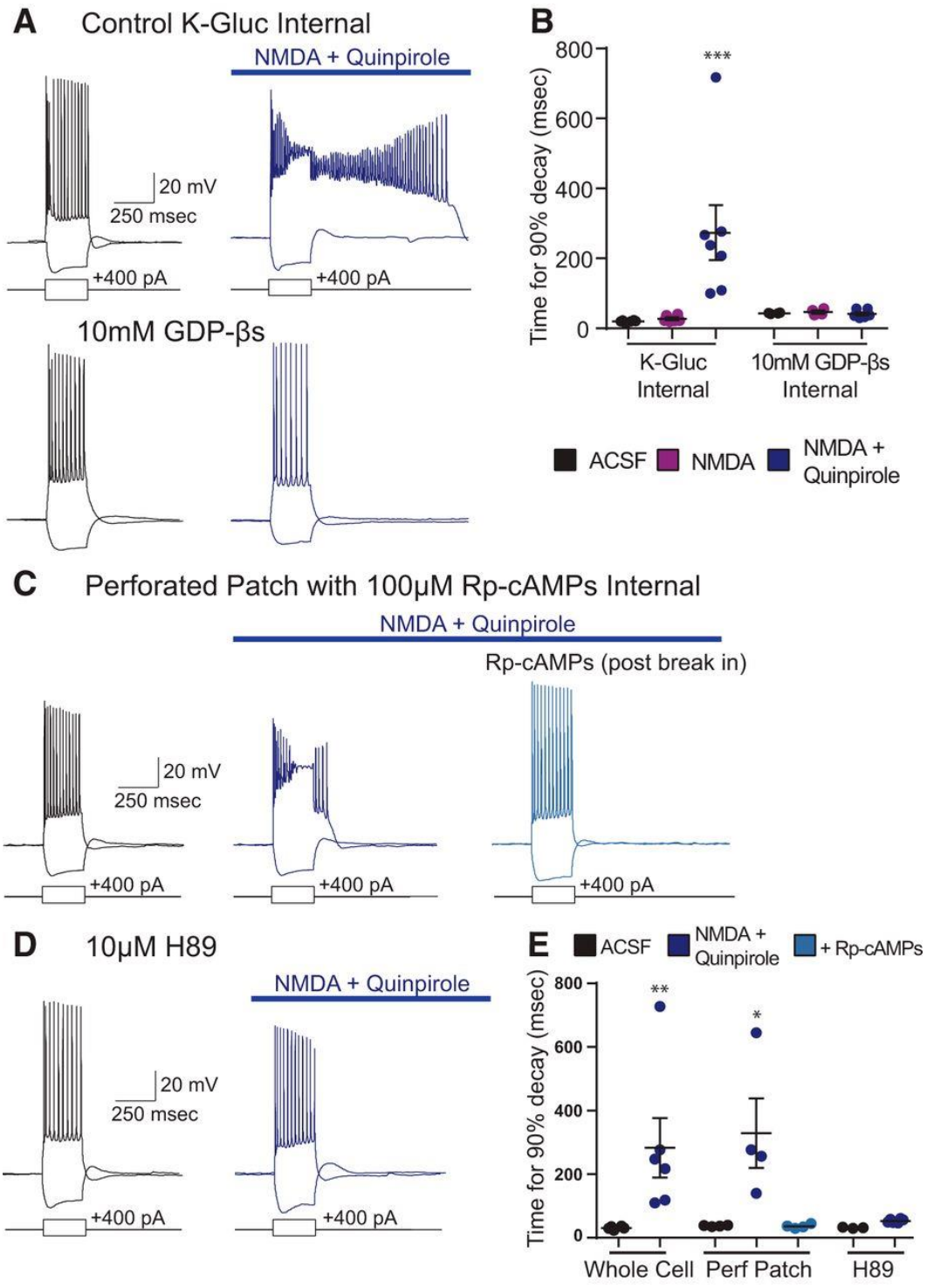

Figure 3. Inhibiting adenylate cyclase / PKA-dependent signaling inhibits the quinpirole-induced ADP

A) Sample traces in ACSF (black) and 4 μM NMDA + 10 μM quinpirole (blue) in control K-gluconate internal as well as internal including 1 mM GDP-βS, a G-protein inhibitor. **B)** GDP-βS blocks the quinpirole-induced ADP in a cell-autonomous fashion. n=7/6, K-gluconate/GDP-βs. ***p = 0.0007. **C)** Sample traces in ACSF (black) and 4 μM NMDA + 10 μM quinpirole (blue, left) in perforated patch and in whole-cell patch clamp dialyzed with internal solution containing 100 μM Rp-cAMPs (blue, right). **D)** Sample traces with bath application of 10 μM H89 in ACSF (black) and 4 μM NMDA + 10 μM quinpirole (blue). **E)** Inhibition of PKA suppresses the quinpirole induced ADP. n = 4 for perforated patch and 6 for H89. *p = 0.0285. **p = 0.0052.

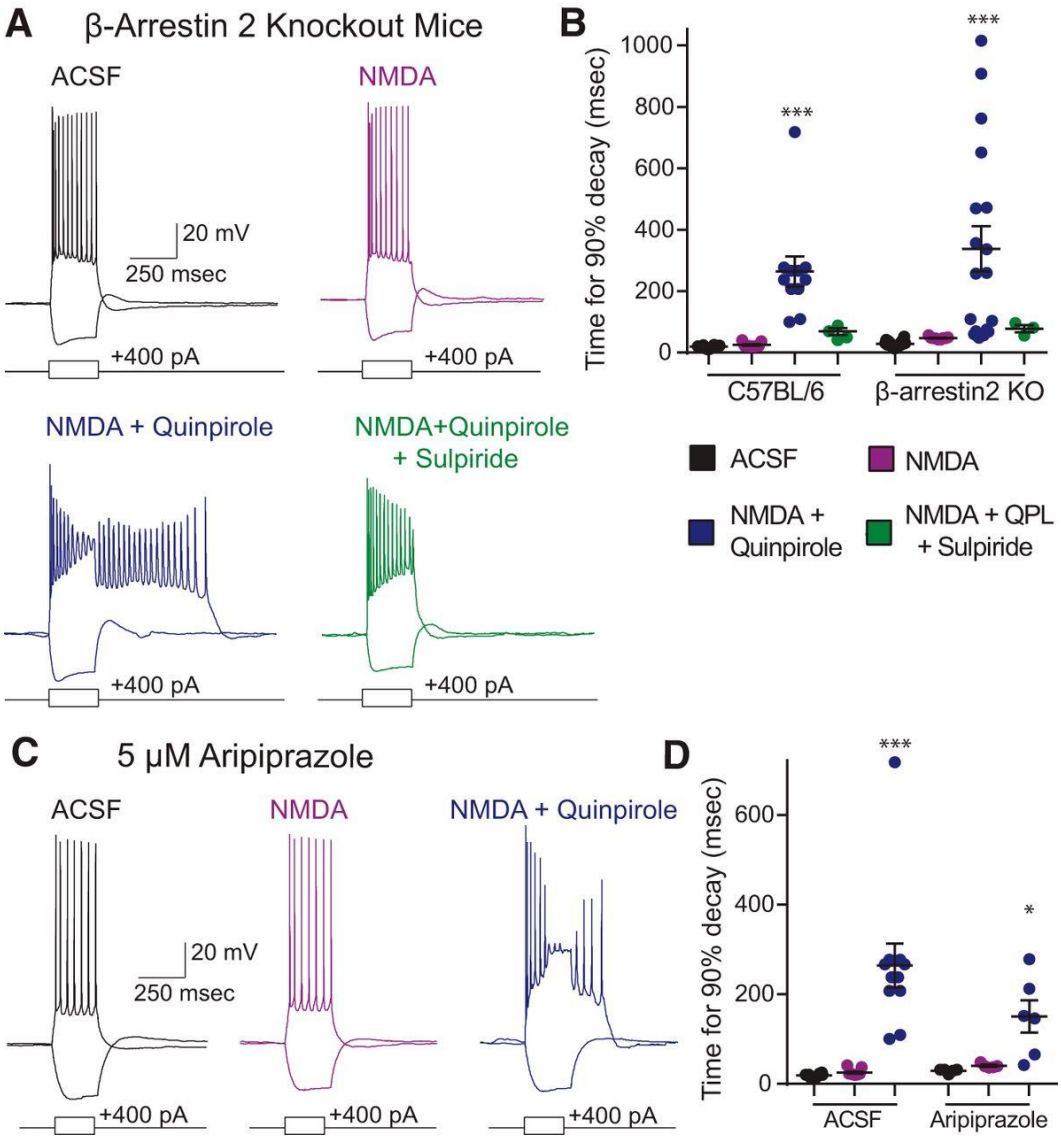

Figure 4. The quinpirole-induced ADP is independent of β-arrestin

A) Example recordings from β–arrestin2 KO mice in ACSF (black) and after application of drug (4 μM NMDA, purple; 4 μM NMDA + 10 μM Quinpirole, blue; 4 μM NMDA + 10 μM Quinpirole + 5μM Sulpiride, green). **B)** The quinpirole-induced ADP persists in β-arrestin2 KO mice. n = 18/11, β-arrestin2 KO / C57BL/6. ***p < 0.0001. **C)** Example traces in 5 M aripiprazole (ARP) at baseline (black) and after application of additional drugs (4 μM NMDA, purple; 4 μM NMDA + 10 μM Quinpirole, blue). **D)** The quinpirole-induced ADP persists in the presence of ARP, a biased D2R ligand that selectively antagonizes □-arrestin signaling. n = 6. ***p < 0.0001, * p=0.0416)

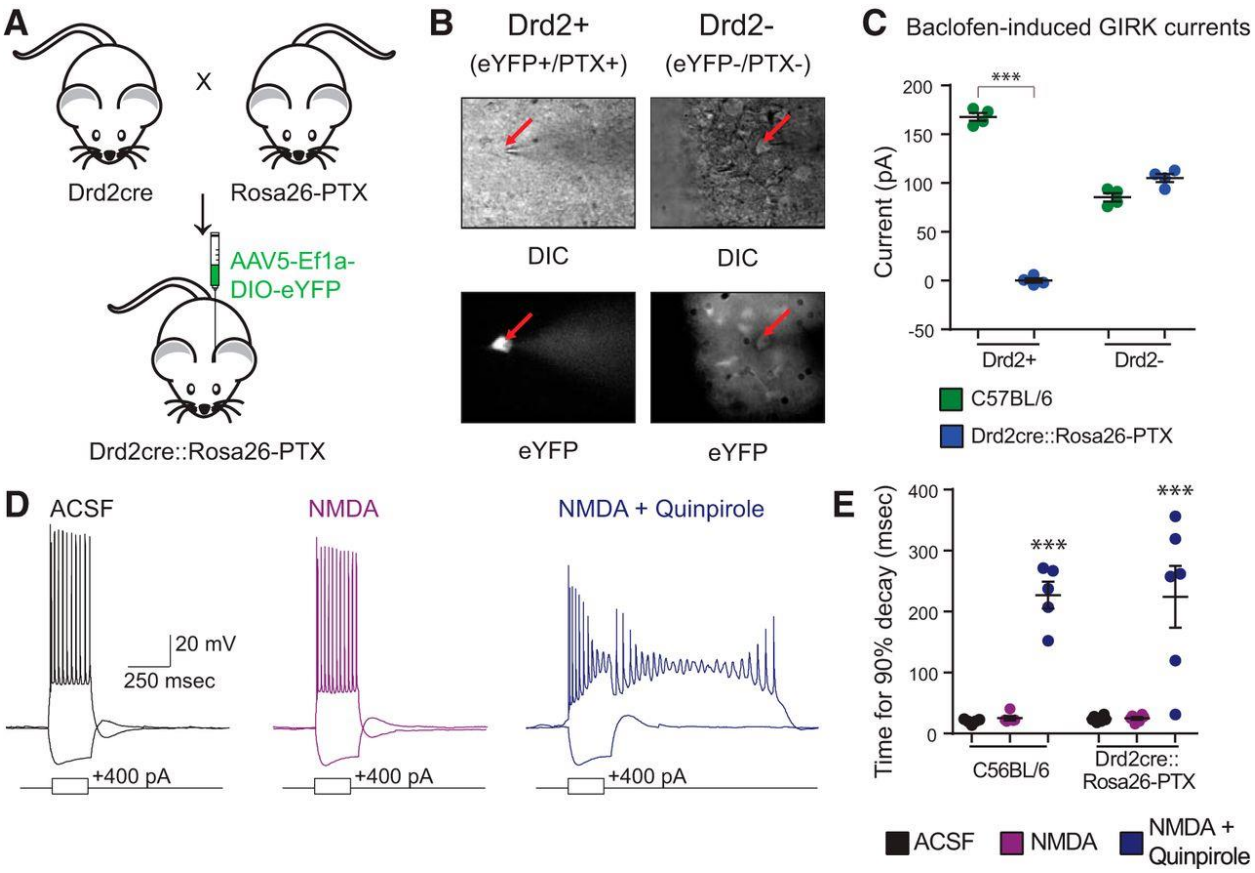

Figure 5. Pertussis toxin blocks G_i-signaling but does not block the quinpirole-induced ADP

A) Experimental design: We crossed D2-Cre mice to Rosa26-PTX mice and injected the offspring in the mPFC with a Cre-dependent virus to drive EYFP expression. **B)** We then recorded from D2+ pyramidal neurons (i.e., EYFP+) and D2-negative pyramidal neurons (i.e., EYFP-negative) in L5 of mPFC. **C)** Pertussis toxin selectively suppresses baclofen-induced GIRK currents in D2+ neurons of Drd2Cre::Rosa26-PTX mice. n = 4. ***p < 0.0001. **D)** Sample traces from Drd2Cre::Rosa26-PTX mice in ACSF (black) and after application of drug (4 µM NMDA, purple; 4 µM NMDA + 10 µM Quinpirole, blue). **E)** The quinpirole-induced ADP is not blocked by pertussis toxin. n = 6/5, Drd2Cre::Rosa26-PTX/C57BL/6. ***p < 0.0001.

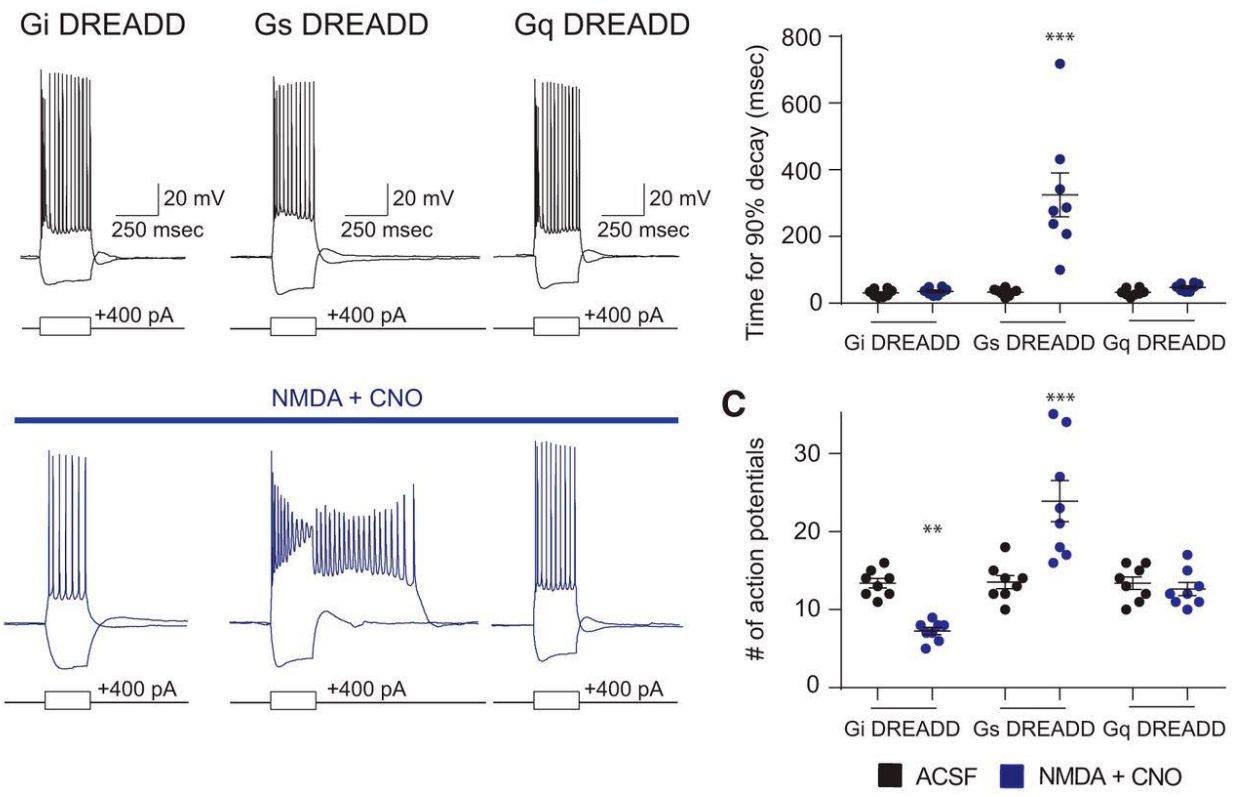

Figure 6. Signaling through G_s but not G_i or G_q coupled DREADDs elicit a quinpirole-like ADP

A) Example traces from L5 mPFC pyramidal neurons from D2-Cre mice injected with virus to derive Cre-dependent expression of either G_i (left), G_s (middle) or G_q (right) coupled DREADDs, at baseline (top, black) or in 4 µM NMDA + 1 µM CNO (bottom, blue). **B)** Activation of the G_s-DREADD with 1 µM CNO together with low dose NMDA elicits an ADP. n = 8. ***p <0.0001. **C)** Activation of the G_i-DREADD with 1 µM CNO reduces the number of action potentials fired when +400pA depolarizing current is injected for 250msec. By contrast, activation of the G_s-DREADD increases the number of action potential during and immediately following the current pulse. n = 8. **p = 0.0065. ***p < 0.0001.

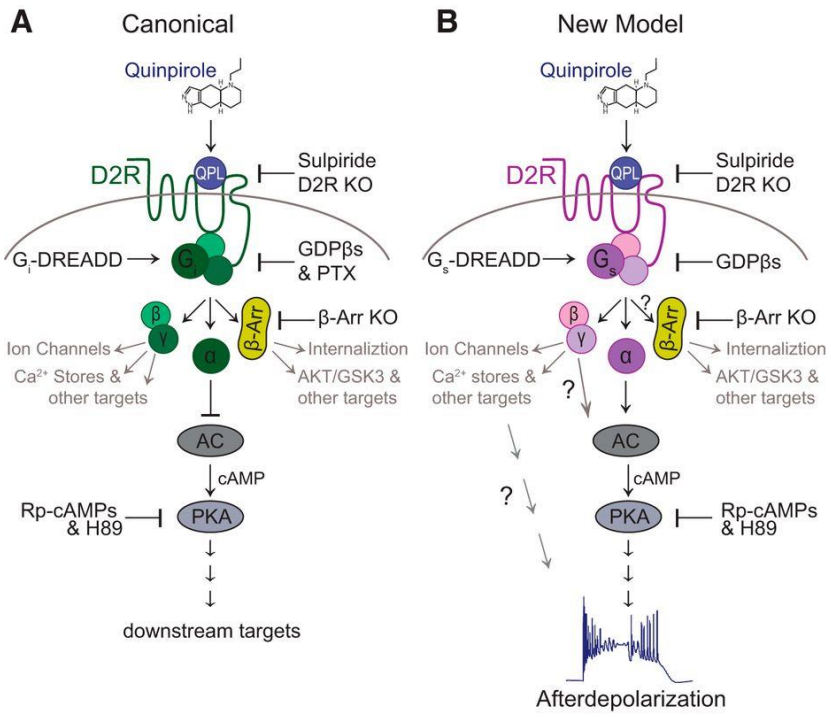

C

Elicits ADP	Suppresses ADP	No Effect
Quinpirole + NMDA	Sulpiride Drd2 KO	CNQX
Quinpirole + Synaptic Stimulation	APV & Nimodipine BAPTA	β-Arrestin2 KO Aripiprazole
G$_s$-DREADD	hyperpolarizing current	Pertussis Toxin
	GDP-βs	G$_q$-DREADD
	Rp-cAMPS H89	G$_i$-DREADD

Figure 7. Schematic models for D2R signaling in mPFC SC-projecting projecting L5 pyramidal neurons

A) Schematic of the canonical D2R signaling cascade acting via Gi to inhibit cAMP/PKA activity. **B)** Schematic of the new model showing how D2R signaling might act via Gs or a Gs-like pathway to stimulate cAMP/PKA and thereby elicit an ADP. **C)** Summary of how various experimental manipulations we tested affected the quinpirole-induced ADP.

References

Beaulieu JM, Gainetdinov RR (2011) The physiology, signaling, and pharmacology of dopamine receptors. Pharmacol Rev 63:182-217.

Beaulieu JM, Sotnikova TD, Marion S, Lefkowitz RJ, Gainetdinov RR, Caron MG (2005) An Akt/beta-arrestin 2/PP2A signaling complex mediates dopaminergic neurotransmission and behavior. Cell 122:261-273.

Bello EP, Mateo Y, Gelman DM, Noain D, Shin JH, Low MJ, Alvarez VA, Lovinger DM, Rubinstein M (2011) Cocaine supersensitivity and enhanced motivation for reward in mice lacking dopamine D2 autoreceptors. Nat Neurosci 14:1033-1038.

Bohn LM, Lefkowitz RJ, Gainetdinov RR, Peppel K, Caron MG, Lin FT (1999) Enhanced morphine analgesia in mice lacking beta-arrestin 2. Science 286:2495-2498.

Bolkan SS, Stujenske JM, Parnaudeau S, Spellman TJ, Rauffenbart C, Abbas AI, Harris AZ, Gordon JA, Kellendonk C (2017) Thalamic projections sustain prefrontal activity during working memory maintenance. Nat Neurosci.

Bonci A, Hopf FW (2005) The dopamine D2 receptor: new surprises from an old friend. Neuron 47:335-338.

Burris KD, Molski TF, Xu C, Ryan E, Tottori K, Kikuchi T, Yocca FD, Molinoff PB (2002) Aripiprazole, a novel antipsychotic, is a high-affinity partial agonist at human dopamine D2 receptors. The Journal of pharmacology and experimental therapeutics 302:381-389.

Clarkson RL, Liptak AT, Gee SM, Sohal VS, Bender KJ (2017) D3 Receptors Regulate Excitability in a Unique Class of Prefrontal Pyramidal Cells. J Neurosci 37:5846-5860.

De Mei C, Ramos M, Iitaka C, Borrelli E (2009) Getting specialized: presynaptic and postsynaptic dopamine D2 receptors. Curr Opin Pharmacol 9:53-58.

Druzin MY, Kurzina NP, Malinina EP, Kozlov AP (2000) The effects of local application of D2 selective dopaminergic drugs into the medial prefrontal cortex of rats in a delayed spatial choice task. Behav Brain Res 109:99-111.

Durstewitz D, Seamans JK (2008) The dual-state theory of prefrontal cortex dopamine function with relevance to catechol-o-methyltransferase genotypes and schizophrenia. Biol Psychiatry 64:739-749.

Floresco SB, Magyar O, Ghods-Sharifi S, Vexelman C, Tse MTL (2006) Multiple dopamine receptor subtypes in the medial prefrontal cortex of the rat regulate set-shifting. Neuropsychopharmacology 31:297-309.

Gee S, Ellwood I, Patel T, Luongo F, Deisseroth K, Sohal VS (2012) Synaptic activity unmasks dopamine D2 receptor modulation of a specific class of layer V pyramidal neurons in prefrontal cortex. J Neurosci 32:4959-4971.

Hnasko TS, Perez FA, Scouras AD, Stoll EA, Gale SD, Luquet S, Phillips PE, Kremer EJ, Palmiter RD (2006) Cre recombinase-mediated restoration of nigrostriatal dopamine in dopamine-deficient mice reverses hypophagia and bradykinesia. Proc Natl Acad Sci U S A 103:8858-8863.

Lammel S, Lim BK, Malenka RC (2014) Reward and aversion in a heterogeneous midbrain dopamine system. Neuropharmacology 76 Pt B:351-359.

Lammel S, Ion DI, Roeper J, Malenka RC (2011) Projection-specific modulation of dopamine neuron synapses by aversive and rewarding stimuli. Neuron 70:855-862.

Madhavan A, Argilli E, Bonci A, Whistler JL (2013) Loss of D2 dopamine receptor function modulates cocaine-induced glutamatergic synaptic potentiation in the ventral tegmental area. J Neurosci 33:12329-12336.

Major G, Polsky A, Denk W, Schiller J, Tank DW (2008) Spatiotemporally graded NMDA spike/plateau potentials in basal dendrites of neocortical pyramidal neurons. J Neurophysiol 99:2584-2601.

Milojkovic BA, Radojicic MS, Antic SD (2005) A strict correlation between dendritic and somatic plateau depolarizations in the rat prefrontal cortex pyramidal neurons. J Neurosci 25:3940-3951.

Minton GO, Young AH, McQuade R, Fairchild G, Ingram CD, Gartside SE (2009) Profound changes in dopaminergic neurotransmission in the prefrontal cortex in response to flattening of the diurnal glucocorticoid rhythm: implications for bipolar disorder. Neuropsychopharmacology 34:2265-2274.

Minzer K, Lee O, Hong JJ, Singer HS (2004) Increased prefrontal D2 protein in Tourette syndrome: a postmortem analysis of frontal cortex and striatum. J Neurol Sci 219:55-61.

Regard JB, Kataoka H, Cano DA, Camerer E, Yin L, Zheng YW, Scanlan TS, Hebrok M, Coughlin SR (2007) Probing cell type-specific functions of Gi in vivo identifies GPCR regulators of insulin secretion. J Clin Invest 117:4034-4043.

Schizophrenia Working Group of the Psychiatric Genomics Consortium (2014) Biological insights from 108 schizophrenia-associated genetic loci. Nature 511:421-427.

Schmitt LI, Wimmer RD, Nakajima M, Happ M, Mofakham S, Halassa MM (2017) Thalamic amplification of cortical connectivity sustains attentional control. Nature 545:219-223.

Seeman P (2002) Atypical antipsychotics: mechanism of action. Can J Psychiatry 47:27-38.

Seong HJ, Carter AG (2012) D1 receptor modulation of action potential firing in a subpopulation of layer 5 pyramidal neurons in the prefrontal cortex. J Neurosci 32:10516-10521.

Simonic I, Gericke GS, Ott J, Weber JL (1998) Identification of genetic markers associated with Gilles de la Tourette syndrome in an Afrikaner population. Am J Hum Genet 63:839-846.

Slifstein M, van de Giessen E, Van Snellenberg J, Thompson JL, Narendran R, Gil R, Hackett E, Girgis R, Ojeil N, Moore H, D'Souza D, Malison RT, Huang Y, Lim K, Nabulsi N, Carson RE, Lieberman JA, Abi-Dargham A (2015) Deficits in prefrontal cortical and extrastriatal dopamine release in schizophrenia: a positron emission tomographic functional magnetic resonance imaging study. JAMA Psychiatry 72:316-324.

St Onge JR, Abhari H, Floresco SB (2011) Dissociable contributions by prefrontal D1 and D2 receptors to risk-based decision making. J Neurosci 31:8625-8633.

Steeves TD, Ko JH, Kideckel DM, Rusjan P, Houle S, Sandor P, Lang AE, Strafella AP (2010) Extrastriatal dopaminergic dysfunction in tourette syndrome. Ann Neurol 67:170-181.

Tseng KY, Lewis BL, Lipska BK, O'Donnell P (2007) Post-pubertal disruption of medial prefrontal cortical dopamine-glutamate interactions in a developmental animal model of schizophrenia. Biol Psychiatry 62:730-738.

Urs NM, Gee SM, Pack TF, McCorvy JD, Evron T, Snyder JC, Yang X, Rodriguiz RM, Borrelli E, Wetsel WC, Jin J, Roth BL, O'Donnell P, Caron MG (2016) Distinct cortical and striatal actions of a beta-arrestin-biased dopamine D2 receptor ligand reveal unique antipsychotic-like properties. Proc Natl Acad Sci U S A 113:E8178-E8186.

Usiello A, Baik JH, Rouge-Pont F, Picetti R, Dierich A, LeMeur M, Piazza PV, Borrelli E (2000) Distinct functions of the two isoforms of dopamine D2 receptors. Nature 408:199-203.

Wang M, Vijayraghavan S, Goldman-Rakic PS (2004) Selective D2 receptor actions on the functional circuitry of working memory. Science 303:853-856.

Winterer G, Weinberger DR (2004) Genes, dopamine and cortical signal-to-noise ratio in schizophrenia. Trends Neurosci 27:683-690.

Yoon DY, Gause CD, Leckman JF, Singer HS (2007) Frontal dopaminergic abnormality in Tourette syndrome: a postmortem analysis. J Neurol Sci 255:50-56.

Zhang L, Yang H, Zhao H, Zhao C (2011) Calcium-related signaling pathways contributed to dopamine-induced cortical neuron apoptosis. Neurochem Int 58:281-294.

Zhang Y, Bertolino A, Fazio L, Blasi G, Rampino A, Romano R, Lee ML, Xiao T, Papp A, Wang D, Sadee W (2007) Polymorphisms in human dopamine D2 receptor gene affect gene expression, splicing, and neuronal activity during working memory. Proc Natl Acad Sci U S A 104:20552-20557.

CHAPTER III

Inducible expression of mutant human DISC1 in mice abolishes quinpirole-induced afterdepolarization in mPFC

Introduction

Schizophrenia is a debilitating psychiatric disorder affecting millions of individuals (Cloutier *et al.*, 2016). Patients with schizophrenia often experience a combination of 'positive' symptoms, including delusions and hallucination, 'negative' symptoms, including affective flattening and avolition , as well as cognitive impairments including deficits in working memory, cognitive flexibility, and executive functions (Meltzer, 1997; Evans *et al.*, 2004). The prefrontal cortex (PFC) has been shown to play a critical role in many of these cognitive functions impaired in schizophrenia (Druzin *et al.*, 2000; Floresco *et al.*, 2006; Durstewitz and Seamans, 2008). Many neurological disorders including schizophrenia have been associated with imbalances in dopamine neurotransmission (Winterer and Weinberger, 2004). It has been suggested that balance between dopamine D1 receptor (D1R) and dopamine D2 receptor (D2R) activation is crucial for optimizing the signal-to-noise ratio of local microcircuits and thereby normal PFC function (Winterer and Weinberger, 2004; Winterer *et al.*, 2004; Durstewitz and Seamans, 2008; Durstewitz *et al.*, 2010).

The dopamine hypothesis of schizophrenia theorizes that excessive D2R activation within the PFC contributes to many of the cognitive impairments associated with the disorder (Coyle *et al.*, 2012; Urs *et al.*, 2017). The two early cornerstones of this hypothesis were the findings that antipsychotic drugs block D2Rs and increase presynaptic dopamine metabolism and that dopamine-mimetics are psychotogenic (Seeman *et al.*, 1976; Beaulieu, Gainetdinov and Caron, 2009). Further studies have shown that infusion of D2R agonists and antagonists into the rodent PFC modulates cognitive functions disrupted in schizophrenia, including working memory and set-shifting (Druzin *et al.*, 2000; Floresco *et al.*, 2006; St Onge *et al.*, 2011). Current antipsychotics, however, are not effective at reversing cognitive deficits associated with schizophrenia. Improving our understanding of

how normal dopaminergic modulation is perturbed in schizophrenia, and other neuropsychiatric diseases, can aid in the development of safer and more effective drug therapies.

Transgenic animal models of psychiatric disease can be useful tools for dissecting the function of individual components of neurotransmitter systems and their contribution to aberrant behaviors (Gainetdinov *et al.*, 2001; Marcotte *et al.*, 2001). *Disrupted-in-Schizophrenia 1 (DISC1)* is a gene known as a risk factor for mental illness and has been associated with impairments in dopamine neuromodulation (Jacobs *et al.*, 1970). Several different DISC1 mutant animal models exhibit behavioral as well as neurochemical feature relevant to human schizophrenia pathologies (Su *et al.*, 2014; Dahoun *et al.*, 2017).

DISC1 is a scaffold protein which interacts with several other proteins in the dopamine system, including serine/threonine protein kinase B (Akt) and glycogen synthase kinase-3 (GSK-3). In DISC1 mouse models there is an upregulation of D2R expression in the mPFC and striatum altering typical D2R neuromodulation (Niwa *et al.*, 2013). Dopamine receptors are G protein-coupled receptors (GPCRs) and D2Rs are canonically thought to act via coupling to inhibitory G-proteins (G_i) and thereby acting to inhibit adenylate cyclase, reducing intercellular levels of cAMP and protein kinase A (PKA) activation (Bonci and Hopf, 2005). However, β-arrestin, normally involved in receptor internalization after prolonged activation, can also form a complex with D2R and initiate signaling cascades which are independent from the D2R-G-protein signaling pathway (Lefkowitz, 2013). Activation of this β-arrestin pathway by dopamine inactivates Akt by dephosphorylation resulting in activation of its negatively regulated substrate (Beaulieu *et al.*, 2005, 2007). Aripiprazole, a new generation antipsychotic acts as a biased agonist of the D2R pathway, partially agonizing G-protein signaling and antagonizing β-arrestin, suggesting that this non-canonical signaling pathway has a role in its antipsychotic effects (Urs *et al.*, 2016, 2017). Interestingly

the D2R-DISC1 complex has also been shown to contribute to the antipsychotic effects of D2R antagonists(Su *et al.*, 2014). DISC1 has also been shown to play important roles in regulating the cAMP pathway as well as Akt / GSK3 (El-Hassar *et al.*, 2014; Su *et al.*, 2014).

It is still not fully understood how D2Rs, G-proteins, β-arrestin, and DISC1 interact to modulate neuronal activity in response to dopamine or how these signaling complexes are impaired in schizophrenia. As discussed in chapter II, we have identified a new mechanism through which D2R activation can enhance excitability of pyramidal neurons in the PFC via pathways associated with G_s-, rather and G_i-, coupled proteins(Robinson and Sohal, 2017). We found that in layer 5 (L5) subcortical (SC) projection neurons, pharmacological activation of D2Rs by the agonist quinpirole elicits a profound afterdepolarization (ADP). Given that *DISC1* is a susceptibility gene for schizophrenia and other psychiatric disorders and that the DISC1-D2R complex has been shown to regulate other non-canonical D2R signaling pathways including cAMP and Akt / GSK3 pathways, we investigated the role of DISC1 in the quinpirole-induced afterdepolarization. In this chapter, I will present results that subcortically (SC) projecting D2R positive layer 5 (L5) pyramidal neurons in mice with a dominant-negative mutation in disrupted in schizophrenia 1 (DISC1) lack the G_i and β-arrestin independent quinpirole-induced afterdepolarization (ADP).

Materials and Methods

Animals

Control experiments were conducted using wild-type C57BL/6J mice (www.jax.org/strain/000664). DISC1 experimental animals were breed by crossing Tg(tetO-DISC1*)1001Plet/J transgenic mice (https://www.jax.org/strain/008790, Pletnikov *et al.*, 2008), which express a *myc* peptide-tagged, mutant (truncated) human *disrupted-in-schizophrenia 1 (DISC1)* gene under control of the tetracycline operator (tetO), with CaMKII-tTA transgenic mice (https://www.jax.org/strain/003010) expressing tetracycline-controlled transactivator protein (tTA) under regulatory control of the forebrain-specific calcium-calmodulin-dependent kinase II (CamkIIa) promoter thereby creating a bitransgenic animal expressing mutant *DISC1* in CamkIIa expressing neurons (**Fig. 1A**).

Electrophysiology

Electrophysiological recordings were performed as described in Chapter II, Materials and Methods, “Electrophysiology.” In brief, coronal mPFC slices were made from adult mice of either sex at post-natal day (P)56-70. Following 30 minutes incubation at 32°C in ACSF recording solution, slices were moved to room temperature. Whole-cell current clamp recordings were then performed in mPFC L5, using a K+-gluc-based internal solution as reported in Chapter II. Pyramidal neuron subtypes were identified based on characteristic firing patterns, specifically h-current-induced “sag” greater than 3mV in response to hyperpolarizing current pulses (Gee *et al.*, 2012). In some experiments, D2R expressing subcortically-projecting neurons were often identified by fluorescent visualization of retrograde tracer Alexafluor-tagged cholera toxin subunit B (Ctb) injected into the MD thalamus 3-5 days prior to electrophysiological experiments. All bath-applied drugs were dissolved in water (4 µM NMDA and 10 µM (-)quinpirole) before being diluted in ACSF.

CTb injection for retrograde tracing.

Injections were performed using standard mouse stereotactical methods. Mice were anesthetized for the duration of the surgery using isoflurane gas. After cleaning, an incision was made in the scalp, the skull was leveled, and small burr holes were drilled over the brain region of interest using a dental drill. Alexa Fluor 488 conjugated to cholera toxin subunit B (CTb-488) was injected through the burr holes into the mediodorsal (MD) thalamus using a microinjector at a speed of 150 nL/minute and the scalp was closed using tissue adhesive (Vetbond). MD thalamus injection coordinates were A/P = -1.7, M/L = +/- 0.3, D/V = -3.45. (**Fig. 1B**)

Experimental Design and Statistical Analysis

All data are shown as mean +/- 1 SEM. Statistical significance was accepted at the level $p < 0.05$. All statistical computations were performed using GraphPad Prism 7.0 software. We used student's t-test to compare pairs of groups if data were normally distributed (verified using Lillie test). If more than two groups were compared, we used ANOVA with post-hoc tests between groups corrected for multiple comparisons (Holm-Sidak or Bonferroni). The specific post-hoc test as well as exact F and corrected p values can be found in the text.

Results

DISC1 mutants have increased input resistance in layer 5 pyramidal neurons.

To investigate the function of *disrupted in schizophrenia 1 (DISC1*), we generated a bitransgenic mouse expressing a dominant-negative mutant human *DISC1* gene under control of the CaMKII promoter by utilizing the Tet-off expression system and a crossing a transgenic animal with inducible expression of the mutant human *DISC1* gene (Pletnikov *et al.*, 2008) and a transgenic animal expressing tTA under regulatory control of CaMKII (**Fig. 1A**).

Since the DISC1-D2R complex has been strongly implicated in schizophrenia, we wanted to investigate the role of DISC1 in dopamine D2 receptor (D2R) expressing neurons within the mPFC. We took advantage of the fact that in deep layers of the mPFC, D2Rs are mainly expressed by subcortical (SC) projection neurons, and injected a retrogradely transported fluorescent tracer (Alexa Fluor 488 conjugated cholera toxin subunit B; CTb-488) into the mediodorsal (MD) thalamus at P52-67 to label SC projection neurons and therefore putative mPFC D2R+ neurons. Then, 3 to 5 days after injection, we performed whole-cell current-clamp recordings, measuring their voltage responses to a series of hyperpolarizing and depolarizing pulses (250 msec duration) from L5 mPFC SC-projecting neurons identified by Ctb-488 fluorescence (**Fig. 1B**).

D2R+ pyramidal neurons can also be identified based on their prominent hyperpolarization-activated cation currents (Ih), which are mediated by hyperpolarization-activated cyclic nucleotide-gated (HCN) channels (Gee *et al.*, 2012; Clarkson *et al.*, 2017). In D2R+ neurons, Ih gives rise to a characteristic “sag” and rebound during and following hyperpolarizing current injection. We first estimated Ih by measuring the membrane potential sag and rebound elicited by a –250 pA current step (**Fig. 1C**) confirming this characteristic sag and rebound property in SC projection neurons labeled by Ctb-488. For

wildtype C57BL/6 and CaMKII::DISC1 mice, there was no difference in this estimate for Ih in SC projection neurons (**Fig. 1G**: n = 9/10, C56BL6/CaMKII::DISC1; unpaired t-test: $t_{(17)}$ = 0.04, n.s.). We also characterized other intrinsic electrophysiological properties in Ctb-488+ L5 pyramidal neurons within mPFC. We found no difference in resting membrane potential between neurons from wildtype and CaMKII::DISC1 mice (**Fig. 1D**: n = 9/10, C56BL/6 /CaMKII::DISC1; unpaired t-test: $t_{(17)}$ = 0.06, n.s.) but did observe an increase in input resistance when subjected to a −50 pA current pulse in L5 SC projection neurons from CaMKII::DISC1 mice (**Fig. 1E**: n = 9/10, C56BL6/CaMKII::DISC1; unpaired t-test: $t_{(17)}$ = 3.01, p =0.0079).

***DISC1* mutants lack the quinpirole-induced ADP.**

As previous shown in Chapter II of this dissertation, D2R activation elicits afterdepolarizations (ADPs) in this population of SC-projecting pyramidal neurons within L5 of the mPFC. These D2R-induced ADPs only occur following synaptic input which activates NMDA receptors (NMDARs) (Gee *et al.*, 2012; Robinson and Sohal, 2017). To investigate whether mutant DISC1 disrupts this D2R-dependent ADP, we analyzed the neurons voltage responses to depolarizing current pulses (+400pA, 250 msec duration). To quantify the ADP, we measured the amount of time required for the membrane potential to return to baseline following the depolarizing current pulse (more precisely, the time for 90% decay). In C57BL/6 wildtype mice we confirmed that ADPs are absent following depolarizing current pulses in ACSF or the presence of just NMDA (4 μM), however, following the addition of the D2R agonist (-)quinpirole (10 μM) to the bath, we observed a robust ADP for ~100-300 msec after the end of each depolarizing current pulse (**Fig. 1C(top), F**: C57BL/6 n = 8, baseline / NMDA / QPL; Oneway ANOVA, $F_{(3,21)}$ =45.3, p < 0.0001; t-test, Tukey correction, baseline vs QPL: $q_{(14)}$ = 11.83, p < 0.0001, NMDA vs QPL: $t_{(14)}$ = 11.47, p < 0.0001). The

time for 90% decay back to baseline following the depolarizing current pulse is not statistically different between C57BL/6 wildtype and CaMKII::DISC1 mice in either control ACSF (**Fig. 1F**: n = 8/10, C56BL6/CaMKII::DISC1; unpaired t-test: $t_{(16)} = 1.773$, n.s.) or NMDA (**Fig. 1F**: n = 8/6, C56BL6/CaMKII::DISC1; unpaired t-test: $t_{(12)} = 1.909$, n.s.). However, in CaMKII::DISC1 mice, the quinpirole-induced ADP is completely abolished (**Fig. 1F**: CaMKII::DISC1 n = 7, baseline / NMDA / QPL; Oneway ANOVA, $F_{(3,21)} = 2.397$, n.s.; n = 8/7, C56BL6/CaMKII::DISC1; unpaired t-test: $t_{(13)} = 6.32$, $p < 0.0001$), suggesting that the normal DISC1 function is necessary for the quinpirole-induced ADP.

Discussion

Here we follow up our earlier work (Gee *et al.*, 2012; Robinson and Sohal, 2017), which described a new mechanism through which dopamine D2 receptor (D2R) activation could elicit an increase in excitability, specifically an ADP, within subcortically projecting L5 pyramidal neurons in the mPFC by stimulating cAMP / PKA signaling that is downstream of G_s (Chapter II, Figure 7).

As discussed in Chapter II of this dissertation, D2R mediated signaling is diverse and the results presented in Chapter II only serve to enlarge the family of possible signaling pathways downstream of D2R activation. The work presented in both this chapter and Chapter II, focus on cellular physiology and do not elucidate the molecular or biochemical details of this pathway. Many recent studies suggest that D2Rs exist in heterogeneous forms, which may explain how D2Rs can couple to various intercellular signaling pathways, giving rise to distinct effect on neuronal excitability, in different neuronal populations. Disrupted-in-schizophrenia 1 (DISC1) is a scaffolding protein known to complex with D2R. Recent studies suggest important roles for this D2R-DISC1 complex in regulation of β-arrestin binding and internalization of the D2R as well as regulation of downstream signaling pathway including cAMP and Akt / GSK3. It will be interesting for future studies to characterize the D2R-DISC1 complex and the molecular mechanisms of its regulatory role on D2R intracellular signaling pathways.

Clinical Implications

Dysfunction of the dopamine system is heavily implicated in schizophrenia. Although the precise nature of such dysfunction remains unclear, many studies raise the possibility that prefrontal D2R function specifically may be abnormal in schizophrenia: mutations in D2Rs are associated with schizophrenia (Schizophrenia Working Group of the Psychiatric

Genomics Consortium, 2014), all known clinically effective antipsychotics block D2Rs (Seeman, 2002), and D2R agonists and antagonists modulate several cognitive functions disrupted in schizophrenia(Druzin *et al.*, 2000; Floresco *et al.*, 2006a; St Onge, Abhari and Floresco, 2011).

An Interesting line of future investigation involves studying the impact of this novel mechanism for D2R-dependent enhancement of layer 5 mPFC excitability on performance during PFC-dependent behavioral tasks. In vivo cannula infusion of CNO into the mPFC of awake behaving mice injected with G_s-DREADD (AAV5-hSyn-DIO-rM3D(Gs)-mCherry) could mimic the quinpirole-induced ADP providing a mechanism for investigating the impact of this novel mechanism. While recent concerns have been raised regarding CNO being metabolized to clozapine, this is unlikely to occur over the time course of slice experiments and can be accounted for in behavior experiments with a CNO control group of uninjected animals(Smith *et al.*, 2016; Gomez *et al.*, 2017). It would be interesting to determine whether CNO paired with synaptic stimulation can elicit an ADP in CamKII::DISC1 mice injected with G_s-DREADD indicating whether DISC1 acts up or downstream of G_s. DISC1 mice have already been shown to have deficits in social interaction and behavioral flexibility. An interesting set of experiments would be to attempt to rescue performance during PFC-dependent behavior tasks by induction of the D2R/G_s-mediated ADP in CaMKII::DISC1 mice.

Improving our understanding of the D2R signaling mechanisms which are altered in schizophrenia will provide great insight aiding in the development of new and improved therapies to treat the symptoms of cognitive dysfunction with fewer adverse side effects.

Conclusion

Dopamine D2 receptors can enhance the excitability of subcortically-projecting pyramidal neurons in layer 5 of medial prefrontal cortex through a pathway that depends on

These results show that this unusual physiological phenomenon, in which D2Rs enhance cellular excitability in a manner that depends on synaptic input and is mediated through G_s associated signaling pathways is disrupted in at least one DISC1 mouse model of schizophrenia. As better models for schizophrenia are developed, it will be interesting to study whether this unusual form of prefrontal D2R signaling is also altered. Important next steps will be understanding how this phenomena contributes to normal brain function and is disrupted in other models of schizophrenia or psychiatric disease.

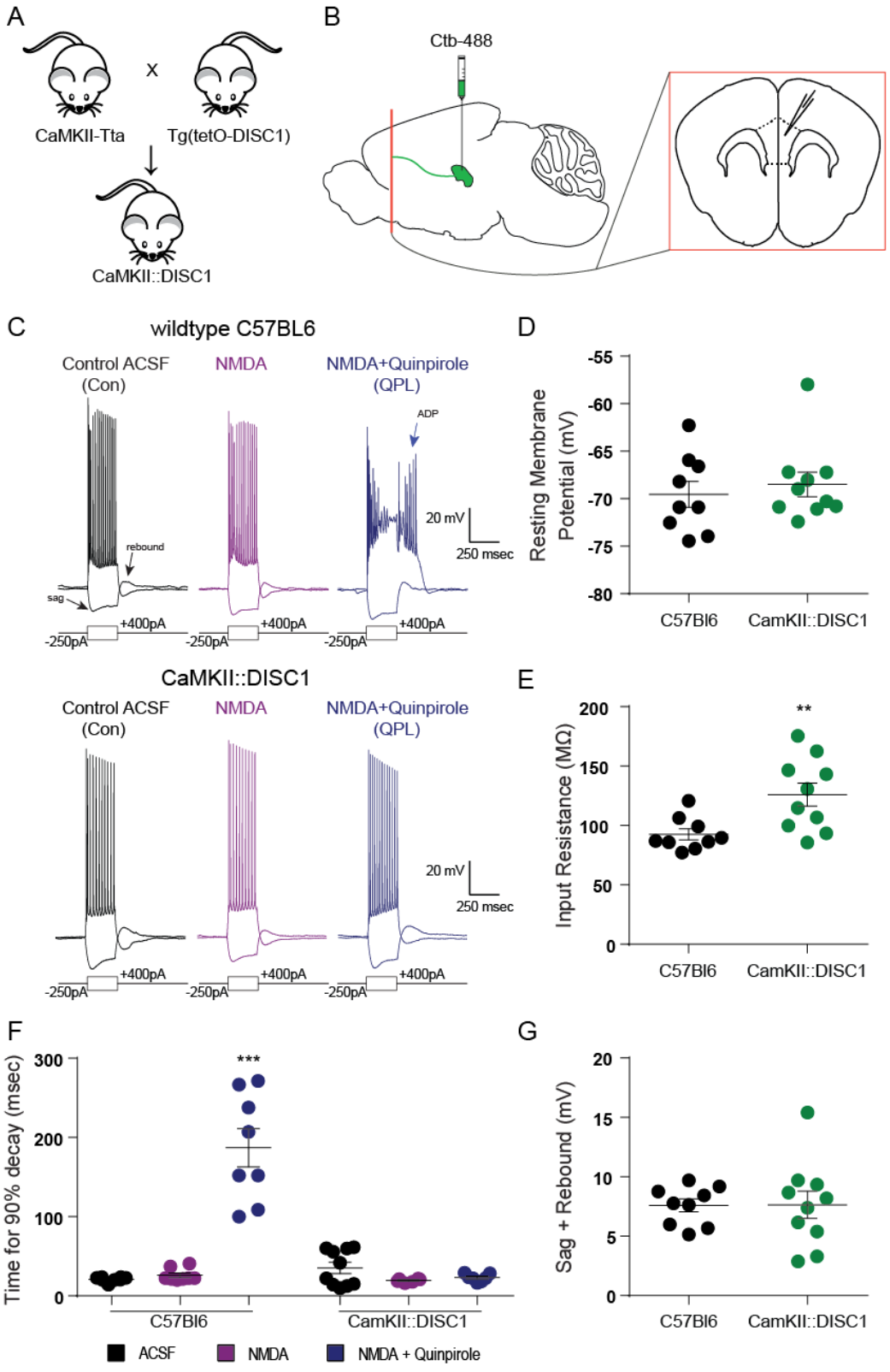

Figure 1. L5 mPFC neurons from *DISC1* mutants have increased input resistance and lack the quinpirole-induced ADP.

A) Experimental design: We crossed Tg(tetO-DISC1) mice to CaMKII-tTA mice to drive expression of inducible mutant human *DISC1* under control of the CaMKII promoter. **B)** We injected offspring in the mediodorsal thalamus with Ctb-488 to identify SC-projecting pyramidal neurons within the mPFC. 3 to 5 days later we recorded from Ctb-488+ pyramidal neurons in L5 of mPFC. **C)** Example pyramidal cell responses to hyperpolarizing (-250pA) and depolarizing (+400pA) current steps at baseline (black) and after application of drug (4 µM NMDA, purple; 4 µM NMDA + 10 µM Quinpirole, blue) in wildtype C57BL/6 mice (top) and CaMKII::DISC1 mice (bottom). Blue arrow indicates the quinpirole-induced afterdepolarization (ADP). **D-G)** Intrinsic electrophysiological properties determined by whole-cell patch clamp recordings from SC-projecting layer 5 mPFC at P56-70 show that expression of dominant-negative mutant human *DISC1* results in an increased input resistance **(E)**, but does not alter resting membrane potential **(D)**, or current through HCN channels as indicated by sag and rebound **(G)**. This characteristic “sag” and “rebound” during and following hyperpolarizing current (-250pA) injection is mediated by hyperpolarization-activated cyclic nucleotide-gated (HCN) channels. **F)** CaMKII::DISC1 mice lack the quinpirole-induced ADP characteristic of normal D2R+ L5 mPFC pyramidal neurons, quantified by the amount of time required for the membrane potential to return to baseline following the depolarizing current pulse (more precisely, the time for 90% decay), after pharmacological manipulations listed above. **p = 0.0079. ***p < 0.0001.

References

Beaulieu, J.-M. *et al.* (2005) 'An Akt/beta-arrestin 2/PP2A signaling complex mediates dopaminergic neurotransmission and behavior.', *Cell*, 122(2), pp. 261–73.

Beaulieu, J.-M. *et al.* (2007) 'Regulation of Akt signaling by D2 and D3 dopamine receptors in vivo.', *The Journal of neuroscience : the official journal of the Society for Neuroscience*, 27(4), pp. 881–5.

Beaulieu, J.-M., Gainetdinov, R. R. and Caron, M. G. (2009) 'Akt/GSK3 signaling in the action of psychotropic drugs.', *Annual review of pharmacology and toxicology*, 49, pp. 327–47.

Bonci, A. and Hopf, F. W. (2005) 'The dopamine D2 receptor: new surprises from an old friend.', *Neuron*, 47(3), pp. 335–8.

Clarkson, R. L. *et al.* (2017) 'D3 Receptors Regulate Excitability in a Unique Class of Prefrontal Pyramidal Cells.', *The Journal of neuroscience : the official journal of the Society for Neuroscience*, 37(24), pp. 5846–5860.

Cloutier, M. *et al.* (2016) 'The Economic Burden of Schizophrenia in the United States in 2013', *The Journal of Clinical Psychiatry*, 77(6), pp. 764–771.

Coyle, J. T. *et al.* (2012) 'Novel Antischizophrenia Treatments'. Edited by M. A. Geyer and G. Gross. Berlin, Heidelberg: Springer Berlin Heidelberg (Handbook of Experimental Pharmacology), 213, pp. 267–295.

Dahoun, T. *et al.* (2017) 'The impact of Disrupted-in-Schizophrenia 1 (DISC1) on the dopaminergic system: a systematic review', *Translational Psychiatry*, 7(1), p. e1015.

Druzin, M. Y. *et al.* (2000) 'The effects of local application of D2 selective dopaminergic drugs into the medial prefrontal cortex of rats in a delayed spatial choice task.', *Behavioural brain research*, 109(1), pp. 99–111.

Durstewitz, D. *et al.* (2010) 'Abrupt Transitions between Prefrontal Neural Ensemble States Accompany Behavioral Transitions during Rule Learning', *Neuron*, 66(3), pp. 438–448.

Durstewitz, D. and Seamans, J. K. (2008) 'The Dual-State Theory of Prefrontal Cortex Dopamine Function with Relevance to Catechol-O-Methyltransferase Genotypes and Schizophrenia', *Biological Psychiatry*, 64(9), pp. 739–749.

El-Hassar, L. *et al.* (2014) 'Disrupted in schizophrenia 1 modulates medial prefrontal cortex pyramidal neuron activity through cAMP regulation of transient receptor potential C and small-conductance k(+) channels.', *Biological psychiatry*. Elsevier, 76(6), pp. 476–85.

Evans, J. D. *et al.* (2004) 'Cognitive and clinical predictors of success in vocational rehabilitation in schizophrenia.', *Schizophrenia research*, 70(2–3), pp. 331–42.

Floresco, S. B. *et al.* (2006a) 'Multiple Dopamine Receptor Subtypes in the Medial Prefrontal Cortex of the Rat Regulate Set-Shifting', *Neuropsychopharmacology*, 31(2), pp. 297–309.

Floresco, S. B. *et al.* (2006b) 'Multiple dopamine receptor subtypes in the medial prefrontal cortex of the rat regulate set-shifting.', *Neuropsychopharmacology : official publication of the American College of Neuropsychopharmacology*, 31(2), pp. 297–309.

Gainetdinov, R. R., Mohn, A. R. and Caron, M. G. (2001) 'Genetic animal models: focus on schizophrenia', *TRENDS in Neurosciences*, 24(9), pp. 527–533.

Gee, S. *et al.* (2012) 'Synaptic activity unmasks dopamine D2 receptor modulation of a specific class of layer V pyramidal neurons in prefrontal cortex.', *The Journal of neuroscience*, 32(14), pp. 4959–71.

Gomez, J. L. *et al.* (2017) 'Chemogenetics revealed: DREADD occupancy and activation via converted clozapine.', *Science (New York, N.Y.)*. American Association for the Advancement of Science, 357(6350), pp. 503–507.

Jacobs, PA; Brunton, M; Frackiewicz, A; Newton, M; Cook, PJL; Robson, E. (1970) 'Studies on a family with three cytogenetic markers.', *Annals of Human Genetics*, 33, pp. 325–336.

Lefkowitz, R. J. (2013) *Arrestins come of age: a personal historical perspective.* 1st edn, *Progress in molecular biology and translational science*. 1st edn. Elsevier Inc.

Marcotte, E. R., Pearson, D. M. and Srivastava, L. K. (2001) 'Animal models of schizophrenia: a critical review.', *Journal of psychiatry & neuroscience : JPN*. Canadian Medical Association, 26(5), pp. 395–410.

Meltzer, H. Y. (1997) 'Treatment-Resistant Schizophrenia - The Role of Clozapine', *Current Medical Research and Opinion*, 14(1), pp. 1–20.

Niwa, M. *et al.* (2013) 'Adolescent Stress-Induced Epigenetic Control of Dopaminergic Neurons via Glucocorticoids', *Science*, 339(6117), pp. 335–339.

Pletnikov, M. V *et al.* (2008) 'Inducible expression of mutant human DISC1 in mice is associated with brain and behavioral abnormalities reminiscent of schizophrenia.', *Molecular psychiatry*, 13(2), pp. 173–86, 115.

Robinson, S. E. and Sohal, V. S. (2017) 'Dopamine D2 Receptors Modulate Pyramidal Neurons in Mouse Medial Prefrontal Cortex through a Stimulatory G-Protein Pathway', *The Journal of Neuroscience*, 37(42), pp. 10063–10073.

Schizophrenia Working Group of the Psychiatric Genomics Consortium (2014) 'Biological insights from 108 schizophrenia-associated genetic loci', *Nature*, 511(7510), pp. 421–427.

Seeman, P. *et al.* (1976) 'Antipsychotic drug doses and neuroleptic/dopamine receptors.', *Nature*, 261(5562), pp. 717–9.

Seeman, P. (2002) ‘Atypical antipsychotics: mechanism of action.’, *Canadian journal of psychiatry. Revue canadienne de psychiatrie*, 47(1), pp. 27–38.

Smith, K. S. *et al.* (2016) ‘DREADDs: Use and Application in Behavioral Neuroscience’, *Behavioral neuroscience*, 130(2), pp. 137–155.

St Onge, J. R., Abhari, H. and Floresco, S. B. (2011) ‘Dissociable contributions by prefrontal d1 and d2 receptors to risk-based decision making.’, *The Journal of neuroscience : the official journal of the Society for Neuroscience*, 31(23), pp. 8625–33.

Su, P. *et al.* (2014) ‘A Dopamine D2 Receptor-DISC1 Protein Complex may Contribute to Antipsychotic-Like Effects’, *Neuron*, 84(6), pp. 1302–1316.

Urs, Nikhil M.; Peterson, Sean M.; Caron, M. G. (2017) ‘New Concepts in Dopamine D2 Receptor Biased Signaling and Implications for Schizophrenia Therapy’, *Biological Psychiatry*. Elsevier, 81(1), pp. 78–85.

Urs, N. M. *et al.* (2016) ‘Distinct cortical and striatal actions of a β-arrestin-biased dopamine D2 receptor ligand reveal unique antipsychotic-like properties.’, *Proceedings of the National Academy of Sciences of the United States of America*. National Academy of Sciences, 113(50), pp. E8178–E8186.

Winterer, G. *et al.* (2004) ‘Prefrontal Broadband Noise, Working Memory, and Genetic Risk for Schizophrenia’, *American Journal of Psychiatry*. American Psychiatric Publishing, 161(3), pp. 490–500.

Winterer, G. and Weinberger, D. R. (2004) ‘Genes, dopamine and cortical signal-to-noise ratio in schizophrenia.’, *Trends in neurosciences*, 27(11), pp. 683–90.

CHAPTER IV

Functional importance of *Tbr1* during later stages of cortical development

Introduction

The cortical circuits have central roles in brain functions (Rakic, 2009). While cortical evolution has endowed the human brain with robust computing abilities, these advances in cortical structure and its circuitry may have increased susceptibility to neuropsychiatric disorders (Johnson et al., 2009). Thus, elucidating the genetic underpinnings of cortical development and function are essential in understanding human disorders such as Autism Spectrum Disorders (ASDs).

Autism Spectrum Disorders (ASDs) are defined by impairments in reciprocal social interaction, often accompanied by abnormalities in language development as well as repetitive behaviors and/or restricted interests. Currently, several hundred genes are implicated in ASD risk, based on *de novo* copy-number variations or *de novo* point mutations (De Rubeis et al., 2014; Iossifov et al., 2014; Willsey et al., 2013). Thus, emerging biological insights from genetic and imaging studies have provided evidence that abnormal cortical development underlies at least some forms of ASD (Minshew & Keller, 2010; Willsey et al., 2013).

Cortical development requires the coordinated execution of a series of developmental processes, including regional and areal specification (Rash & Grove, 2006), the specification of neuronal and glia identity (Leone et al., 2008; Molyneaux et al., 2007), cell migration (Kwan et al., 2012), and wiring of neural circuits (De la Rossa et al., 2013). System analysis of co-expression networks of high-confidence ASD genes (hcASD) provided evidence that several of these genes are expressed in immature layer 5 and 6 cortical projection neurons (Willsey et al., 2013). This has provided a strong rationale for studying the function of these ASD genes in cortical development. Among the list of hcASD genes whose expression converges during development of deep cortical layers, several of the genes are already known to regulate mouse cortical development, including *Tbr1*,

Foxp1, and *Bcl11a* (Cánovas et al., 2015; De Rubeis et al., 2014; Dias et al., 2016; Dwyer & O'Leary, 2001; Han et al., 2011; Hisaoka et al., 2010; Huang et al., 2014; Iossifov et al., 2014; Sanders et al., 2012; Willsey et al., 2013). Here we have focused our work on defining the function of *Tbr1* on the earliest-born cortical projection neurons of layer 6 and the subplate using conditional mutagenesis.

T-brain-1 (Tbr1), a T-box transcription factor (TF), was the first gene shown to regulate development of early-born pallial projection neurons, including Cajal Retzius cells, subplate cells and layer 6 projection neurons (Bedogni et al., 2010; Bulfone et al., 1995; Hevner et al., 2001). In the telencephalon *Tbr1* is expressed (beginning ~E10.5) only in postmitotic differentiating cortical projection neurons, and turns on following *Tbr2* expression in the subventricular zone (Bulfone et al., 1995; Díaz-Alonso et al., 2015; Hevner et al., 2002; Hevner et al., 2003; Hevner et al., 2001; Vasistha et al., 2015). *Tbr1* is expressed in the excitatory neurons of the neocortex (subplate, layer 6, rostral layer 5, layers 2/3), hippocampus, entorhinal cortex, pallial amygdala, piriform cortex, olfactory bulb and Cajal Retzius neurons (Hevner et al., 2003; Hevner et al., 2001). Analysis of *Tbr1* constitutive null (*Tbr1*$^{constitutive\ null}$) mice showed that it regulates layer 6 identity and the growth of their corticothalamic axons to the thalamus (Bedogni et al., 2010; Bulfone et al., 1998; Hevner et al., 2002). *Tbr1* promotes the identity of layer 6 neurons by repressing the *Fezf2* and *Bcl11b* TFs that promote layer 5 fate with subcerebral projections (McKenna et al., 2011). *Tbr1*$^{constitutive\ null}$ also have defects in cortical arealization (Bedogni et al., 2010; Hevner et al., 2001). Thus, early *Tbr1* expression regulates neural fate in which the mutant has defects in molecular specification, neural lamination, and cortical connectivity with the thalamus (Alfano et al., 2014; Hevner et al., 2002; Hevner et al., 2001; McKenna et al., 2011; Mihalas & Hevner, 2017; Remedios et al., 2007). Most *Tbr1*$^{constitutive\ null}$ mice die at birth. TBR1 molecular functions are beginning to be elucidated. For instance TBR1 protein

interacts with the CASK (calcium/calmodulin dependent serine protein kinase) (Wang et al., 2004). The CASK-TBR1 complex promotes *Grin2b* transcription by directly binding to its promoter (Chuang, Huang, & Hsueh, 2014). *Tbr1* promotes expression of many other genes, including those that encode regulators of cell adhesion and synaptogenesis including *Cdh8, Cntn2, Ntng1* and *Wnt7b* (Huang et al., 2014).

While neocortical development appears normal in $Tbr1^{constitutive\ heterozygous}$ mice, parts of their pallial amygdala are abnormal. They have abnormal inter- and intra-amygdalar axonal projections, reduced NMDAR expression and the central nucleus of amygdala is particularly susceptible to *Tbr1* haploinsufficiency (Chuang, Huang, & Hsueh, 2015; Huang et al., 2014). The reduced NMDAR may be due to *Tbr1* driving expression of the NMDAR subunit *Grin2b* (Chuang et al., 2014). These studies provide evidence that reduced *Tbr1* dosage lead to abnormal brain wiring and excitation/inhibition imbalance (NMDAR hypo-activity), two prominent models for ASD etiology (Canitano & Pallagrosi, 2017; Chuang et al., 2014; Huang et al., 2014; Rubenstein, 2010, 2011; Rubenstein & Merzenich, 2003). This is particularly important, as ASD patients with mutations in hcASD genes are typically heterozygous.

Recurrent *de novo* disruptive mutations in the *TBR1* gene have been found in patients with ASDs (De Rubeis et al., 2014; Sanders et al., 2012; Willsey et al., 2013). *De novo* truncating and missense mutations impairs TBR1's subcellular localization and transcriptional repression (Deriziotis et al., 2014). Furthermore, TBR1 interacts with FOXP2 (Deriziotis et al., 2014), a transcription factor that is implicated in cortical development (Tsui et al., 2013) and speech/language disorders (Huang & Hsueh, 2017). ChIP-Seq, transcriptomic and computational analyses of TBR1 provided strong evidence that TBR1 regulates expression of multiple ASD risk genes (Notwell et al., 2016).

Given the complex spatio-temporal pattern of *Tbr1* expression, we focused on its function in deep neocortical neurons using Cre-lox conditional mutagenesis by creating a *Tbr1*^{layer6} and a *Tbr1*^{layer5} mutant. Furthermore, we focused on its function beginning around the day of birth, nearly 10 days after the onset of its expression. We did not eliminate its expression in Cajal Retzius and thereby did not cause a radial migration/lamination defect. Both the *Tbr1*^{layer5} and *Tbr1*^{layer6} mutants are viable enabling the analysis of cortical physiology and behavior. We found that late gestation/neonatal *Tbr1* function is required to maintain many aspects layer 6 identity.

The *Tbr1*^{layer6} mutant neurons transformed towards identity of layer 5 neurons, which include their transcriptome, their dendritic pattern and physiology. Previous studies have shown that different prefrontal pyramidal cell classes express varying degrees of hyperpolarizing-activated cyclic nucleotide-gated (HCN) channels (Dembrow *et al.*, 2010; Gee *et al.*, 2012; Seong and Carter, 2012). Quantification of the current through HCN channels, h-current (I_h), can be used to distinguish dopamine D2 receptor (D2R) expressing neuron within the pre-frontal cortex (Clarkson *et al.*, 2017). While layer 5 pyramidal neurons are of heterogeneous populations with various degrees of h-current, layer 6 pyramidal neurons classically lack h-current. The *Tbr1*^{layer6} mutant neurons had reduced excitatory and inhibitory synaptic density. Importantly, the physiological and synaptic phenotypes were also seen in *Tbr1*^{layer6} heterozygous. We found that this reduction in excitatory and inhibitory synapse density functionally translates into reduced spontaneous EPSCs and IPSCs in mouse brain slices.

RNA-seq of FACS purified layer 5 neurons from the *Tbr1*^{layer5} mutants did not show Tbr1 as a differentially regulated gene (data not shown). This is likely due to the heterogeneous nature of L5 cortical neurons (Clarkson *et al.,* 2017; Dembrow *et al.*, 2010). A more precise analysis of differential gene regulation in *Tbr1*^{layer5} mutant neurons could be

obtained by performing single-cell RNA-seq. Interestingly, electrophysiological properties of the *Tbr1*^{layer5} mutant neurons suggest a homogenization of the L5 population towards prominent h-current suggestive of D2Rpositive neuron identity (Clarkson *et al.,* 2017). The *Tbr1*^{layer5} mutant neurons also had reduced excitatory and inhibitory synaptic density. We found that this reduction in excitatory and inhibitory synapse density functionally translates into reduced spontaneous EPSCs and IPSCs in mouse brain slices.

In the present study, we have demonstrated the neurobiology behind *Tbr1* loss of function in layer 5 and layer 6 glutamatergic neurons as a part of a concerted effort to understand the neurobiology of Autism Spectrum Disorder (ASD) mutations. ASD is characterized by severe and sustained impairment in social communication and interactions. Humans with ASD also suffer from a range of additional behavior problems, including anxiety, compulsive behaviors, and aggression (Gadow *et al.*, 2004; McClintock *et al.,* 2003). We have also discovered that loss of *Tbr1* function in layer 5 leads to a pronounced decrease in social behaviors consistent with ASD associated behaviors. Interestingly, loss of function of *Tbr1I* in layer 6 does not reduce social interaction but instead leads to increased anxiety and aggressive behavior. Aggressive behaviors are commonly observed in individuals diagnosed with autism spectrum disorder (ASD) and may be a phenotypic indicator of different subtypes within ASD. Interestingly, loss of function mutations of *Tbr1* in layer 5 versus layer 6 have differential impacts on behavioral outcomes.

Materials and Methods

Animals

The *Tbr1*^{flox} allele was generated by inGenious Targeting Laboratory (Ronkonkoma, NY). LoxP sites were inserted into introns 1 and 3, flanking *Tbr1* exons 2 and 3 (Fig. 1A). To enable selection of homologous recombinants, the LoxP site in intron 3 was embedded in a *neo* cassette that was flanked by *Flp* sites. The *neo* cassette was removed by mating to a *Flp*-expressing mouse (Rodriguez et al., 2000) to generate the *Tbr1*^{flox} allele. Cre excision removes exons 2 and 3, including the T-box DNA binding region, similar to the constitutive null allele (Bulfone et al., 1998). *Ntsr1-cre* mice were used to delete *Tbr1* in layer 6 projection neurons. *tdTomato*$^{fl/+}$ (*Ai14*) mice were crossed with *Tbr1*$^{f/f}$ mice and used as an endogenous reporter. *Tbr1* layer 6 knockout mice (*Tbr1*^{layer6} mutant) were generated by crossing *Tbr1*$^{f/f}$*::tdTomato*$^{f/+}$ mice with *Tbr1*$^{f/+}$*::Ntsr1-cre*$^{+}$. *Rbp4-cre* mice were used to delete *Tbr1* in layer 5 projection neurons. *tdTomato*$^{fl/+}$ (*Ai14*) mice were crossed with *Tbr1*$^{f/f}$ mice and used as an endogenous reporter. *Tbr1* layer 5 knockout mice (*Tbr1*^{layer5} mutant) were generated by crossing *Tbr1*$^{f/f}$*::tdTomato*$^{f/+}$ mice with *Tbr1*$^{f/+}$*::Rbp4-cre*$^{+}$. All strains were maintained on a C57Bl/6 background. Animals were housed in a vivarium with a 12hr light, 12hr dark cycle. Postnatally, experimental animals were kept with their littermates.

For timed pregnancies, noon on the day of the vaginal plug was counted as embryonic day 0.5. Animal care and procedures were performed according to the University of California San Francisco Laboratory Animal Research Center (LARC) guidelines.

Genomic DNA extraction and genotyping

Tissue samples were digested in a solution containing 1 mg/mL of proteinase K, 50 mM Tris-HCl pH 8.0, 100 mM EDTA, 100 mM NaCl and 1% SDS. Genomic DNA was extracted using a standard ethanol precipitation protocol. Genotyping was performed with PCR-based

assays using purified genomic DNA, and various primer-pair combinations flanking the deleted region and detecting *Cre* and *tdTomato* alleles.

RNA extraction and cDNA synthesis

Total RNA was extracted from the cortices of wildtype and *Tbr1* constitutive null mice at E15.5 and P0 using RNeasy Plus® Mini Kit (QIAGEN) following the manufacturer's protocol. First strand cDNA was synthesized using Superscript reverse transcriptase II following manufacturer's protocol (Thermofisher).

Quantitative real time PCR (qRT-PCR)

Quantitative RT-PCR was performed to measure RNA levels using SYBR Green (Bio-Rad) and 7900HT Fast Real-Time PCR System. Gene-specific primers for *Tbr1* exons 1, 2 and 4, *Bcl11a*, *Grin2b* and *Hcn1* as well as ***ef1α*** housekeeping genes (HKG) were designed using the Primer 3 program (Rozen & Skaletsky, 1999). The expression levels of the genes in both wildtype and *Tbr1* mutant mice were normalized to the expression levels of ***ef1α***. Subsequently, the gene expression levels in *Tbr1* mutant mice were measured relative to the wildtype littermates (Darbandi & Franck, 2009; Pfaffl, 2001).

Western blot

Cortices of 2 *Tbr1* constitutive null and 2 wildtype brains were dissected at E15.5 and P0 in ice-cold PBS. Tissues were homogenized in 300 μL ice-cold RIPA lysis buffer. Following an incubation at 4°C for 2 hrs with agitation, the samples were centrifuged at 13,500 rpm for 20 min at 4°C. 20-30 μg total protein was combined with Laemmli buffer supplemented with 1:20 β-mercaptoethanol and was heat to 95°C for 5 min. The protein

lysate was electrophoresed using Mini-PROTEIN®TGX 4-20% precasted gels (Bio-Rad) and ran for 1-2 hrs at 100V. The fractionated proteins were transferred to a nitrocellulose membrane (GE Amersham Protran). The membrane was blocked with 7.5% nonfat dried milk, washed 3X with 1X PBS with 0.1% Tween-20, and then was incubated for 12 hrs with the primary antibody at 4°C. The following day, the membrane was washed 3X with 1X PBS with 0.1% Tween-20, incubated with the Goat Anti-Rabbit-HRP secondary for 1 hr. Signals were detected using a DAB system (Vector Laboratories) following manufacturer's protocol.

RNA-seq on FAC-Sorted Cells

Layer specific transcriptome profiling was conducted by using RNA-seq on FAC-Sorted cells from somatosensory cortex of *Tbr1*^{wildtype}, *Tbr1*^{layer5}*, and Tbr1*^{layer6} mutants. The somatosensory cortex was dissected in HBSS from P5 mice (Thermofisher). Cortices were dissociated using a Papain Dissociation System (Worthington Biochemical Corporation) following manufacturer's protocol. tdTomato^{+} cells were sorted using BD FACS Aria II Cell Sorter at Center for Advanced Technology (UCSF). Approximately 25,000 cells were collected from each sample and immediately proceeded with RNA extraction using RNeasy® Plus Micro Kit (QIAGEN) following manufacturer's protocol. RNA quality was assessed using Agilent RNA 6000 Nano Kit (Agilent Technologies) and ran on Bioanalyzer 2100 (Agilent Technologies). RNA-seq libraries were generated by TruSeq® Stranded Total RNA Library Prep Kit with Ribo-Zero Gold Set A (Illumina). The quality of the libraries was assessed using Bioanalyzer 2100 (Agilent Technologies) and Agilent High Sensitivity DNA Kit (Agilent Technologies) following manufacturer's protocol. Libraries were validated using qPCR and sequenced on Hiseq 4000 at Center for Advanced Technology (UCSF).

Bioinformatics analysis of FAC-Sorted layer 6 RNA-Seq

Collectively, we analyzed 8 RNA-Seq libraries, which comprised of 4 *Tbr1*^{wildtype} and 4 *Tbr1*^{layer6} mutant RNA-Seq libraries. Sequencing was conducted on HiSeq 4000 using Paired-End 100 (PE100) with the Library fragment size of approximately 300 bp.

RNA-Seq alignment, and quality control

The RNA-Seq reads were aligned to the mm9 mouse genome reference using STAR in gene annotation mode. Picard was utilized to generate alignment quality control (QC) metrics for every RNA-Seq samples. Principle component analysis (PCA) of the quality control matrices was employed to determine the presence of RNA-Seq sample outliers (The outliner is defined as a sample whose QC metrics are at least three standard deviations away from the mean in any of the first three principal components). The analysis did not indicate any outliers in these datasets.

Gene expression estimation and normalization

Gene expression was quantified with HTSeq in intersection-strict mode. Out of 24,015, 16,805 genes have at least one read in more than 50% of the samples. These 16,805 genes were normalized for gene length, GC content, and sample library size using CQN R-package. Gene length is obtained directly from the gene annotation file (.GTF) of mouse mm9 genome build reference. Bedtools is used to compute the gene GC content.

After normalization, the genes whose expression value doesn't change across all samples are removed. PCA is applied to identify any sample outliners with those filtered and normalized gene expression. The expression values were scaled and centered before PCA. PCA over gene expression shows that there are not outliners in this dataset.

Differential gene expression analysis (DEX analysis):

To identify differentially expressed genes (DEX genes), we identified all possible confounding variables including ribosomal bases in the mapped reads, percentage of bases in intronic region, RIN, Sex and RNA concentration to produce a reliable conclusion. Thousands of negative binomial regression models are built to model expressions of each gene. The best model is formed using Bayesian information criterion (BIC) and forward stepwise algorithm. The DEX analysis was performed with edgeR (McCarthy, 2012; Robinson, 2010). Genes that pass the 0.05 significance threshold are considered as significantly differentially expressed genes.

Gene Co-expression network analysis with gene expression residual:

To avoid effect of confounding variables in gene co-expression network analysis, we mathematically removed the effects of variables, Sex and percentage of UTR region bases by computing the estimated gene expression with linear model coefficients and over-dispersion parameters output by edgeR. We use the estimated gene expression to construct a signed gene co-expression network. Hierarchical clustering with the average linkage method is employed to create modules of genes. Genes in one module have similar expression patterns in the data. The expression of genes belonging to a module is summarized using the eigengene expression of the module. We evaluated the degree of association between '*Tbr1*^{layer5} mutant vs. Control' as well as '*Tbr1*^{layer6} mutant vs. Control' status and module eigengene expression using Pearson correlation. Gene module which are statistically significant (adjusted p-value $\leq$0.05) correlated ($\geq$0.9 or $\leq$-0.9) with status are reported. We conducted the GO pathway analysis using ToppFun

(https://toppgene.cchmc.org/enrichment.jsp) online tool to understand the biological meaning of those gene modules.

TBR1 Chromatin immunoprecipitation (ChIP)

Transcription factor ChIP was performed as previously published with a few modifications (McKenna et al., 2011; Sandberg et al., 2016). P2 somatosensory cortices were dissected and dissociated by pipetting in cold PBS. Dissociated cells were fixed in 1% formaldehyde for 10 min at RT and neutralized with 1 mL 2.5M glycine. Fixed chromatin was lysed and sheared into 200 - 1,000 bp fragments using a Covaris S2 (13 cycles of duty cycle = 5%, intensity = 3 and cycles per burst = 200). Immunoprecipitation (IP) reactions of two biological replicates at P2 were performed using 5 μg TBR1 polyclonal antibody (Santa Cruz Biotech, SC48816 X (M-200)). 20X molar excess TBR1 blocking peptide was used as negative control. Protein/antibody complexes were collected using Dynabeads (20 mL protein A + 20 mL protein G) and processed as previously described (Vokes et al., 2007). ChIP-seq libraries were generated using Ovation Ultralow System V2 (NuGEN) following manufacturer's protocol. Generated libraries were size selected (180–350 bp) and sequenced at the Center for Advanced Technology at UCSF (http://cat.ucsf.edu/) and the Genomics Core Facility (http://humangenetics.ucsf.edu/genomics-services/).

ChIP-Seq Computational Analysis

Clustering, base calling, and quality metrics were performed using standard Illumina software. Sequenced libraries were analyzed for overall quality and were filtered, and reads were mapped to the mouse genome (mm9) as previously described (Sandberg et al., 2016).

Primary Cell Culture and Luciferase assay

Plasmids: To generate luciferase constructs candidate regulatory elements of mouse *Tbr1* (hs416, chr2: 61494203-61494886, 683bp)*, Foxp2* (chr6: 15097241-15098146, 905 bp), *Grin2b* (chr6: 135813640-135814770, 1,130 bp), *Bcl11a* (chr11: 24270818-24271924, 1,383 bp), *Drd1* (chr13: 54074453-54075131, 678 bp), *Hcn1* (chr13: 118669041-118670541, 1,500 bp), *Fezf2* (hs434, chr14: 13170235-13171693, 1,458bp), *Foxp1* (chr6: 99325484-99327361, 1,877 bp), and *DlxI5/6i* enhancer (chr6: 6819420-6819819, 400 bp) were amplified by PCR, and cloned into the pGL4.23 vector (Promega). The vectors were transformed with *DH5α E. coli* cells at 42°C.

Luciferase assay: Primary cortical neurons were harvested from P0 wildtype cortex and transfected using Lipofectamine 2000 (Invitrogen) and one of the regulatory element luciferase vectors that were generated as described above. To test whether TBR1 modified the regulatory elements activity, *pCAG-Tbr1-IRES-eGFP* was co-transfected together with one of the aforementioned regulatory element vectors. A renilla luciferase plasmid (pRL, Promega) was co-transfected to control for transfection efficiency. The luciferase assay was performed 48hrs after transfection using the dual-luciferase kit (Promega) according to manufacturer's instructions. Reporter activity was measured using Veritas™ Microplate Luminometer (Turner BioSystems, Model# 9100-001).

Histology

At the time of experiment, for P0 and P3 experiments, animals were anesthetized on ice while postnatal (P21 and P56) animals were anesthetized with intraperitoneal avertin (0.015 ml/g of a 2.5% solution) injection. Animals were perfused transcardially with cold

PBS and then with 4% PFA in PBS, followed by brain isolation, 1-2 hr post-fixation, cryoprotected in 30% sucrose in PBS, and cut frozen (coronally or sagittally) on a sliding microtome at 40µm for immunohistochemistry or *in situ* hybridization. All primary and secondary antibodies were diluted in PBS containing 10% Normal Serum, 0.25% Triton X-100 and 2% BSA. The following primary antibodies were used: Chicken anti-GFP (1:2000, Aves), mouse anti-Vglut1 (1:200, Synaptic Systems), rabbit anti-Vgat (1:500, Synaptic Systems), rabbit anti-PSD95 (1:200, Cell Signaling), mouse anti-gephyrin (1:200, Synaptic Systems). The secondary antibodies for immunofluorescence were Alexa Fluor-conjugated and purchased from Thermofisher. For synapse immunohistochemistry, sections were pre-treated with pepsin to enhance the staining as described before (Corteen, Cole, Sarna, Sieghart, & Swinny, 2011). Immunofluorescence specimens were counterstained with 1% DAPI to assist the delineation of cortical layers. For *in situ* hybridization a rostro-caudal coronal series of at least ten sections were examined. Anti-sense riboprobes for *Tbr1*, *Foxp2*, *Wnt7b*, *Tle4*, *Nr4a2*, *Bcl11b*, *Fezf2*, *Foxp1*, *Sst*, *Ntng1*, *Cntn2*, and *Drd1* were prepared as previously described (Cobos et al., 2005; Long, Garel, Depew, Tobet, & Rubenstein, 2003). ISH was performed using digoxigenin-labeled riboprobes as previously described (Stanco et al., 2014).

Image Acquisition and Analysis

Fluorescent and brightfield images were taken using a Coolsnap camera (Photometrics) mounted on a Nikon Eclipse 80i microscope using NIS Elements acquisition software (Nikon). Confocal images were taken using Zeiss LSM 880 Confocal Microscope with a 63X objective at 1,024×1,024 pixels resolution using ZEN 2.0 software at Molecular Imaging Center (UC Berkeley). Brightness and contrast were adjusted and images merged

using Photoshop or ImageJ software. ImageJ software was used for image processing. For synapse counting (presynaptic and postsynaptic boutons), confocal image stacks (0.4µm step size) were processed with ImageJ software. In brief, background subtraction and smooth filter were applied to each stack. Using a threshold function, each stack was converted into a 'masks' image. Furthermore, the channels were co-localized with the Image Calculator plugging. Lastly, the number of co-localizations were counted and the length of each dendrite was measured in each of the focal plane. Staining for control and mutant were done in parallel as well as the image capturing.

Cell counting

For assessing cell density in the neocortex on fluorescence sections 10X images at were taken of the somatosensory cortex, encompassing all neocortical layers, from both hemispheres for each replicate. Images were opened with ImageJ to delimit and measure the region of interest (ROI).

Electrophysiology

Coronal brain slices (250 µm) including medial prefrontal cortex were made from mice age p21-28 and p56-p80. Slicing solution was chilled to 4°C and contained (in mM): 234 sucrose, 26 $NaHCO_3$, 11 glucose, 10 $MgSO_4$, 2.5 KCl, 1.25 NaH_2PO_4, 0.5 $CaCl_2$, bubbled with 5% CO_2/ 95% O_2. Slices were incubated in artificial cerebrospinal fluid (aCSF) at 32°C for 30 minutes and then at room temperature until recording. aCSF contained (in mM): 123 NaCl, 26 $NaHCO_3$, 11 glucose, 3 KCl, 2 $CaCl_2$, 1.25 NaH_2PO_4, 1 $MgCl_2$, also bubbled with 5% CO_2/ 95% O_2.

Neurons were visualized using differential interference contrast or DODT contrast microscopy on an upright microscope (Olympus). Ntsr1cre positive neurons were identified

by fluorescent visualization of cre-dependent tdTomato. We obtained somatic whole-cell patch clamp recordings using a Multiclamp 700B (Molecular Devices) amplifier and acquired with pClamp. Patch pipettes (2-5 MΩ tip resistance) were filled with the following (in mM): 130 KGluconate, 10 KCl, 10 HEPES, 10 EGTA, 2 $MgCl_2$, 2 MgATP, 0.3 Na_3GTP. All recordings were made at 32-34°C. Series resistance was compensated in all current clamp experiments and monitored throughout recordings. Recordings were discarded if Rs changed by >25%. For spontaneous EPSC and IPSC recordings cells were held in voltage clamp at -70 mV and +10mV, respectively. In both cases patch pipettes were filled with the following (in mM): 135 Cesium Methanesulfonate, 8 NaCl, 10 HEPES, 0.3 EGTA, 5 QX314, 4 MgATP, 0.3 Na_3GTP.

Viral injection for expression of fluorescent reporters

Viral injections were performed using standard mouse stereotactical methods. Mice were anesthetized for the duration of the surgery using isoflurane gas. After cleaning, an incision was made in the scalp, the skull was leveled, and small burr holes were drilled over the brain region of interest using a dental drill. Virus was injected through the burr holes using a microinjector at a speed of 150 nL/minute and the scalp was closed using tissue adhesive (Vetbond).

For expression anterograde fluorescent reporters, we injected a Cre-dependent ChR2-eYFP virus (AAV5-Ef1-DIO-ChR2-eYFP, 0.5 µL). In*Tbr1*^{layer5} mutant and *Tbr1*^{control} mice, these viral injections targeted mPFC and medial dorsal thalamus (mdT) where as in*Tbr1*^{layer6} mutant and *Tbr1*^{control} mice we targeted S1 and ventromedial (VM) thalamus of each mouse line (p21-p28) and waited 3-4 weeks for trafficking of ChR2 to the axon terminals in mPFC. For retrograde labelling, Alexafluor-tagged cholera toxin subunit B 488 (CTb488; ThermoFisher) was first dissolved in PBS to make a 1.0mg/mL solution. 350nL of

CTb488 were then injected into the MD thalamus at a rate of 100nL/min and waited 3-5 days before histology experiments. md thalamus injection coordinates were A/P = -1.7, M/L = +/- 0.3, D/V = -3.45. mPFC injection coordinates were A/P = +1.7, M/L = +/- 0.3, D/V = -2.75.VM thalamus injection coordinates were A/P = -1.7, M/L = ± 0.7, D/V = -4.1. S1 injection coordinates were A/P = -0.75, M/L = ± 2.5, D/V = -1.75

Behavior Assays

Mice are transferred to experimental room and allowed to habituate for at least 45 minutes each day. All behavior assays were performed on mice age P56 to P80. We were blind to genotype during scoring of videos.

Open-field test: An individual mouse was placed near the wall-side of 50 x 50 cm open-field arena, and the movement of the mouse was recorded by a video camera for 10 min. The recorded video file was later analyzed with Any-Maze software (San Diego Instruments). Time in the center of the field (a 25 x 25 cm square) was measured. The open field arena was cleaned with 70% ethanol and wiped with paper towels between each trial.

Elevated plus maze test: An individual mouse was placed at the junction of the open and closed arms, facing the arm opposite to the experimenter, of an apparatus with two open arms without walls (30 x 5 x 0.5 cm) across from each other and perpendicular to two closed arms with walls (30 x 5 x 15 cm) with a center platform (5 x 5 cm), and at a height of 40 cm above the floor. The movement of the mouse was recorded by a video camera for 10 min. The recorded video file was later analyzed and time in the open arms of the apparatus

was measured. The arms of the elevated plus maze apparatus was cleaned with 70% ethanol and wiped with paper towels between each trial.

Rotarod test: The assay consisted of four trials per day over the course of 2 days with the rotarod set to accelerate from 4rpm to 45rpm over 5 minutes. The trial started once five mice were placed on the rotarod rotating at 4rpm in separate partitioned compartments. Each trial ended when a mouse fell off, made three complete revolutions while hanging on, or reached 300 s. Digital videos of the mice on the rotarod were recorded from behind.

Social interaction and novel object task: An individual mouse was allowed to habituate for 5 minutes in their home cage prior to starting the trial. A juvenile (3-4 weeks old) mouse of the same strain and sex was introduced to the home cage. After 5 minutes, the juvenile was removed from the home cage. After a 5 minute break a novel object (typically a plastic test tube cap) was introduced into the home cage for five minutes. We scored videos offline, blind to genotype. We measured the number of seconds the mouse spent with its nose in direct contact with the novel object or engaged in social interaction with the juvenile (defined as sniffing, close following, or allo-grooming) in the 300 seconds following the time the juvenile or object was introduced into the cage. In addition, we noted any aggressive-appearing behaviors toward the juvenile, freezing, and grooming behaviors.

Statistical Analysis

All statistical analyses were done on GraphPad Prism 7.0 software. All data are shown as mean $\pm$ SEM. Statistical significance was accepted at the level $p < 0.05$. We used student's t-test to compare pairs of groups if data were normally distributed (verified using

Lillie test). If more than two groups were compared, we used one-way ANOVA with post-hoc tests between groups corrected for multiple comparisons (Holm-Sidak or Tukey). The specific post-hoc test as well as exact F and corrected p values can be found in the text and corresponding figure legends.

Results

Characterization of the *Tbr1* conditional mutant allele.

To investigate the function(s) of *Tbr1* in specific subtypes of cortical neurons at later stages of development, we generated a *Tbr1* conditional mutant (*Tbr1*^{flox}) allele. We constructed a targeting vector that inserts LoxP sites into introns 1 and 3 (Fig. 1A). Therefore, upon Cre-recombination, exons 2 and 3 (including the T-box DNA binding region) will be deleted; similar to the constitutive null allele previously published (Bulfone et al., 1998).

We validated recombination of *Tbr1*$^{flox/flox}$ alleles with the *β-actin-cre* allele, to examine whether the conditional allele would result in *Tbr1* loss of function upon Cre recombination. We measured *Tbr1* RNA levels from the cortex (E15.5 and P0) via RT-qPCR using primers to exons 1 and 2, and to exons 1 and 4. Only the exon 1-2 reaction showed no signal in the *Tbr1* mutant consistent with the location of the Cre-mediated deletion (Fig. 1C). We next investigated *Tbr1* transcripts using *in situ* hybridization (ISH) at P0, using either a *Tbr1* full-length (FL) probe, or a probe that only hybridizes to exons 2 and 3 (E2-3; the part deleted by Cre recombination). We did not observe any signal with the *Tbr1* E2-3 probe; whereas we observed strong signal from the FL *Tbr1* probe (Fig. 1D), suggesting that a stable truncated RNA is still produced in the conditional mutant.

We performed a western blot (WB) on cortical proteins from *Tbr1* null and wildtype littermates at E15.5 and P0 to determine whether the *Tbr1* truncated RNA generates a stable protein (Fig. 1E). The TBR1 antigen is encoded by exon 1 and maps to the N-terminus of TBR1 (red; Fig. 1A, 1B). The TBR1 protein is ~75 kDa in the wildtype E15.5 and P0 cortex; however, no signal was detected in the *Tbr1* null cortex at E15.5 and P0 (Fig. 1E). Thus, it appears the *Tbr1*^{flox} allele generates a conditional *Tbr1* allele that does not generate a stable TBR1 protein, and thus is likely to function as a null allele.

***Tbr1* maintains layer 6 identity in postnatal cortex.**

We next studied the effect of deleting *Tbr1* in layer 6 and subplate approximately 5-6 days after *Tbr1* expression begins in these neurons using *Ntsr1-cre* (Madisen et al., 2010). We refer to these as $Tbr1^{layer6}$ mutants. *Ntsr1-cre* expression, detected using the Ai14 tdTomato Cre-dependent reporter, begins in layer 6 and subplate neurons around E16.5-E17.5 (data not shown). To identify dysregulated RNAs in layer 6 and subplate of $Tbr1^{layer6}$ mutants we performed RNA sequencing (RNA-Seq) on FAC-sorted cells from the $Tbr1^{wildtype}$ and $Tbr1^{layer6}$ mutant somatosensory cortex at P5. We assessed a total of 8 samples, including 4 $Tbr1^{layer6}$ mutants and 4 $Tbr1^{wildtype}$ controls. After alignment, quality control, and normalization, we identified differentially expressed (DEX) genes in the $Tbr1^{layer6}$ mutant versus the $Tbr1^{wildtype}$ control with EdgeR (McCarthy, 2012; Robinson, 2010). We detected 178 genes DEX after correction for multiple comparisons (false discovery rate ≤ 0.05), including *Tbr1* (fold change [FC] = -1.93, $p = 3.83 \times 10^{-7}$). These 178 genes are enriched for gene ontology (GO) terms related to nervous system development, neurogenesis, and neuron development (Fig. 2), consistent with the known functions of *Tbr1* (Bedogni et al., 2010; Bulfone et al., 1995; Bulfone et al., 1998; Hevner et al., 2001).

The observed transcriptome changes provide evidence that *Tbr1* is required to maintain the identity of layer 6 neurons. Several key regulators of layer 6 identity are downregulated in the $Tbr1^{layer6}$ mutants, including *Tle4* (FC = -2.11, $p = 2.99 \times 10^{-8}$) and *Wnt7b* (FC = -2.08, $p = 1.83 \times 10^{-6}$). Furthermore, we observed ectopic expression of regulators of layer 5 identity and properties, including *Foxp1* (FC = 1.41, p = 0.029), *Fezf2* (FC = 1.68, p = 0.000176), *Grin3a* (FC = 2.36, $p = 4.65 \times 10^{-7}$) and *Epha7* (FC = 1.95, $p = 1.21 \times 10^{-6}$; Fig. 2). We conducted ISH on a subset of these genes to verify the changes observed in the RNA-seq data. Fig. 4 shows the results in the somatosensory cortex at P3. We confirm that *Tbr1* and *Wnt7b* expression is reduced in layer 6 of $Tbr1^{layer6}$ mutants (Fig.

4H-H′, J-J′). This decrease appears to be accompanied by an increase in *Tbr1 and Wnt7b* in the superficial layers of the somatosensory cortex (Fig. 4H-H′, J-J′). We also observe that *Nr4a2* expression is reduced in the subplate (Fig. 4I-I′). We also confirmed the previously mentioned ectopic expression of layer 5 regulators in layer 6; for example, *Bcl11b* (Fig. 4K-K′), *Fezf2* (Fig. 4L-L′) and *Foxp1* (Fig. 4M-M′).

Overall, the RNA expression data (RNA-Seq and ISH; Figs 2 and 4) provide evidence that *Tbr1* is required not only to induce layer 6 identity (Hevner, Miyashita-Lin, & Rubenstein, 2002; Hevner et al., 2001), but is also essential approximately 5-6 days after *Tbr1* expression is established to maintain layer 6 identity.

Tbr1 directly regulates the transcription of genes that control layer 6 identity.

To determine whether the changes in genes expression in *Tbr1*^{layer6} mutants is due to direct regulation by TBR1, we performed chromatin immunoprecipitation followed by high-throughput sequencing (ChIP-Seq) on P2 cortex and assessed whether TBR1 binds to the promoter and/or other candidate regulatory elements (REs) of key DEX genes. We also performed ChIP-Seq against H3K27Ac, a histone variant associated with active enhancers (Creyghton et al., 2010).

In P2 cortex, TBR1 binds to 27,228 regions genome-wide. To stratify these binding sites, we defined promoters as 1 kb upstream of the 5’ UTR, all other regions as putative intragenic or distal regulatory regions. Approximately 40% of peaks overlap promoters and approximately 60% overlap intragenic or distal regulatory regions. To narrow to putative functional binding sites, we intersected these peaks with H3K27Ac peaks generated from the same tissue. To gain further evidence that these peaks represent candidate active regulatory elements influenced by TBR1, we assessed the number of genes with putative

TBR1 regulatory loci that are dysregulated in the *Tbr1*^{layer6} mutants. TBR1 binds to the 89% of the promoter regions and 77% of the candidate REs near the genes dysregulated in the *Tbr1*^{layer6} mutants (Fig. 5). Given the putative functional connection between *Tbr1* dysregulation and these regulatory elements, we next directly tested the activity of several REs, and their relationship to TBR1.

Thus, we cloned 9 REs into pGL4.23 luciferase expression vector upstream of a minimal promoter. We then transfected these into primary cultures made from P0 cortex, and assayed luciferase activity 3 days later. In parallel experiments, we co-transfected the RE vectors with a *Tbr1* expression vector. We tested 3 classes of candidate REs that were candidates for regulating genes that were (1) downregulated (*Tbr1, Foxp2, Grin2b, Bcl11a* and *Drd1*), (2) upregulated (*Hcn1*, *Fezf2* and *Foxp1*) and (3) unchanged (*DlxI5/6i*) in the *Tbr1*^{layer6} mutants (Fig. 5). Luciferase activity was driven by all of the REs (Fig. 3), except the negative control *DlxI5/6i* interneuron specific enhancer (Zerucha et al., 2000). On the other hand, *Tbr1* co-transfection only activated the *Tbr1, Foxp2, Grin2b, Bcl11a* and *Drd1* candidate REs, consistent with down-regulation of these cognate genes in the *Tbr1*^{layer6} mutants (Fig. 2). In addition, *Tbr1* co-transfection reduced luciferase expression with the *Hcn1*, *Fezf2* and *Foxp1* REs, which corresponded to genes whose expression increased in the *Tbr1*^{layer6} mutants (Fig. 2).

Thus, using TBR1 ChIP-Seq and a RE functional assay, we have identified RE and provided evidence that they function either as activators or repressors of expression in the presence of TBR1. This data solidifies our evidence that TBR1 directly controls the molecular properties of layer 6 pyramidal neurons, and that TBR1 functions as an activator or a repressor depending on the nature of the RE.

***Tbr1* specifies a program that patterns apical dendritic lamination of layer 6 neurons.**

A key feature of a neuron's identity is its dendritic pattern (Lefebvre, Sanes, & Kay, 2015; Russ & Kaltschmidt, 2014). Normally, the apical dendrites of layer 6 pyramidal neurons grow into layer 4 where they elaborate their branches (Ledergerber & Larkum, 2010). We used tdTomato expression that was driven by *Ntsr1-cre* in layer 6 and the subplate, to compare the dendritic pattern of wild type and *Tbr1*^{layer6} mutants (Fig. 6). In the wildtype control, the apical dendrites of the layer 6 glutamatergic neurons extend to layer 4 at P3, P21 and P60 (Fig. 6A-C). On the other hand, in the *Tbr1*^{layer6} mutants the apical dendrites extend to layer 1 at P3, P21 and P60 (white arrowheads, Fig. 6A′-C′). This change in the morphology of the dendrite is consistent with the hypothesis that the layer 6 neurons have changed fate to a layer 5 identity.

***Tbr1* is required after E17.5 for corticothalamic projections into the anteromedial thalamus.**

Layer 6 and subplate projection neurons have a characteristic axon projection pattern that involves axons that extend through the basal ganglia to the thalamus, where they form a stereotypic topographic map between cortical areas and specific thalamic nuclei (Crandall, Cruikshank, & Connors, 2015). *Tbr1* constitutive null mutant axons fail to grow to the thalamus (Hevner et al., 2002; Hevner et al., 2001). Here, we investigated corticothalamic projections in *Tbr1*^{layer6} mutants in two ways. First, we injected a Cre-dependent anterograde label (DIO-ChR2-EYFP) into the somatosensory cortex of wild type and *Tbr1*^{layer6} mutants at P21. Histological analyses were performed at P60. Importantly, *Ntsr1-Cre* recombination of *Tbr1* does not extend into many cortical regions, including the olfactory bulb, medial prefrontal neocortex, dorsomedial neocortex (cingulate and

retrosplenial), hippocampus and parahippocampus, piriform cortex, and pallial amygdala; therefore we targeted the somatosensory cortex where there is significant overlapping expression of *Ntsr1*-cre and endogenous *Tbr1* (data not shown). Despite the evidence that *Tbr1*^{layer6} mutant layer 6 pyramidal neurons have molecular and dendritic properties of layer 5 pyramidal neurons (Figs. 2, 3, 4, 6), the mutant layer 6 neurons, like in the wildtype, have corticothalamic projections that enter the thalamus (Fig. S1). However, the *Tbr1*^{layer6} mutants have reduced thalamic projections, which is most strongly seen in the anterior and anteromedial thalamus (seen in the rostral coronal sections). We confirmed this phenotype using a second approach using tdTomato expression that was driven in layer 6 neurons using *Ntsr1-cre.* This method also highlighted a reduction of mutant layer 6 cortical projections in the striatum.

To evaluate whether the phenotype was due to a failure to maintain the projections, or a failure to establish them, we studied neonatal *Tbr1*^{layer6} mutants at P3 (Fig. S2). The P3 and P21 phenotypes were very similar. This result supports a conclusion that *Tbr1* expression in layer 6 and subplate neurons is required after ~E17.5 for the growth of corticothalamic projections in the anterior and anteromedial thalamus. Thus, while *Tbr1* is required prior to E17.5 for corticothalamic projections to emerge from the subpallium and enter the diencephalon (Hevner et al., 2002; Hevner et al., 2001), these processes take place in the *Tbr1*^{layer6} mutants. However, the latter mutants show that after ~E17.5 *Tbr1* is required for the maturation of corticothalamic connectivity preferentially in the anterior and anteromedial thalamus.

Excitatory synapse numbers are reduced in *Tbr1*^{layer6} and *Tbr1*^{layer5} mutants.

We next investigated excitatory synapses numbers of layer 6 neurons in the *Tbr1*^{layer6} mutants as well as layer 5 neurons in the *Tbr1*^{layer5} mutants. We used

immunofluorescence to label excitatory presynaptic terminals (VGlut1^{+}) that are apposed to dendritic postsynaptic zones (PSD95^{+}) in control, and *Tbr1* heterozygous and homozygous mutants on the apical spines at P21 (layer 6, Fig. 7I; layer 5, Fig. 8I) and P56 (layer 6, Supplementary Fig 3I; layer 5, Data not shown). We continued to examine the loss of *Tbr1* within layer 6, driven by *Ntsr1-Cre* recombination, in the somatosensory cortex. In the *Tbr1*^{layer5} mutants we targeted the medial prefrontal neocortex, a brain region strongly implicated in ASD dysfunction (Bachevalier and Mishkin, 1986; Morgan *et al*., 1993), because *Rbp4-Cre* recombination of *Tbr1* occurred throughout many cortical regions including the mPFC (data not shown).

Tbr1 postnatally regulate the number of excitatory synapses at P21 and P56 in coronal sections from the somatosensory cortex (layer 6, Fig. 7A) and the medial prefrontal cortex (layer 5, Fig. 8A). We analyzed the number of excitatory terminals (VGlut1^{+} presynaptic structures) that are apposed to dendritic postsynaptic zones (PSD95^{+}) of *Tbr1*$^{\text{wildtype}}$, *Tbr1* heterozygous mutants and *Tbr1*homozygous mutants at P21 (layer 6, Fig 7I; layer 5, Fig. 8I) and P56 (layer 6, Supplementary Fig 3I; layer 5, data not shown).

As depicted in Fig. 7I, brain sections from somatosensory cortex (Fig. 7A) of *Tbr1*$^{\text{wildtype}}$ (*Ntsr1-cre::tdTomato*$^{f/+}$, Fig. 7D-D′), *Tbr1*^{layer6} heterozygous mutants (*Tbr1*$^{f/+}$*::Ntsr1-cre::tdTomato*$^{f/+}$, Fig. 7E-E′) and *Tbr1*^{layer6} homozygous mutants (*Tbr1*$^{f/f}$*::Ntsr1-cre::tdTomato*$^{f/+}$, Fig. 7F-F′) were tested. Confocal fluorescent microscopy analysis of the synapse numbers showed a ~35% reduction in excitatory synaptic punctae on *Tbr1*^{layer6} heterozygous (BD= 0.786, $p<0.0001$) and a ~75% decrease in *Tbr1*^{layer6} homozygous mutants (BD= 0.303, $p<0.0001$) at P21 (Fig. 7G). The decrease in excitatory synapse numbers is also present at P56 (Supplementary Fig. 3G), in which the excitatory synapses

have decreased ~35% in *Tbr1*^{layer6} heterozygous (BD=0.501, p<0.0001) and ~64% in *Tbr1*^{layer6} homozygous mutants (BD= 0.362, p<0.0001; Supplementary Fig. 3G). Reduced excitatory synaptic density at P21 (Fig. 7D-G) and P56 (Supplementary Fig. 3D-G), led us to measure spontaneous EPSCs using whole-cell patch clamp at both P21 and P56. We recorded from neurons expressing *Ntsr1-cre*, identified using the fluorescent Ai14 tdTomato Cre-dependent reporter, in the somatosensory cortex (S1) from coronal slices (Fig. 7A) of *Tbr1*^{wildtype}, *Tbr1*^{layer6} heterozygous, and *Tbr1*^{layer6} homozygous mutant mice at P21 or P56. To examine the sEPSC, we made voltage clamp recordings at -70mV using a cesium-based intracellular solution. The frequency of sEPSC are reduced in *Tbr1*^{layer6} homozygous mutants as compared to cells from *Tbr1*^{wildtype} mice at P21 (Fig. 7H, 7I: n = 7/7/7, wildtype/ heterozygous/ homozygous; One-way ANOVA, $F_{(2,18)} = 6.625$, p = 0.007; t-test, Tukey correction, wildtype v. homozygous: $q_{(18)} = 5.123$, p = 0.0053). The decrease in sEPSC frequency was also present at P56 (Supplementary Fig. 3H, 3I: n = 7/7/7, wildtype/ heterozygous/ homozygous; One-way ANOVA, $F_{(2,18)} = 10.17$, p = 0.0011; t-test, Tukey correction, wildtype v. homozygous: $q_{(18)} = 6.371$, p = 0.0008).

As depicted in Fig. 8I, brain sections from mPFC (Fig. 8A) of *Tbr1*^{wildtype} (*Rbp4-cre::tdTomato*$^{f/+}$, Fig. 8D-D′), *Tbr1*^{layer5} heterozygous mutants (*Tbr1*$^{f/+}$*::Rbp4-cre::tdTomato*$^{f/+}$, Fig. 8E-E′) and *Tbr1*^{layer5} homozygous mutants (*Tbr1*$^{f/f}$*::Rbp4-cre::tdTomato*$^{f/+}$, Fig. 8F-F′) were tested. Confocal fluorescent microscopy analysis of the synapse numbers showed a ~35% reduction in excitatory synaptic punctae on *Tbr1*^{layer5} heterozygous (BD= 0.786, p<0.0001) and a ~75% decrease in *Tbr1*^{layer5} homozygous mutants (BD= 0.303, p<0.0001) at P21 (Fig. 8D). The decrease in excitatory synapse numbers is also present at P56 (data not shown).

Reduced excitatory synaptic density at P21 (Fig. 8D-G) and P56 (data not shown), led us to measure spontaneous EPSCs using whole-cell patch clamp at both P21 and P56. We recorded from neurons expressing *Rbp4-cre*, identified using the fluorescent Ai14 tdTomato Cre-dependent reporter, in the mPFC from coronal slices (Fig. 8A) of *Tbr1*^{wildtype}, *Tbr1*^{layer5} heterozygous, and *Tbr1*^{layer5} homozygous mutant mice at P21 or P56. To examine the sEPSC, we made voltage clamp recordings at -70mV. The frequency of sEPSC are reduced in *Tbr1*^{layer5} homozygous mutants as compared to cells from *Tbr1*^{wildtype} mice at P21 (Fig. 8H, 8I: n = 6/6/6, wildtype/ heterozygous/ homozygous; One-way ANOVA, $F_{(2,15)}$ = 23.18, $p < 0.001$; t-test, Tukey correction, wildtype v. homozygous: $q_{(15)} = 9.416$, $p < 0.0001$; heterozygous v. homozygous: $q_{(15)} = 6.455$, $p = 0.001$). The decrease in sEPSC frequency was also present at P56 (Fig. 8H, 8I: n = 6/6/6, wildtype/ heterozygous/ homozygous; One-way ANOVA, $F_{(2,15)} = 19.76$, $p < 0.0001$; t-test, Tukey correction, wildtype v. homozygous: $q_{(15)} = 8.582$, $p < 0.0001$).

Tbr1^{layer6} and _Tbr1_^{layer5} mutants have altered cortical interneuron lamination and reduced inhibitory synaptic density at P21 and P56.

The pattern of SST^{+} cortical interneuron (CIN) lamination is abnormal in P3 *Tbr1*^{layer6} mutants (Supplementary Fig. 4). In *Tbr1*^{layer6} mutants, the distribution of SST+ CINs are reduced in layer 6, unchanged in layer 5 and increased in layers 2-4 (Supplementary Fig. 4A-A′′). These changes are consistent with previous studies that have demonstrated the role of cortical pyramidal neurons in regulating the distribution of cortical interneurons (Lodato et al., 2011)

This result, in conjunction with the reduction in excitatory synapses (layer 6, Fig. 7I; layer 5, Fig 8I) led us to measure inhibitory synapse numbers in the *Tbr1*^{layer6} and *Tbr1*^{layer5} mutants. From confocal images, we counted the numbers of inhibitory terminals (VGat^{+}

presynaptic structures) apposed to dendritic postsynaptic zones (Gephyrin^{+}) of *Tbr1*^{wildtype} (layer 6, Fig. 7J-J′, Supplementary Fig. 3J-J′; layer 5, Fig. 8. J-J'), *Tbr1* heterozygous mutants (layer 6, Fig. 7K-K′, Supplementary Fig. 3K-K′; layer 5, Fig. 8 K-K') and *Tbr1*^{layer6} homozygous mutants (layer 6, Fig. 7L-L′, Supplementary Fig. 3L-L′; layer 5, Fig. 8L-L') onto the apical dendrites of layer 6 pyramidal neurons at P21 (Fig. 7II) and P56 (Supplementary Fig. 3II) as well as onto the apical dendrites of layer 5 pyramidal neurons at P21 (Fig. 8II) and P56 (data not shown).

Confocal fluorescent microscopy analysis of the synapse numbers demonstrated a ~37% reduction in inhibitory synaptic density in *Tbr1*^{layer6} heterozygous mutants (BD= 0.574, p<0.0001) and a ~72% decrease in *Tbr1*^{layer6} homozygous mutants (BD= 0.252, P<0.0001) at P21 (Fig. 7J). The decrease in inhibitory synapse numbers is also present at P56 (Supplementary Fig. 3M), in which the inhibitory synapses have decreased ~33% in *Tbr1*^{layer6} heterozygous mutants (BD= 0.673, p<0.0001) and ~66% in *Tbr1*^{layer6} homozygous mutants (BD= 0.346, p<0.0001; Fig. 6M).

To measure the inhibitory synaptic input onto the layer 6 and layer 5 pyramidal neurons *in vivo*, we measured spontaneous IPSCs (sIPSC) using whole-cell patch clamp at both P21 and P56. We made voltage clamp recordings at +10mV using a cesium-based intracellular solution. In slices from P21 *Tbr1*^{layer6} homozygous mutant mice, we observed reduced sIPSC frequency (Fig. 7N, 7O: n = 7/6/7, wildtype/ heterozygous/ homozygous; One-way ANOVA, $F_{(2,17)} = 4.738$, p = 0.023; t-test, Tukey correction, wildtype v. homozygous: $q_{(17)} = 3.847$, p = 0.037, heterozygous v. homozygous: $q_{(17)} = 3.635$, p = 0.0495). sIPSC frequency remained reduced at P56 (Supplementary Fig. 3N, 3O: n = 8/8/7, wildtype/ heterozygous/ homozygous; One-way ANOVA, $F_{(2,20)} = 12.44$, p = 0.0003; t-test,

Tukey correction, wildtype v. homozygous: $q_{(20)} = 6.907$, $p = 0.0003$, heterozygous v. homozygous: $q_{(20)} = 4.901$, $p = 0.0066$).

In slices from P21 *Tbr1*^{layer5} homozygous mutant mice, we observed reduced sIPSC frequency (Fig. 8N, 8O: : n = 7/7/7, wildtype/ heterozygous/ homozygous; One-way ANOVA, $F_{(2,18)} = 5.159$, $p = 0.0169$; t-test, Tukey correction, wildtype v. homozygous: $q_{(18)} = 4.534$, $p = 0.0129$). sIPSC frequency remained reduced at P56 (Fig. 8N, 8O: n = 7/7/7, wildtype/ heterozygous/ homozygous; One-way ANOVA, $F_{(2,18)} = 6.694$, $p = 0.0067$; t-test, Tukey correction, wildtype v. homozygous: $q_{(18)} = 5.15$, $p = 0.005$).

Tbr1 mutants have an increase in hyperpolarization-activated cation currents (Ih).

Given that L6 pyramidal neurons in *Tbr1*^{layer6} mutants exhibit anatomical changes suggestive of L5 phenotypes (Fig. 4, 6), we wondered whether similar changes might be present in the intrinsic physiology of L6 pyramidal neurons in *Tbr1*^{layer6} mutants. We used whole-cell patch clamp to measure intrinsic physiological properties of labelled *Ntsr1*-cre expressing pyramidal neurons within L6 of S1 (Fig. 9a & b). At P56 and P21, resting membrane potential (Fig. 9a B, Supplementary Fig. 5B) and input resistance (Fig. 9a C, Supplementary Fig. 5C) were not different between *Tbr1*^{wildtype}, *Tbr1*^{layer6} heterozygous, and *Tbr1*^{layer6} homozygous mutant cells (n=8 of each genotype). A prominent feature of many L5 pyramidal neurons that is largely absent from L6, is hyperpolarization-activated cation current (I_h) mediated by HCN channels (Gee et al., 2012). I_h causes a characteristic “sag” and “rebound” in current clamp recordings of responses to steps of hyperpolarizing current. We examined responses to a -200 pA step, and found that S1 L6 pyramidal neurons from P56 *Tbr1*^{layer6} heterozygous and homozygous mutant mice exhibited significantly increased sag + rebound compared to *Tbr1*^{wildtype} controls, suggesting increased h-current, while other intrinsic electrophysiological properties were largely unaltered (Fig. 9a D: n = 7/6/7,

wildtype/ heterozygous/ homozygous; One-way ANOVA, $F_{(2,17)} = 13.18$, $p = 0.0003$; t-test, Tukey correction, wildtype v. heterozygous: $q_{(17)} = 3.693$, $p = 0.0457$; wildtype v. homozygous: $q_{(17)} = 7.258$, $p = 0.0002$).

The neurons from *Tbr1*^{layer6} homozygous mutants at P21 also exhibited an increased sag and rebound compared to *Tbr1*^{wildtype} controls, suggesting increased h-current (Supplementary Fig. 5D: n = 8/8/8, wildtype/ heterozygous/ homozygous; One-way ANOVA, $F_{(2,21)} = 17.68$, $p < 0.001$; t-test, Tukey correction, wildtype v. homozygous: $q_{(21)} = 8.331$, $p < 0.0001$; heterozygous v. homozygous: $q_{(21)} = 5.16$, $p = 0.0041$). Other intrinsic electrophysiological properties were largely unaltered at P21 (Supplementary Fig. 5B, 5C).

In deep layer neocortical pyramidal neurons, the presence of I_h shifts the resonant frequency towards higher frequencies (Dembrow, Chitwood, & Johnston, 2010). Therefore, to further characterize potential increases in I_h, we estimated the resonant frequency. For this, we injected constant current to hold *Ntsr1-cre* positive neurons in current clamp near -70mV, then introduced a sinusoidal current stimulus with constant amplitude (100 pA peak-to-peak) and a frequency that increased linearly from 0 to 20 Hz over 20 seconds (Fig. 9a E). We used the ratio of the fast Fourier transform of the voltage response (Fig. 9a E top) to the fast Fourier transform of the sinusoidal current stimulus (Fig. 9a E middle) to calculate the impedance amplitude profile (Fig. 9a E bottom). We defined the resonant frequency as the frequency at which the impedance profile reached its peak. At P56-80, both *Tbr1*^{layer6} heterozygous and *Tbr1*^{layer6} homozygous mutants exhibit an increase in their resonant frequency compared to *Tbr1*^{wildtype} controls (Fig. 9b G: n = 7/8/8, wildtype/ heterozygous/ homozygous; One-way ANOVA, $F_{(2,20)} = 16.24$, $p < 0.0001$; t-test, Tukey correction, wildtype v. heterozygous: $q_{(20)} = 7.075$, $p = 0.0002$; wildtype v. homozygous: $q_{(20)} = 7.038$, $p = 0.0002$).

Finally, we blocked I_h by bath applying the specific HCN channel antagonist ZD7288 (25 μM; Fig. 9b F). The resonant frequency was reduced by over 50% in the *Tbr1*^{layer6} heterozygous (Fig. 9b G: n = 8; paired T-test, t(7) = 7.723, p < 0.0001) and *Tbr1*^{layer6} homozygous mutants (Fig. 9b G: n = 8; paired T-test, t(7) = 8.194, p < 0.0001). However, the resonant frequency was not significantly altered by ZD7288 in the neurons from the *Tbr1*^{wildtype} mice, indicating that I_h significantly shifts the resonant frequency of mutant, but not wild-type, L6 pyramidal neurons.

To compare electrophysiological abnormalities linked to loss of *Tbr1* layer 5 cortical neurons we used whole-cell patch clamp to measure intrinsic physiological properties of labelled *Rbp4*-cre expressing pyramidal neurons within L5 of mPFC. At P21-28, resting membrane potential (Fig 10B) and input resistance (Fig 10C), were not different between *Tbr1*^{wildtype}, *Tbr1*^{layer5} heterozygous, and *Tbr1*^{layer5} homozygous mutant cells (n = 7 of each genotype).

A prominent feature of a subpopulation of dopamine D2 receptor (D2R) expressing L5 pyramidal neurons is hyperpolarization-activated cation current (I_h) mediated by HCN channels (Gee et al. 2012; Clarkson et al., 2017). We found that L5 mPFC neurons from P21-28 *Tbr1*^{layer5} homozygous mutants have increased sag and rebound compared to *Tbr1*^{wildtype} controls, suggesting increased h-current (Fig 10D: n = 7/7/7, wildtype/ heterozygous/ homozygous; One-way ANOVA, $F_{(2,18)} = 8.823$, p = 0.0021; t-test, Tukey correction, wildtype v. heterozygous: $q_{(18)} = 4.27$, p = 0.0192; wildtype v. homozygous: $q_{(18)} = 5.712$, p = 0.0021) .

We also measured the intrinsic properties of mPFC L5 *Rbp4-cre* positive neurons from slices from P56-80 mice. Again, neurons from both *Tbr1* heterozygous and homozygous mutant mice have significantly increased sag + rebound compared to controls,

while other intrinsic electrophysiological properties were largely unaltered (Fig 10H: n = 7/7/7, wildtype/ heterozygous/ homozygous; One-way ANOVA, $F_{(2,18)} = 10.11$, $p = 0.0011$; t-test, Tukey correction, wildtype v. heterozygous: $q_{(18)} = 4.565$, $p = 0.0123$; wildtype v. homozygous: $q_{(18)} = 6.115$, $p = 0.0011$).

Additionally, to further characterize potential increases in I_h, we estimated the resonant frequency *Tbr1*^{layer5} mutant neurons as described for *Tbr1*^{layer6} mutants in Figure 9. At P56-80, both *Tbr1*^{layer5} heterozygous and *Tbr1*^{layer5} homozygous mutants exhibit an increase in their resonant frequency over *Tbr1*^{wildtype} (Fig 11C: n = 8/6/8, wildtype/ heterozygous/ homozygous; One-way ANOVA, $F_{(2,19)} = 23.93$, $p < 0.0001$; t-test, Tukey correction, wildtype v. heterozygous: $q_{(19)} = 6.229$, $p = 0.008$; wildtype v. homozygous: $q_{(19)} = 9.57$, $p < 0.0001$). Finally, we blocked I_h by bath applying the specific HCN channel antagonist ZD7288 (25 μM; Fig 11B). The resonant frequency was reduced by over 50% in the *Tbr1*^{wildtype} mice (Fig 11C: n = 8; paired T-test, $t(7) = 4.646$, $p = 0.0024$), *Tbr1*^{layer5} heterozygous (Fig 11C: n = 6; paired T-test, $t(5) = 8.099$, $p = 0.0005$) as well as in the *Tbr1*^{layer5} homozygous mutants (Fig 10C: n = 8; paired T-test, $t(7) = 8.576$, $p < 0.0001$).

Tbr1^{layer6} mutants exhibit increased aggressive behaviors.

To identify behavioral abnormalities linked to loss of *Tbr1* function in L6 neurons, we performed multiple behavioral assays in littermate cohorts of *Tbr1*^{wildtype}, *Tbr1*^{layer6} heterozygous, and *Tbr1*^{layer6} homozygous mutant male and female mice between P56-80. Because *Tbr1* is a high confidence ASD gene, we explored the impact of *Tbr1* loss of function mutation in layer 6 on ASD associated behaviors such as motor ability, anxiety, and social interaction. *Tbr1*^{layer6} heterozygous and *Tbr1*^{layer6} homozygous mutants did not show impairments in locomotion as measured by speed in the open field (Fig. 12A) or in motor coordination as measured by performance on a rotarod (Fig. 12 C) compared to wildtype

controls. *Tbr1*^{layer6} mutants did not show significant difference in anxiety, measured by time spent in the center of a novel open field (Fig. 12 B). However, in the elevated plus maze *Tbr1*^{layer6} heterozygous, and *Tbr1*^{layer6} homozygous mutants did spend an increased time in the closed arms (Fig. 12D: n = 11/8/9, wildtype/ heterozygous/ homozygous; One-way ANOVA, $F_{(2,25)} = 4.155$, $p = 0.028$; t-test, Tukey correction, wildtype v. heterozygous: $q_{(25)} = 4.065$, $p = 0.022$).

To assay social behavior, we measured the time each experimental mouse spent exploring a novel juvenile wildtype mouse of the same sex introduced to its home cage. Subsequently, we measured the amount of time the subject mouse spent exploring a novel object introduced to its home cage. We did not find differences in the time *Tbr1*^{layer6} mutants spent exploring a novel object (Fig. 12E). However, in the *Tbr1*^{layer6} homozygous mutants, we observed a significant increase in the total amount of time the adult spent with the novel juvenile mouse (Fig. 12F: n = 11/8/9, wildtype/ heterozygous/ homozygous; One-way ANOVA, $F_{(2,25)} = 4.534$, $p = 0.021$; t-test, Tukey correction, wildtype v. homozygous: $q_{(25)} = 3.731$, $p = 0.0364$). To further assess the type of interaction, we divided this time into "social interaction," defined as time spent in sniffing, close following (not followed by periods of aggression), or allo-grooming, vs. "aggressive" behavior, defined as biting, fighting, or close following associated with periods of active fighting. *Tbr1*^{wildtype}, *Tbr1*^{layer6} heterozygous, and *Tbr1*^{layer6} homozygous mutants spent similar time in social interaction, particularly during the first 2 minutes of the 5 minutes social interaction task (Fig. 12F). *Tbr1*^{layer6} homozygous mutants, however, also exhibited prolonged periods of aggressive interaction with the juvenile (Fig. 12F: n = 11/8/9, wildtype/ heterozygous/ homozygous; One-way ANOVA, $F_{(2,25)} = 10.97$, $p = 0.0004$; t-test, Tukey correction, wildtype v. homozygous: $q_{(25)} = 6.237$, $p = 0.0005$).

$Tbr1^{layer5}$ mutants exhibit increased open arm exploration and decreased social interaction.

We assessed ASD-related behaviors, specifically motor ability, anxiety, and social interaction, on littermate cohorts of $Tbr1^{wildtype}$, $Tbr1^{layer5}$ heterozygous, and $Tbr1^{layer5}$ homozygous mutant male and female mice between P56-80. $Tbr1^{layer5}$ heterozygous and $Tbr1^{layer5}$ homozygous mutants did not show impairments in locomotion as measured by speed in the open field (Fig 13A) or in motor coordination as measured by performance on a rotarod (Fig 13C) compared to wildtype controls. $Tbr1^{layer5}$ mutants did not show significant difference in anxiety, measured by time spent in the center of a novel open field (Fig 13B). However, in the elevated plus maze $Tbr1^{layer5}$ homozygous mutants did spend an increased time in the open arms (Fig 13D: n = 11/8/9, wildtype/ heterozygous/ homozygous; t-test, wildtype v. heterozygous: $t_{(19)} = 2.355$, $p = 0.0294$) suggesting decreased anxiety or increased exploratory drive in the $Tbr1^{layer5}$ homozygous mutant mice.

To specifically assay social behavior, we measured the time the experimental mouse spent exploring a novel juvenile wildtype mouse of the same sex introduced to its home cage. Subsequently, we measured the amount of time the subject mouse spent exploring a novel object introduced to its home cage. We did not find differences in the time $Tbr1^{layer5}$ mutants spent exploring a novel object (Fig 13E). However, in the $Tbr1^{layer5}$ homozygous mutants, we observed a significant decrease in the time spent interacting with the novel juvenile mouse (Fig 13F: n = 11/5/12, wildtype/ heterozygous/ homozygous; One-way ANOVA, $F_{(2,25)} = 16.51$, $p < 0.0001$; t-test, Tukey correction, wildtype v. homozygous: $q_{(25)} = 7.124$, $p < 0.0001$; heterozygous v. homozygous: $q_{(25)} = 6.295$, $p = 0.0004$). This pronounced reduction of social exploration in the $Tbr1^{layer5}$ homozygous mutants is suggestive of core ASD behavioral characteristics.

Discussion

Persistent *Tbr1* function drives a partially irreversible sequence of developmental processes: Neonatal Tbr1 specifies properties of a sublamina of neocortical layer 6 (corticothalamic) and represses layer 5 (corticofugal) identity.

Tbr1 is expressed in the excitatory neurons of the neocortex (subplate, layer 6, rostral layer 5, layers 2/3), hippocampus, entorhinal cortex, pallial amygdala, piriform cortex, olfactory bulb and Cajal Retzius neurons (Hevner, Neogi, Englund, Daza, & Fink, 2003; Hevner et al., 2001). Analysis of $Tbr1^{constitutive}$ null mice demonstrated its function in the differentiation of the first waves of pallial glutamatergic neurons including Cajal Retzius cells, olfactory bulb mitral cells, subplate cells and layer 6 cells (Bedogni et al., 2010; Bulfone et al., 1998; Hevner, Miyashita-Lin, & Rubenstein, 2002). Further analyses of $Tbr1^{constitutive}$ null mice revealed that *Tbr1* promotes the identity of layer 6 neurons by repressing layer 5 molecular properties in layer 6 pyramidal neurons (McKenna et al., 2011).

In the present study, using conditional mutagenesis, we have demonstrated that *Tbr1* is required in maintaining subplate and layer 6 identity. The impaired differentiation of subplate and layer 6 neurons is indicated both molecularly (Figs. 2, 3, 4) and by dendritic defects (Fig. 6). Molecularly, $Tbr1^{layer6}$ mutant neurons have reduced expression of layer 6 markers including *Wnt7b*, *Foxp2* and *Tle4* (Figs. 2, 4) and possess an increased expression of genes controlling layer 5 molecular properties including *Bcl11b*, *Fezf2*, *Foxp1, Epha7 and Grin3a* (Figs. 2, 4 and Supplementary Fig. 4). Strikingly, the expression of *Tle4* and *Foxp2* is mainly reduced in the deep layer 6 neurons (layer 6b), even though *Tbr1* expression is uniformly reduced in the layer 6 of $Tbr1^{layer6}$ mutant (Fig. 4). This phenomenon may suggest that *Tbr1* may have preferential function within layer 6. The ectopic expression of layer 5 markers in the $Tbr1^{layer6}$ mutants suggests that layer 6 neurons have changed fate to a layer

5 identity (Fig. 2, 4). The change in the dendritic patterning of the *Tbr1*^{layer6} mutants further strengthens the hypothesis that the layer 6 neurons have changed fate to a layer 5 identity, in which the *Tbr1*^{layer6} mutants extends their apical dendrites superficially into the marginal zone (Fig. 6) (Lefebvre, Sanes, & Kay, 2015).

Preliminary investigation into gene regulation by *Tbr1* in layer 5 neurons did not draw any conclusive results. Batch-FACS RNA-seq on *Tbr1*^{layer5} mutant cells did not find any significant variations in RNA expression suggesting differential gene regulation in *Tbr*^{wildtype} versus *Tbr1*^{layer5} mutants. Previous studies have described layer 5 pyramidal neurons throughout somatosensory, visual, and frontal cortices as heterogeneous populations with different projection targets, morphology, electrophysiological properties, and receptor expression (Morishima and Kawaguchi, 2006; Dembrow *et al.*, 2010, Gee *et al.,* 2012; Harris and Shepherd, 2015; Clarkson *et al.,* 2017). Batch RNA-seq likely failed to turn up significant results because of differential gene regulation by *Tbr1* within the different subpopulations of pyramidal neurons within layer 5. In order to address this issue, we are planning to perform single-cell RNA-seq on *Tbr1*^{layer5} mutant cells.

Lastly, both *Tbr1*^{layer6} and *Tbr1*^{layer5} mutant neurons have increased levels of h-current (layer 6, Fig. 9a & b and Supplementary Fig. 5; layer 5, Fig. 10), which is one of the physiological properties of D2R-expressing layer 5 pyramidal neurons (Clarkson *et al.*, 2017; Gee et al., 2012; Lee et al., 2014). Recent studies have demonstrated that there are at least two subclasses of pyramidal neurons within layer 5 (Gee et al., 2012; Seong & Carter, 2012). These pyramidal subtypes are part of distinct circuits. ‘Type B’ pyramidal cells are thin-tufted pyramidal neurons that express *Drd1* gene and are intratelencephalic (IT), with projections to contralateral cortex and lack h-current. ‘Type A’ cells are thick-tufted pyramidal neurons that express *Drd2* gene, with projections to thalamus and pons but not to contralateral cortex and possess h-current (Dembrow, Chitwood, & Johnston, 2010; Gee et

al., 2012). In the *Tbr1*^{layer6} mutants, the decreased expression of *Drd1* (Fig. 2) and increased levels of HCN1 protein (Supplementary Fig. 5) suggests that during the layer 6 to layer 5 fate change, there is a bias towards generating more type A layer 5 pyramidal neurons. Furthermore, the elevated h-current resembles the physiological properties of type A pyramidal neurons that are usually positioned in layer 5b (Clarkson et al., 2017; Dembrow et al., 2010; Gee et al., 2012; Lee et al., 2014). Thus, *Tbr1* persistent function is required to initiate, orchestrate and maintain layer 6 specific program of molecular, dendritic and physiological properties. Although we currently lack conclusive RNA-seq data from *Tbr1*^{layer5} mutants, the electrophysiological characteristic of exaggerated h-current (Fig. 10 and Fig. 11) suggests that loss of *Tbr1* function within layer 5 also drives generation of type A, D2R expressing, pyramidal neurons.

Contrary to the *Tbr1*^{constitutive} null mice where corticothalamic axons fail to grow and enter the thalamus (Hevner et al., 2002; Hevner et al., 2001), *Tbr1*^{layer6} mutants have corticothalamic projections that innervate the thalamus (Supplementary Fig. 1 and 2). However, their ramification within the thalamus is abnormal with decreased thalamic innervation in the anterior and anteromedial structure of thalamus (Supplementary Fig. 1 and 2). This suggests that even though *Tbr1* expression is required to initiate the corticothalamic pathway, it is not required to maintain these axons through P56 in the *Tbr1*^{layer6} mutant. Furthermore, ectopic subcortical projections or corpus callosum projections are not generated by the *Tbr1*^{layer6} mutant. Thus, despite taking on many layer 5 properties, the mutant layer 6 neurons do not grow layer 5-like axonal projections. This suggests that once the layer 6 program regulating axonal pathway choice is established by *Tbr1*, it is irreversibly maintained after approximately E18, once *Tbr1* is eliminated in the layer 6 neurons. On the other hand, *Tbr1* dependent programs for promoting layer 6 gene expression, repression of layer 5 gene expression, layer 6-specific dendritic patterning and

H-current physiological properties remain plastic and are dependent upon *Tbr1* function during later stages of development and adulthood (Fig. 2, 3, 4, and Supplementary Fig. 3 and 4).

Tbr1 directly regulates the transcription of genes that control layer 6 identity

Towards elucidating TBR1-regulated transcriptional pathways that control layer 6 properties, we combined transcriptomic analysis of FACS purified neonatal wildtype and *Tbr1*^{layer6} mutant (Fig. 2), with whole genome neonatal TBR1 ChIP-Seq (Fig. 5). This provides evidence to identify candidate regulatory elements (RE) that are bound by TBR1.

Transcription assays in neonatal neocortical primary cultures demonstrated that TBR1 functions as an activator or repressor of REs adjacent to genes whose expression changes in *Tbr1*^{layer6} mutant neurons (Fig. 3). Importantly, TBR1 activated REs near to genes whose expression was reduced in layer 6, and repressed REs near to genes whose expression was increased in layer 5. Future studies are needed to identify the nuclear co-factors that determine whether TBR1 acts as a transcriptional activator or repressor, although it is conceivable that the DNA sequence of the REs modifies TBR1's confirmation to control its activity. The discovery of these TBR1 regulated REs opens the possibility that these elements will show *in vivo* layer-specific activity which could be elucidated using transgenic experiments. These REs also serve as essential nodes for establishing the transcriptional circuits that drive TBR1 mediated gene expression.

Tbr1 may be involved in the processes that control excitatory and inhibitory synaptic development and maintenance.

A reduced density of excitatory and inhibitory dendritic synapses is a central phenotype of both the *Tbr1*^{layer6} and the *Tbr1*^{layer5} heterozygous and homozygous mutants

as seen in tissue sections from P21 and P56 (layer 6, Fig. 7 and Supplementary Fig. 3; layer 5; Fig. 8). A similar reduction was also seen in primary cultures grown from P2 cortex (data not shown). These findings were substantiated using slice physiology, where the *Tbr1*^{layer6} and *Tbr1*^{layer5} mutant neurons exhibit reduced sEPSCs and sIPSCs at P21 and P56 (layer 6, Fig. 7 and Supplementary Fig. 3; layer 5, Fig. 8).

We took advantage of transcriptome analysis of FAC-sorted RNA-Seq from neonatal layer 6 neurons of wildtype and *Tbr1*^{layer6} mutants to further elucidate and understand the *Tbr1*-regulated pathways that could contribute to the reduced synaptic phenotype (Fig. 2). *Tbr1* regulates the transcription of a large cohort of genes that could be involved in synaptic development and maintenance through regulating processes that may involve retinoic acid levels, G-protein coupled receptors, Wnt canonical signaling, cell adhesion molecules, cell-cell signaling, axonal growth, neurotransmission, etc. (Krishnan & Schiöth, 2015; Leung & Wong, 2017; Lim et al., 2009; Muram, Rowe, & Hirasawa, 2016; Yee & Chen, 2016). For instance, Wnt proteins comprise a large class of signaling molecules that regulate a variety of developmental processes, including synapse formation (Davis, Zou, & Ghosh, 2008; Liebl, McKeown, Yao, & Hing, 2010). Furthermore, it has been demonstrated that *Wnt7b* activates canonical wnt signaling (Davis et al., 2008). The *Wnt7b* activation of the canonical pathway has been linked to increased presynaptic inputs in the developing hippocampus (Davis et al., 2008).

Dysregulation of approximately 33% (66/178) *Tbr1* targets in *Tbr1*^{layer6} mutants of genes that are linked to biological processes such as regulating retinoic acid levels, G-protein coupled receptors, wnt canonical signaling and cell adhesion may contribute to the decreased synaptic density phenotype in the layer 6 mutant neurons (Fig. 7, Supplementary Fig. 3). The reduction in the synaptic transmission may lead to abnormal excitation and

inhibition levels in the cortical circuitry of the *Tbr1*^{layer6} mutants. Although the etiology of ASDs is heterogeneous, the two most prominent models for autism pathogenesis are abnormal brain wiring and an imbalance of excitation/inhibition (Bernardinelli, Nikonenko, & Muller, 2014; Rubenstein & Merzenich, 2003; Walsh, Morrow, & Rubenstein, 2008). These two deficits lead to abnormal information processing and may result in autism-like behaviors. The absence of correct excitatory or inhibitory inputs could alter the activity of the target neurons. These inappropriate levels of neuronal activity may result in abnormal information processing, which may lead to aberrant behaviors.

Tbr1^{layer6} mutants exhibit Autism-like behaviors with increased anxiety and aggressive behaviors.

Tbr1^{layer6} mutants are viable allowing us to interrogate their behavior, which was remarkably normal in many assays including assays of their motor functions, interest in novel objects, an assay of social interaction (Fig. 12). On the other hand, a measure of exploration, (time spent in the closed arms of an elevated plus maze), showed that both heterozygote and homozygotes *Tbr1*^{layer6} mutants spent more time in the closed arms (Fig. 12D), suggesting that they may have increased anxiety in open spaces. Furthermore, homozygous *Tbr1*^{layer6} mutants exhibited prolonged periods of aggressive behaviors with the juvenile mice (Fig. 12F). Increased anxiety and aggressive behaviors have been observed in some human patients with ASD (Gadow *et al.*, 2004; McClintock *et al.,* 2003). That loss of function of *Tbr1* within layer 6 impacts aggressive behaviors without deficits in normal social interactions suggests that *Tbr1* play diverse roles in layer 6 and layer 5 which differentially impact behavior.

Ntsr1-Cre recombination of *Tbr1* does not extend into many cortical regions, including the olfactory bulb, medial prefrontal neocortex, dorsomedial neocortex (cingulate

and retrosplenial), hippocampus and parahippocampus, piriform cortex, and pallial amygdala, ruling out the possibility that defects in *Tbr1*$^{+}$ neurons in these structures contributes to the behavior phenotypes. This is pertinent, as *Tbr1*^{constitutive} heterozygotes have abnormal amygdala connectivity that has been associated with deficits in social interaction, cognitive flexibility and associative memory (Huang et al., 2014). Thus, the highly specific molecular and physiological defects in the early born pyramidal neurons of the neocortical subplate and layer 6 can be implicated in the mutant's increased aggression and anxiety.

Tbr1^{layer5} mutants exhibit Autism-like behaviors with decreased social behaviors.

Unlike *Tbr1*$^{constitutive\ null}$ mice which typically die at birth, *Tbr1*^{layer5} mutants are viable allowing us to study the role of *Tbr1* in mature neurons. The *Tbr1*^{layer5} mutants performance was notably normal in several behavior tasks including assays of their motor functions and exploration of novel objects (Fig. 13). On the other hand in an elevated plus maze, a measure of anxiety and exploration, showed that homozygotes *Tbr1*^{layer5} mutants spent more time in the open arms (Fig. 13D), suggesting that they may have either decreased anxiety or an increased drive for exploration. Furthermore, homozygous *Tbr1*^{layer5} mutants exhibited a pronounced reduction in novel juvenile social interactions (Fig. 13F). Interestingly, loss of *Tbr1* function selectively throughout layer 5 and not layer 6 cortical neurons results in this severe social phenotype, reminiscent of a core ASD behavioral phenotypes in humans.

***Tbr1* loss-of-function mutations are associated with Autism Spectrum Disorders (ASDs).**

Genetic analyses of patients with ASD have identified TBR1 as a high confidence risk factor for ASDs (De Rubeis et al., 2014; Iossifov et al., 2014; Sanders et al., 2012; Willsey et al., 2013). Transcriptome analysis of FACS layer 6 neurons of neonatal wildtype and *Tbr1*^{layer6} mutant revealed that *Tbr1* regulates a small group of ASD genes including *Scn2a1, Foxp1, Wnt7b*, *Nuak1* (De Rubeis et al., 2014; Sanders et al., 2015) and *Foxp2* (Gong et al., 2004; Li, Yamagata, Mori, & Momoi, 2005). Microarray analysis of wildtype and *Tbr1* mutant (data not shown) as well as *in situ* hybridization experiments (Fig. 4H-H′), revealed that *Bcl11a* expression, a probable ASD gene (De Rubeis et al., 2014), is also reduced in *Tbr1* mutants.

De novo and inherited mutations in *TBR1* have been found in patients with ASDs (De Rubeis et al., 2014; Iossifov et al., 2014; Sanders et al., 2012; Willsey et al., 2013). Two of the TBR1 *de novo* mutations result in early termination and generate truncated proteins that lack a functional DNA-binding T-box domain (De Rubeis et al., 2014). It has been demonstrated that the two truncated TBR1 mutants can no longer function in transcription or in interactions with CASK (Huang & Hsueh, 2017; Wang et al., 2004) and FOXP2 (Deriziotis et al., 2014). Furthermore, it has been shown that *de novo* TBR1 mutations change the subcellular distribution of TBR1 (Deriziotis et al., 2014). All together, these studies demonstrated that *de novo* TBR1 mutations in ASD patients impair TBR1 ability to interact with FOXP2 (Deriziotis et al., 2014). Furthermore, FOXP2 and TBR1 are only co-expressed in layer 6 of the cerebral cortex and not in other layers of the cerebral cortex and amygdala. Thus, the interaction with FOXP2 can only partly account for the function of TBR1 during the development of pyramidal neurons of deep cortical layer 6.

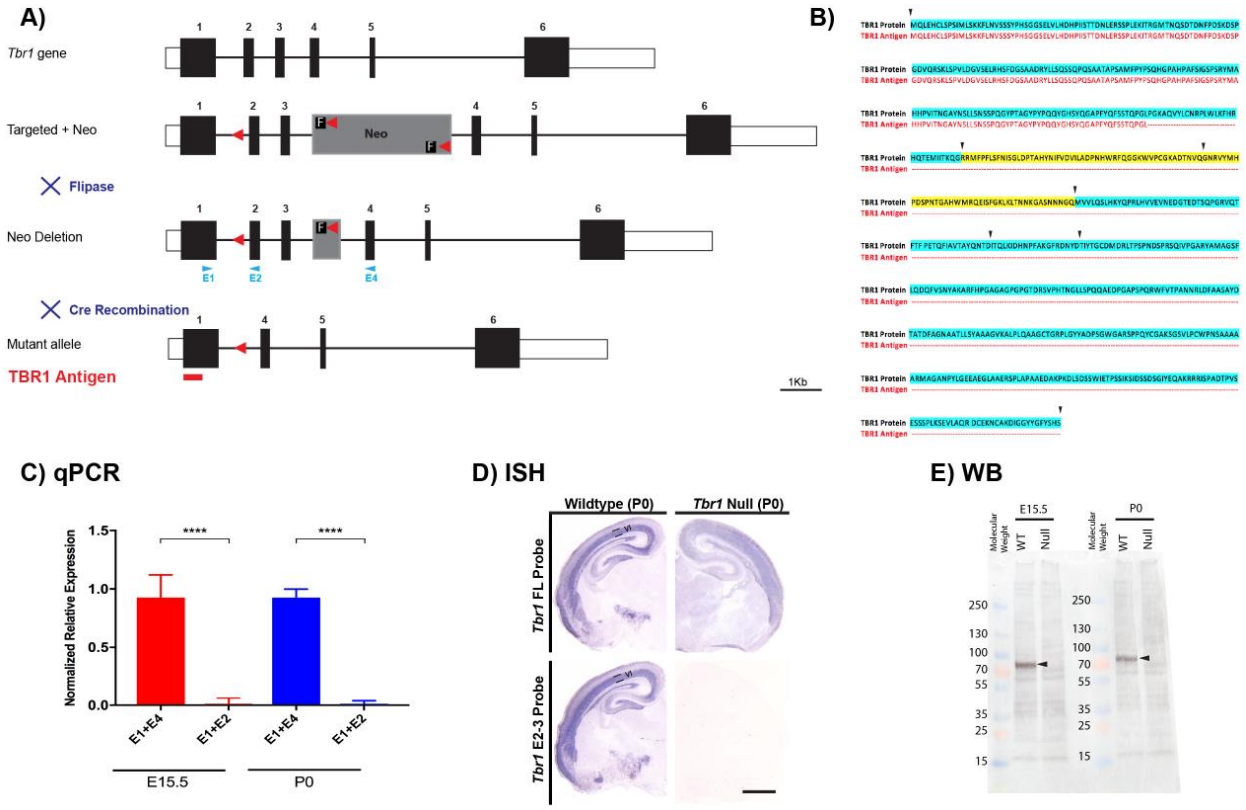

Figure 1. Organization of the *Tbr1* wildtype and conditional mutant (*Tbr1*^{f}) alleles.

(A) Schematic representations of the *Tbr1* wildtype allele, *Tbr1* targeting vector, and *Tbr1* conditional mutant allele (*Tbr1*^{f}). The wildtype *Tbr1* allele has six known exons (numbered black boxes, 1-6); the initiation codon is in exon 1, and the termination codon is in exon 6. The white boxes indicate the 5' and 3' UTRs. Red arrowheads correspond to the location of LoxP sites; the black boxes with an F inside are Frt sites. Flipase removes the Neomycin expression cassette (grey box with Neo inside). Upon Cre recombination, exons 2 and 3 are deleted to generate *Tbr1* mutant allele. The positions of the qPCR primers used for genotyping are indicated with blue arrowheads under exons 1, 2 and 4. The location of TBR1 antigen that was detected with antibodies for western blotting (panel E) and for immunohistochemistry (Figure 5) is indicated by the red line under part of exon 1. **(B)** Amino acid alignment of full-length TBR1 protein (black) with TBR1 antigen (red). Black arrowheads represent exonic boundaries. Region highlighted in yellow indicates the amino acid sequence corresponding to the deleted region in the *Tbr1* mutant allele. **(C)** qRT-PCR results corresponding to relative expression levels of *Tbr1* exons 1 and 2 (E1+E2) as well as exons 1 and 4 (E1+E4) transcripts in the cortex of *Tbr1* constitutive null and wildtype littermates at E15.5 and P0. Gene expression levels were analyzed using two biological replicates, each assayed in experimental triplicates. The error bars represent the standard error of the mean of all replicates; gene expression is normalized relative to a housekeeping gene (*Ef1α*). Relative expression levels in wildtype mice were defined as 1.0 (**P* <0.05) (***P* < 0.01) (****P*<0.001). **(D)** *In situ* hybridization (ISH) on coronal sections of P0 forebrain from

wildtype and *Tbr1* constitutive null. *Tbr1* full-length (FL) probe and *Tbr1* probe corresponding to exons 2 and 3 (E2-3) were used during the hybridization step. Layer 6 is labeled as VI. Scale bar = 50 μm. **(E)** Western blot (WB) to detect TBR1 protein isolated from E15.5 and P0 cortex of a *Tbr1* constitutive null and wildtype littermate. Black arrowhead indicates the TBR1 protein (~75 kDa) detected in wildtype at E15.5 and P0.

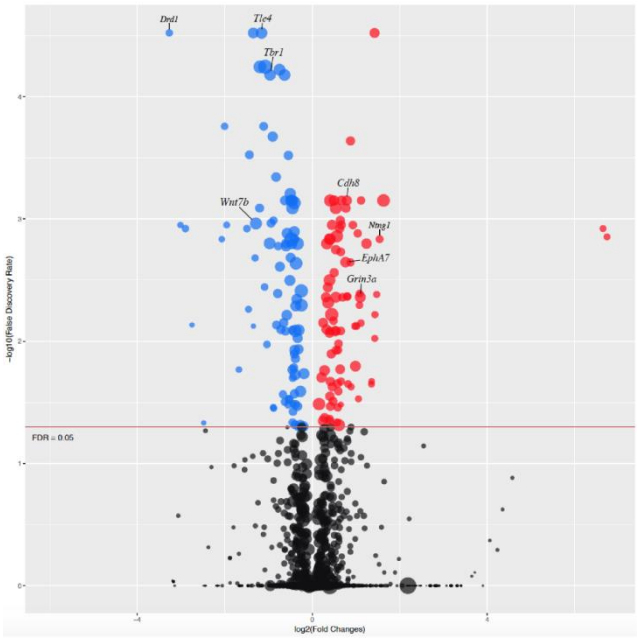

Figure 2. RNA-seq analysis of FACS purified layer 6 neurons shows differentially regulated RNAs between wildtype and *Tbr1*^{layer6} mutants.

Volcano plot of differentially expressed RNAs of *Tbr1*^{wildtype} and *Tbr1*^{layer6} mutant from FAC-sorted cells at P5. Up-regulated and downregulated genes in *Tbr1*^{layer6} mutant are in represented in red and blue respectively. Black dots represent a group of genes that did not reach statistical significance (α=0.05). The size of each point represents the difference in the median gene expression between *Tbr1*^{wildtype} and *Tbr1*^{layer6} mutant samples.

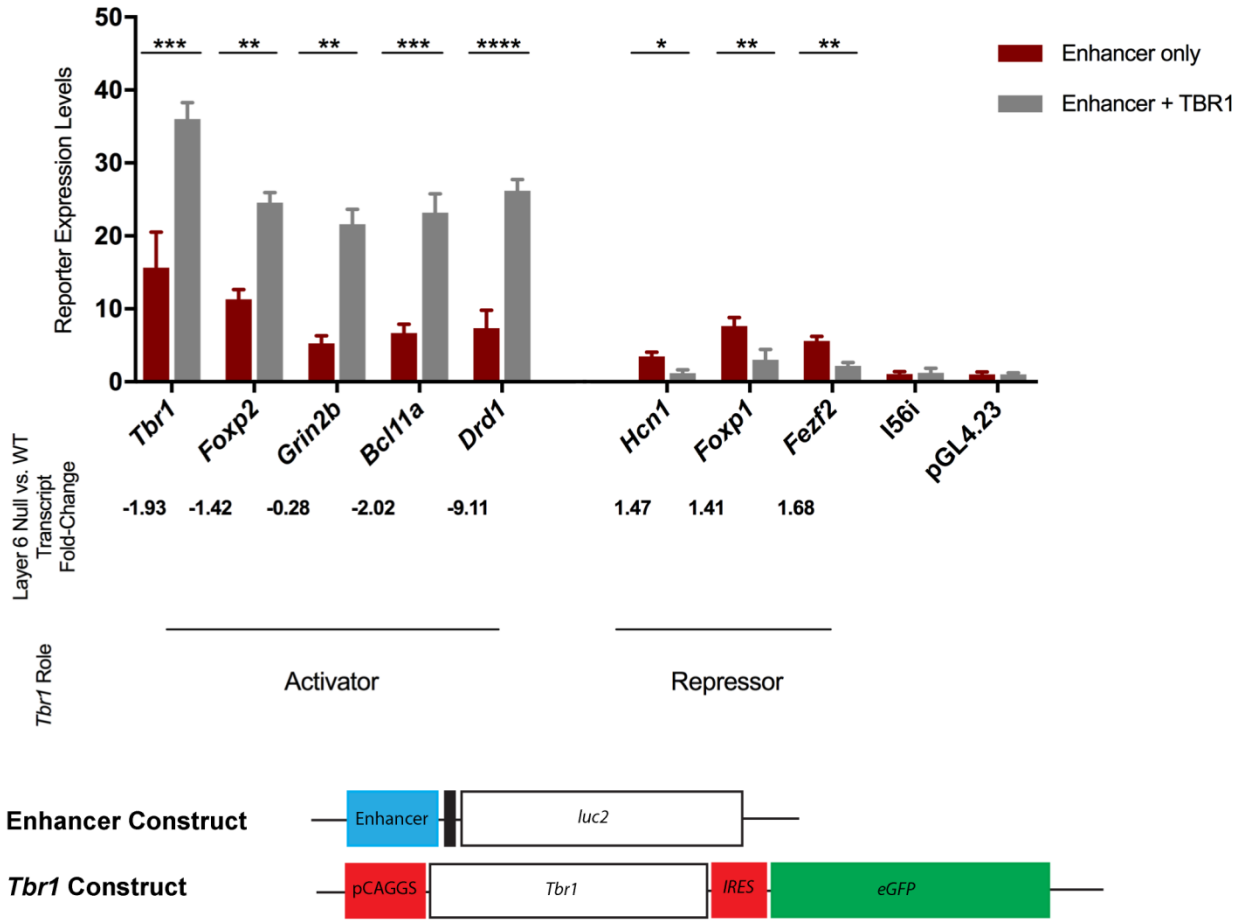

Figure 3. TBR1 transcriptional regulation of candidate enhancer regions in loci adjacent to *Tbr1*-regulated genes.

Luciferase transcription assay was utilized to measure activity of *Tbr1, Foxp2, Grin2b, Foxp1, Fezf2, Drd1, Hcn1* candidate enhancers in primary cultures made from P0 cortex (transfected on 1 DIV; assay on 3 DIV). The reporter activity was measured under enhancer activity alone (red) and enhancer co-transfected with TBR1 (grey). TBR1 activates *Tbr1* (FC= 2.3, p= 0.0007), *Foxp2* (FC= 2.17, p= 0.0023), *Grin2b* (FC= 4.11, p= 0.0015), *Bcl11a* (FC= 3.46, p= 0.0002) and *Drd1*(FC= 3.57, p<0.0001), whereas TBR1 represses *Foxp1* (FC= -2.52, p= 0.0087), *Fezf2* (FC= -2.55, p= 0.0015) and *Hcn1* (FC= -2.9, p=0.0248). I56i enhancer and pGL4.23 empty vector were used as negative controls. The error bars represent the standard error of the mean of all replicates for each enhancer relative to I56i enhancer and the empty pGL4.23 vector (in which the enhancers were inserted). T-test with Welch's correction was used for the statistical analysis of the enhancer alone (red) and enhancer co-transfected with TBR1 (grey). (*p<0.05) (**p< 0.01) (***p<0.001).

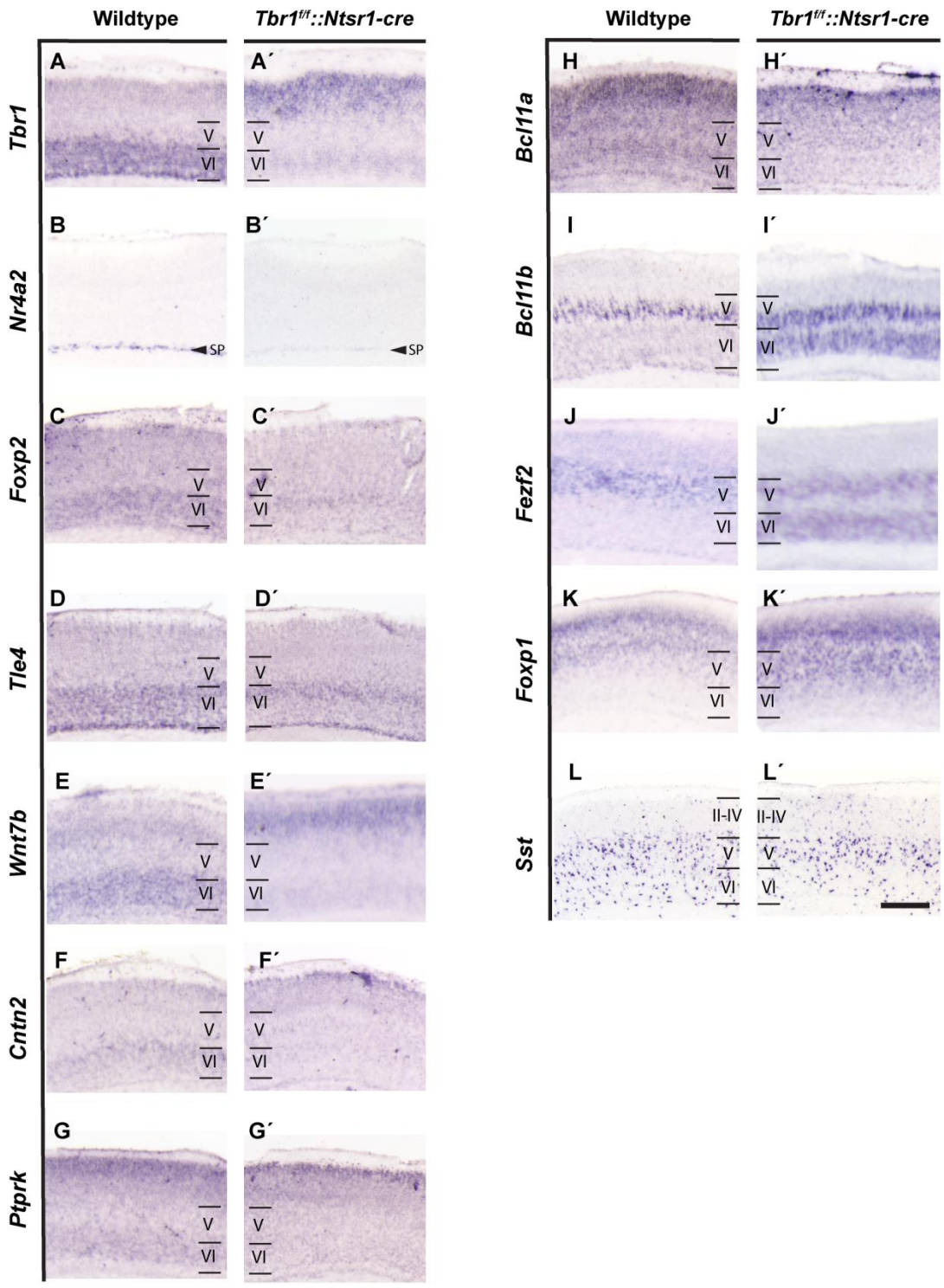

Figure 4. *Tbr1* is required to maintain layer 6 identity in postnatal cortex.

In situ hybridization on coronal sections of P3 somatosensory cortex (S1) of *Tbr1*^{wildtype} **(A-L)** and *Tbr1*^{layer6} homozygous mutants *(Tbr1*$^{f/f}$*::Ntrs1-cre)* **(A´- L´)**. In *Tbr1*^{layer6} mutants, *Tbr1* **(A-A´)**, *Foxp2* **(C-C´)**, *Tle4* **(D-D´)** and *Wnt7b* **(E-E´)**, *Cntn2* **(F-F´)**, *Ptprk* **(G-G´)** and *Bcl11a* **(H-H´)** expressions are reduced in layer 6. This decrease is accompanied by an increase in the expression of *Tbr1* and *Wnt7b* in the superficial layers **(A-A´, E-E´)**. *Nr4a2* expression decreases in the subplate of *Tbr1*^{layer6} mutants **(B-B´)**. *Tbr1*^{layer6} mutants have ectopic layer 6 expression of *Bcl11b* **(I-I´)**, *Fezf2* **(J-J´)** and *Foxp1* **(K-K´)**. In *Tbr1*^{layer6} mutant, *Sst*$^{+}$ CINs are reduced in layer 6, unchanged in layer 5, and increased in layers 2-4 **(L-L´)**. II-IV = layers 2-4, V = layer 5, VI = layer 6. SP: Subplate. Scale bar = 50µm.

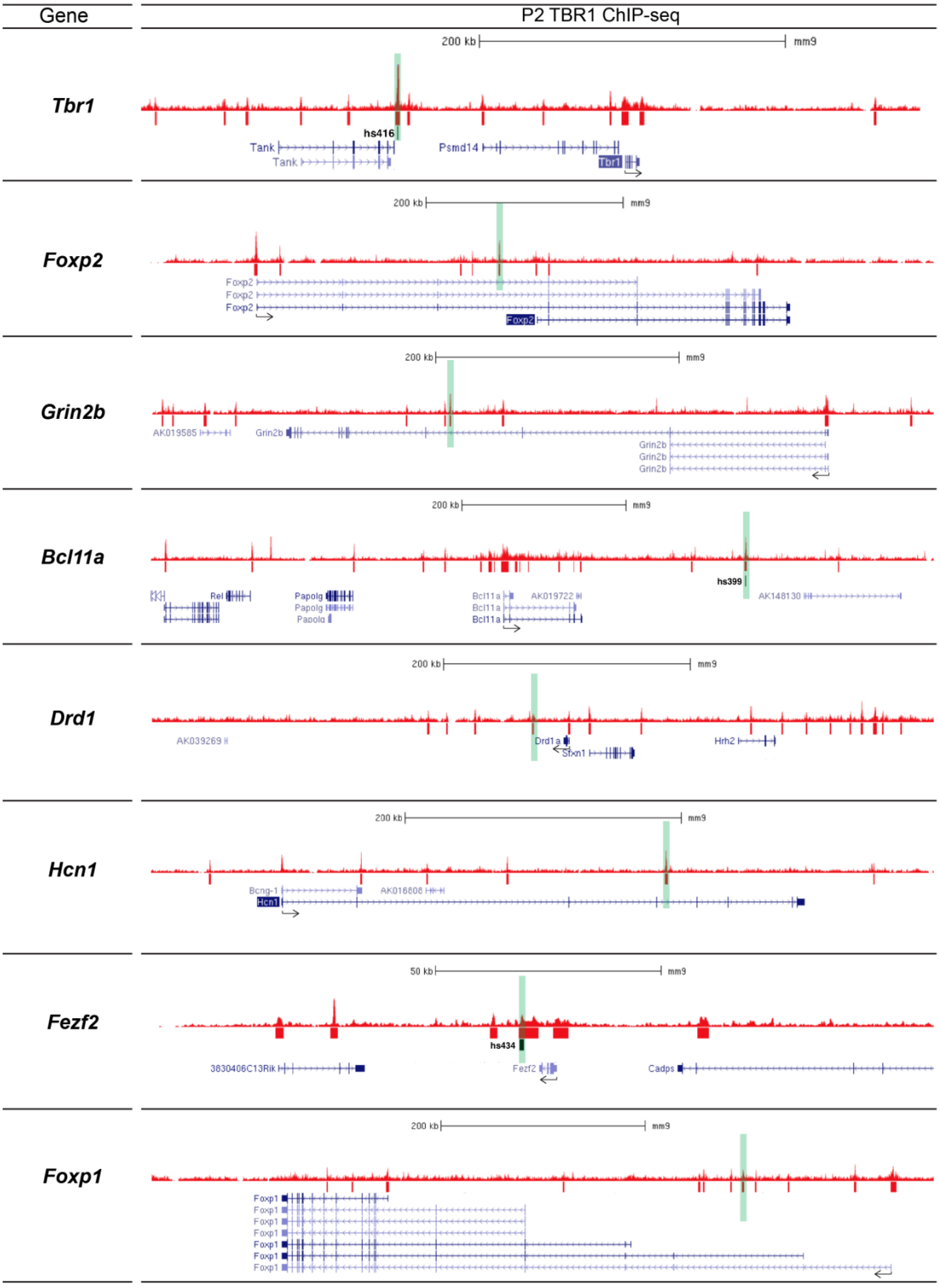

Figure 5. TBR1 binds to the promoter and candidate enhancer regions of genes whose expression changes in *Tbr1* mutant cortex.

TBR1 ChIP-Seq on wildtype whole cortex at P2 (red tracks) demonstrates TBR1 binding to either promoter or candidate enhancer regions. Red boxes below the ChIP-Seq track indicate that TBR1 binding reached statistical significance. Genes (exons and RNA transcripts) are shown in blue. Green boxes highlight the candidate enhancer regions that were tested in the luciferase transcription assay. Black boxes indicate genomic regions used in the luciferase assay, that have proven enhancer activity in the E11.5 cortex corresponding hs416 (*Tbr1* locus), hs434 (*Fezf2* locus) and hs399 (*Bcl11a* locus). Black arrow indicates the direction of transcription. Genomic scale (in kb) are shown for each locus.

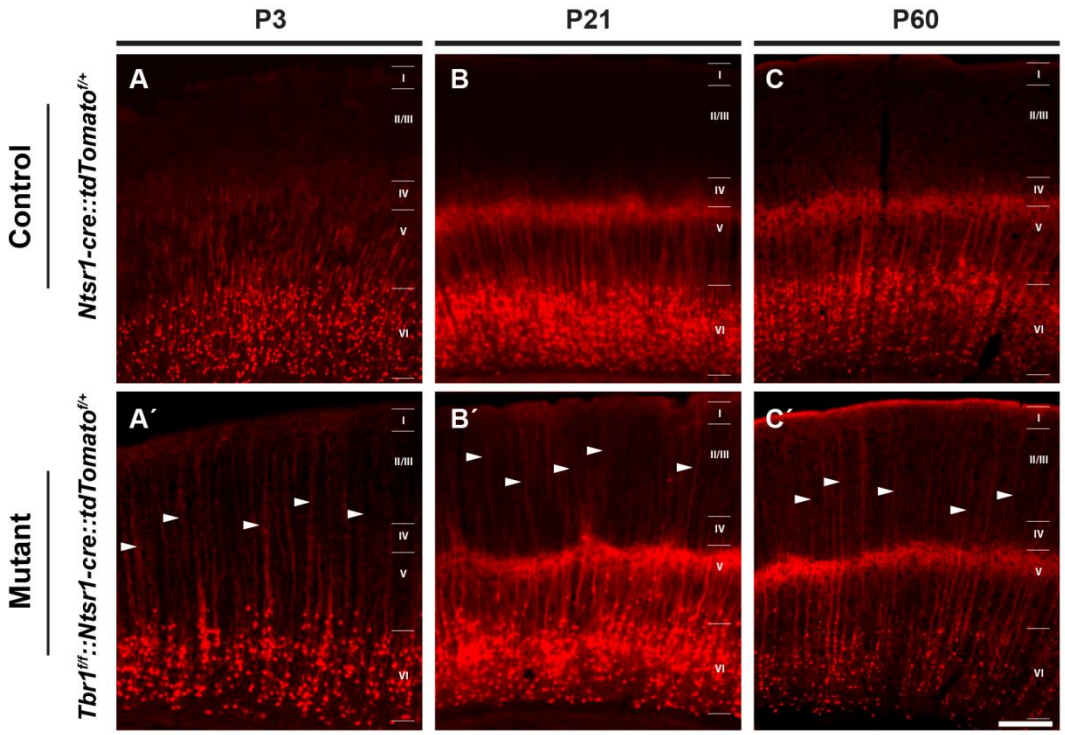

Figure 6. Ectopic growth of layer 6 apical dendrites into superficial layer 1 in *Tbr1*^{layer6} mutants.

The endogenous tdTomato fluorescence (red) in the somatosensory cortex of **(A)** *Tbr1* ^{wildtype} and **(B)** *Tbr1*^{layer6} mutant. These lines had the *Ntsr1-cre::tdTomato*$^{f/+}$ alleles to label the layer 6 cell bodies and their dendrites. White arrowheads in panel A´- C´ indicate some of the apical dendrites extending through layers 2/3 to layer 1 in *Tbr1*^{layer6} mutant. Cortical layers are labelled. Scale bar: 50µm.

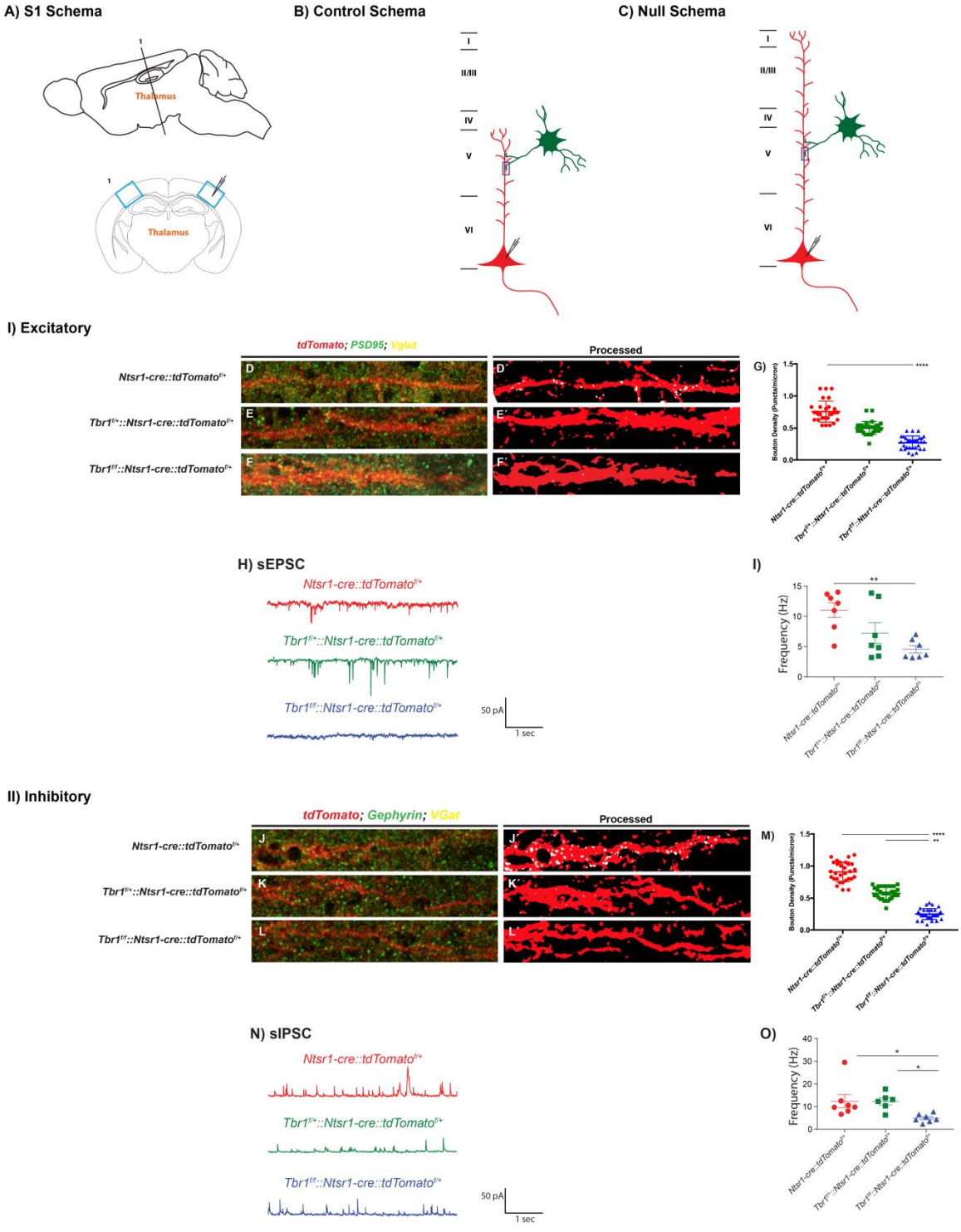

FIGURE 7. Loss of *Tbr1* in layer 6 reduces excitatory (I) and inhibitory (II) synaptic input onto the layer 6 neurons in the somatosensory cortex at P21.

(A) Schematic representation of coronal slice of somatosensory cortex (S1, blue boxes). The blue box represents the region of somatosensory cortex (S1) utilized for imaging and whole-cell patch clamp experiments. **(B, C)** Schema of layer 6 projection neuron (red) in somatosensory cortex of *Tbr1* $^{\text{wildtype}}$ **(B)** and *Tbr1*^{layer6} mutant **(C)**. The rectangles indicate the zone where synapses were analyzed **(B, C)** at P21. Pipette tip indicates that the soma was patched during the electrophysiology recordings **(B, C)**.

(I) Excitatory synaptic input was analyzed via synaptic bouton staining onto apical dendrites of layer 6 neurons **(D-F)** and spontaneous EPSC (sEPSC) recordings from the soma of the layer 6 pyramidal neurons **(H)** of *Tbr1* $^{\text{wildtype}}$ **(D)** *Tbr1*^{layer6} heterozygous mutants, and **(E)** *Tbr1*^{layer6} homozygous mutants **(F)** at P21 **(D, E, F)**. These lines had the *Ntsr1-cre::tdTomato*$^{f/+}$ alleles to label the layer 6 neurons by tdTomato's endogenous fluorescence (red). ImageJ software was used to process confocal images **(D-F)** for quantification **(D´ – F´)**. **(G)** Quantification of VGlut1^{+} boutons and PSD95^{+} clusters co-localizing onto the apical dendrites of layer 6 neurons at P21. **(H)** Sample traces of sEPSC recordings in voltage clamp at -70mV in somatosensory cortex slices from 4 weeks old *Tbr1* $^{\text{wildtype}}$ **(**red**)**, *Tbr1*^{layer6} heterozygous mutants (green), and *Tbr1*^{layer6} homozygous mutants (blue) at P21. **(I)** Quantification of the sEPSC frequency in layer 6 neurons at P21.

(II) Inhibitory synaptic input was examined through synaptic bouton staining onto apical dendrites of layer 6 neurons **(J – L)** and spontaneous IPSC (sIPSC) recordings from the soma of the layer 6 neurons **(N)** of *Tbr1* $^{\text{wildtype}}$ **(J)**, *Tbr1*^{layer6} heterozygote mutants **(K)**, and *Tbr1*^{layer6} homozygous mutants **(L)** at P21 **(J, K, L)**. These lines had the *Ntsr1-cre::tdTomato*$^{f/+}$ alleles to label the layer 6 neurons by tdTomato's endogenous fluorescence (red). ImageJ software was used to process confocal images **(J – L)** for quantification **(J´ – L´)**. **(M)** Quantification of VGat^{+} boutons and Gephyrin^{+} clusters co-localizing onto the apical dendrites of layer 6 neurons at P21. **(N)** Sample traces of sIPSC recordings in voltage clamp at +10mV in somatosensory cortex slices from 4 weeks old *Tbr1* $^{\text{wildtype}}$ **(**red**)**, *Tbr1*^{layer6} heterozygous mutants (green), and *Tbr1*^{layer6} homozygous mutants (blue) at P21. **(O)** Quantification of the sIPSC frequency in layer 6 neurons at P21. Two-way ANOVA was used for the statistical analysis of the control, heterozygous and null. (*p<0.05) (**p< 0.01) (***p<0.001) (****p<0.0001). Scale bar (in F and L) = 5µm.

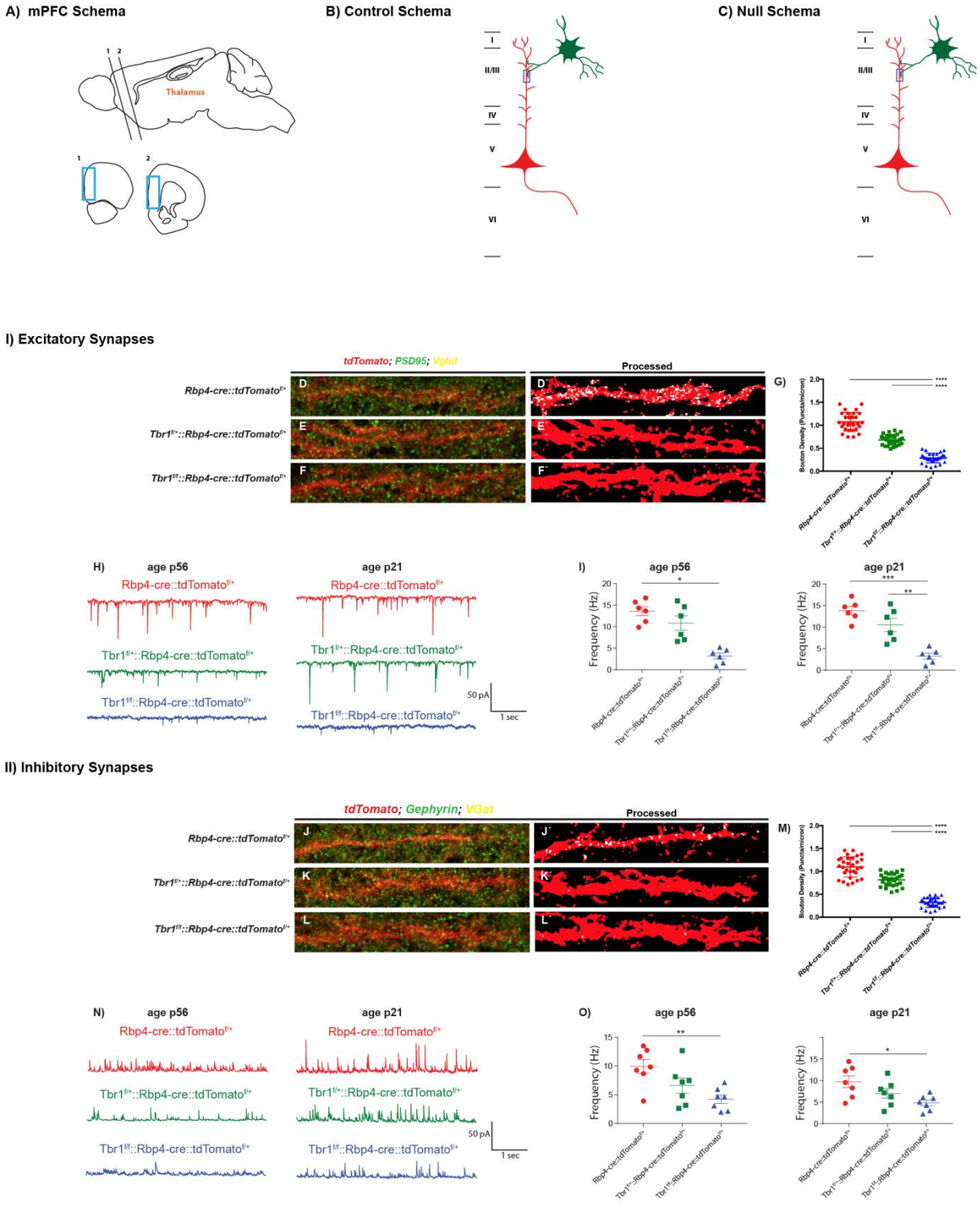

Figure 8. Loss of *Tbr1* in layer 5 reduces excitatory (I) and inhibitory (II) synaptic input onto the layer 6 neurons in the somatosensory cortex.

(A) Schematic representation of coronal slice of medial prefrontal cortex (mPFC, blue boxes). The blue box represents the region of mPFC utilized for imaging and whole-cell patch clamp experiments. **(B, C)** Schema of layer 5 projection neuron (red) in somatosensory cortex of *Tbr1* ^{wildtype} **(B)** and *Tbr1*^{layer5} mutant **(C)**. The rectangles indicate the zone where synapses were analyzed **(B, C)** at P21. Pipette tip indicates that the soma was patched during the electrophysiology recordings **(B, C)**.
(I) Excitatory synaptic input was analyzed via synaptic bouton staining onto apical dendrites of layer 5 neurons **(D-F)** and spontaneous EPSC (sEPSC) recordings from the soma of the layer 5 pyramidal neurons **(H)** of *Tbr1* ^{wildtype}, *Tbr1*^{layer5} heterozygous mutants, and *Tbr1*^{layer5} homozygous mutants at P21 and P56. These lines had the *Rbp4-cre::tdTomato*$^{f/+}$ alleles to label the layer 5 neurons by tdTomato's endogenous fluorescence (red). ImageJ software was used to process confocal images **(D-F)** for quantification **(D´ – F´)**. **(G)** Quantification of VGlut1^{+} boutons and PSD95^{+} clusters co-localizing onto the apical dendrites of layer 5 neurons at P21. **(H)** Sample traces of sEPSC recordings in voltage clamp at -70mV in somatosensory cortex slices from 4 and 8 weeks old *Tbr1* ^{wildtype} **(**red**)**, *Tbr1*^{layer5} heterozygous mutants (green), and *Tbr1*^{layer5} homozygous mutants (blue) at P21 and P56. **(I)** Quantification of the sEPSC frequency in layer 6 neurons at P21 and P56.
(II) Inhibitory synaptic input was examined through synaptic bouton staining onto apical dendrites of layer 5 neurons **(J – L)** and spontaneous IPSC (sIPSC) recordings from the soma of the layer 5 neurons **(N)** of *Tbr1* ^{wildtype}, *Tbr1*^{layer6} heterozygote mutants, and *Tbr1*^{layer6} homozygous mutants at P21 and P56. These lines had the *Ntsr1-cre::tdTomato*$^{f/+}$ alleles to label the layer 5 neurons by tdTomato's endogenous fluorescence (red). ImageJ software was used to process confocal images **(J – L)** for quantification **(J´ – L´)**. **(M)** Quantification of VGat^{+} boutons and Gephyrin^{+} clusters co-localizing onto the apical dendrites of layer 5 neurons at P21. **(N)** Sample traces of sIPSC recordings in voltage clamp at +10mV in somatosensory cortex slices from 4 and 8 weeks old *Tbr1* ^{wildtype} **(**red**)**, *Tbr1*^{layer5} heterozygous mutants (green), and *Tbr1*^{layer5} homozygous mutants (blue) at P21 and P56. **(O)** Quantification of the sIPSC frequency in layer 5 neurons at P21 and P56. Two-way ANOVA was used for the statistical analysis of the control, heterozygous and null. (*p<0.05) (**p< 0.01) (***p<0.001) (****p<0.0001). Scale bar (in F and L) = 5µm.

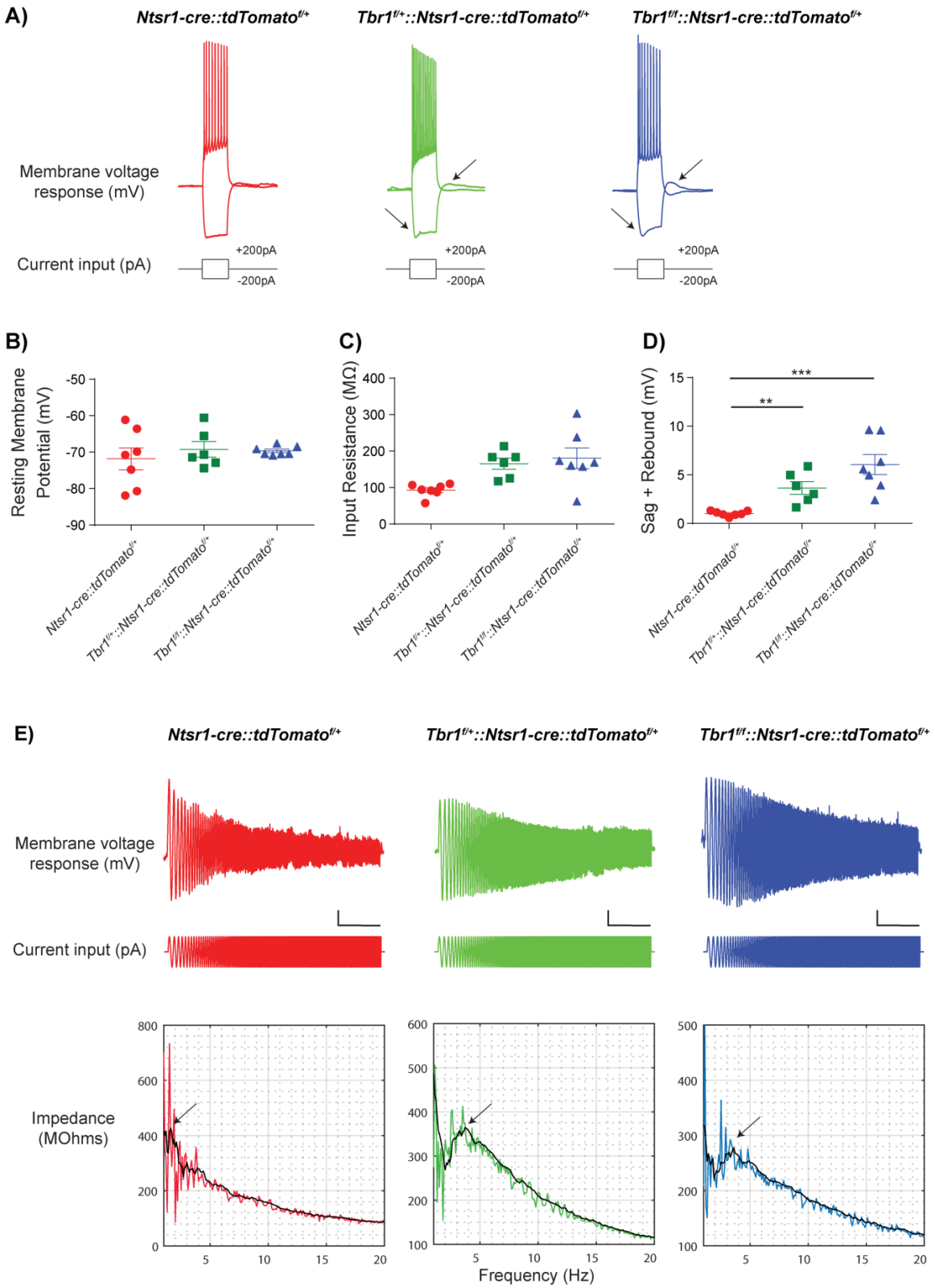

Figure 9a. Loss of *Tbr1* in layer 6 somatosensory cortex results in an increase in hyperpolarization-activated cation currents (Ih).

Whole-cell patch clamp recordings from layer 6 S1 at P56 **(A-D)** show that many intrinsic electrophysiological properties were unaffected by loss of *Tbr1*, including resting membrane potential **(B)**, input resistance **(C)**, and action potential halfwidth (data not shown). We estimated Ih by measuring the membrane potential sag and rebound elicited by a –200 pA current step. This characteristic "sag" and "rebound" during and following hyperpolarizing current injection is mediated by hyperpolarization-activated cyclic nucleotide-gated (HCN) channels. Sag and rebound were increased in $Tbr1^{layer6}$ heterozygous and $Tbr1^{layer6}$ homozygous mutants at P56.

(E) Neurons were held in current clamp at -70mV. We provided a sinusoidal current of constant amplitude (100 pA peak-to-peak) with its frequency linearly increasing from 0 to 20 Hz over 20 seconds. We used the ratio of the fast Fourier transform of the voltage response (top) to the fast Fourier transform of the sinusoidal current stimulus (middle) to calculate the impedance amplitude profile (bottom). We estimated the resonant frequency to be the frequency at which the impedance profile reached its peak (arrows). Scale bar = 5 mV, 5 s.

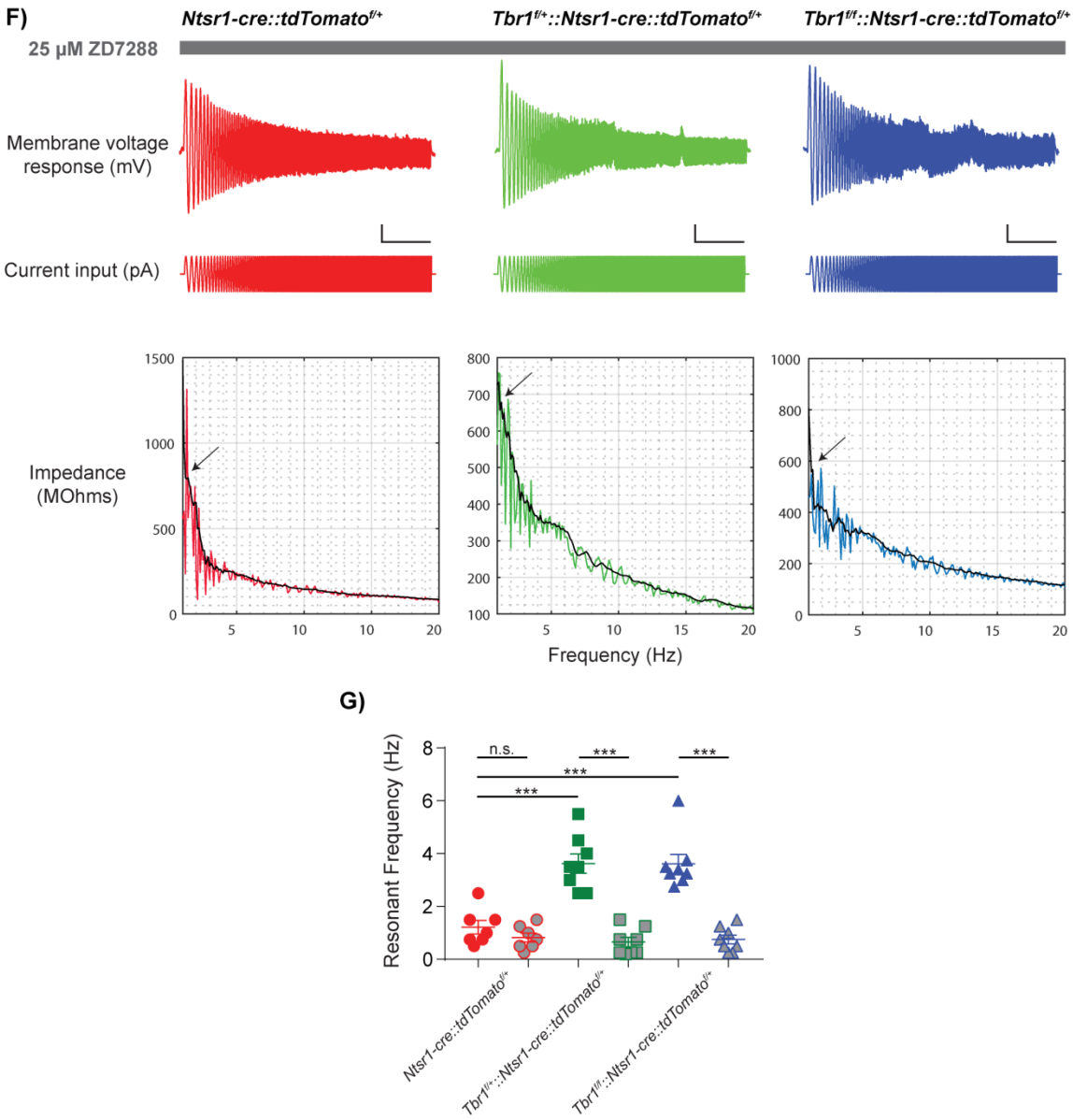

Figure 9a. Increased hyperpolarization-activated cation currents (Ih) in *Tbr1*^{layer6} mutants are blocked by HCN channel blocker ZD7288.

(F) Addition of ZD7288, an HCN channel blocker, did not significantly decrease the resonant frequency of *Tbr1*^{wildtype} (red) but did decrease it by over 50% in *Tbr1*^{layer6} heterozygote mutants (green), and *Tbr1*^{layer6} homozygous mutants (blue). **(G)** Quantification of changes in resonant frequency of *Tbr1*^{wildtype} (red), *Tbr1*^{layer6} heterozygote mutants (green) and *Tbr1*^{layer6} homozygous mutants (blue) after ZD7288 treatment. (**p< 0.01) (***p<0.001).

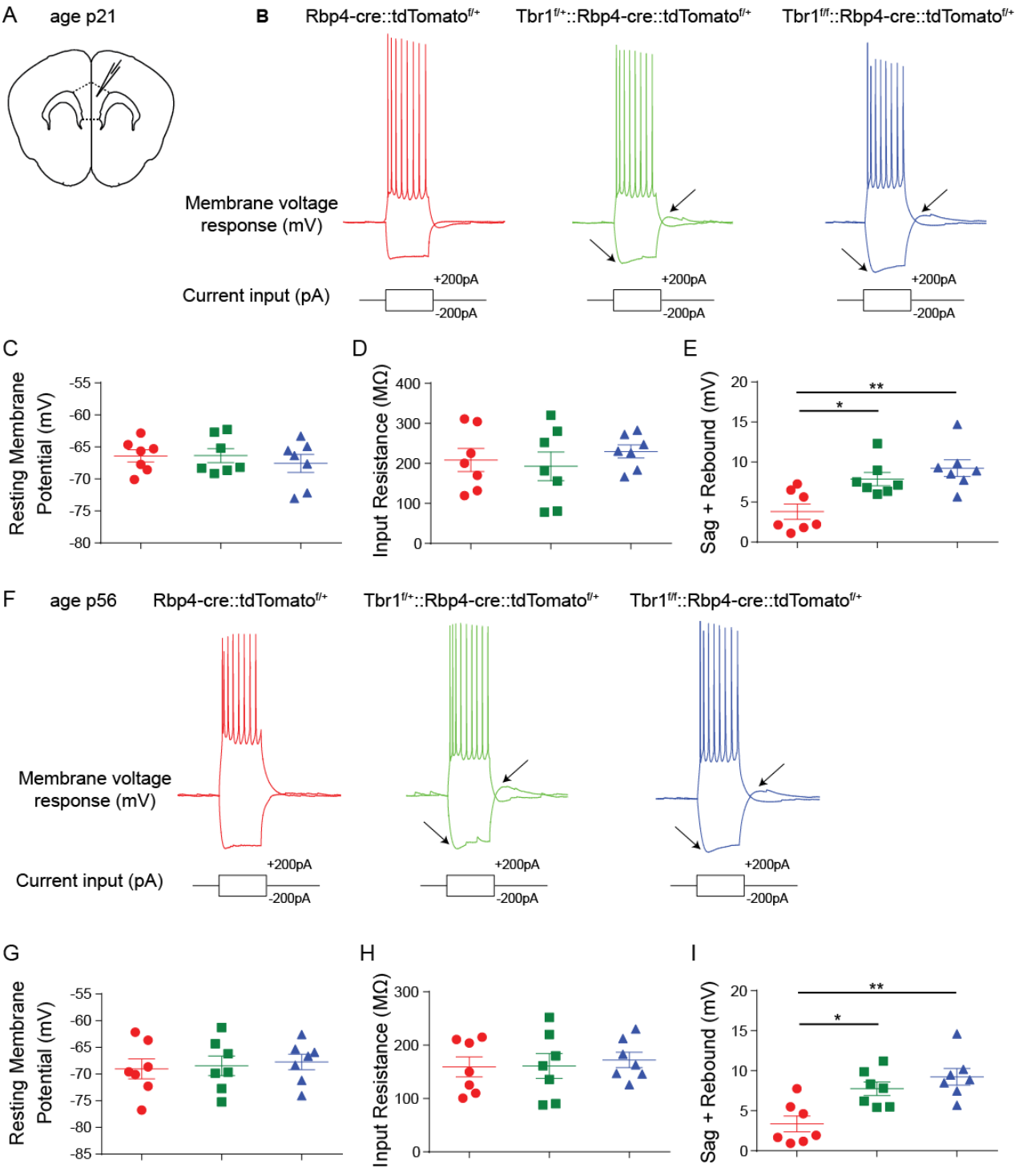

Figure 10. Loss of *Tbr1* in layer 5 mPFC results in an increase in hyperpolarization-activated cation currents (Ih).

Whole-cell patch clamp recordings from layer 5 mPFC at p21-p28 (**A-D**) and p56-p80 (**E-H**) show that many intrinsic electrophysiological properties were unaffected by loss of *Tbr1*, including resting membrane potential (**B, F**), input resistance (**C, G**), and action potential halfwidth (data not shown). We estimated Ih by measuring the membrane potential sag and rebound elicited by a –200 pA current step. This characteristic "sag" and "rebound" during and following hyperpolarizing current injection is mediated by hyperpolarization-activated cyclic nucleotide-gated (HCN) channels. At both ages p21-p28 (**D**) and p56-p80 (**H**), sag and rebound were increased. (*$p<0.05$) (**$p< 0.01$).

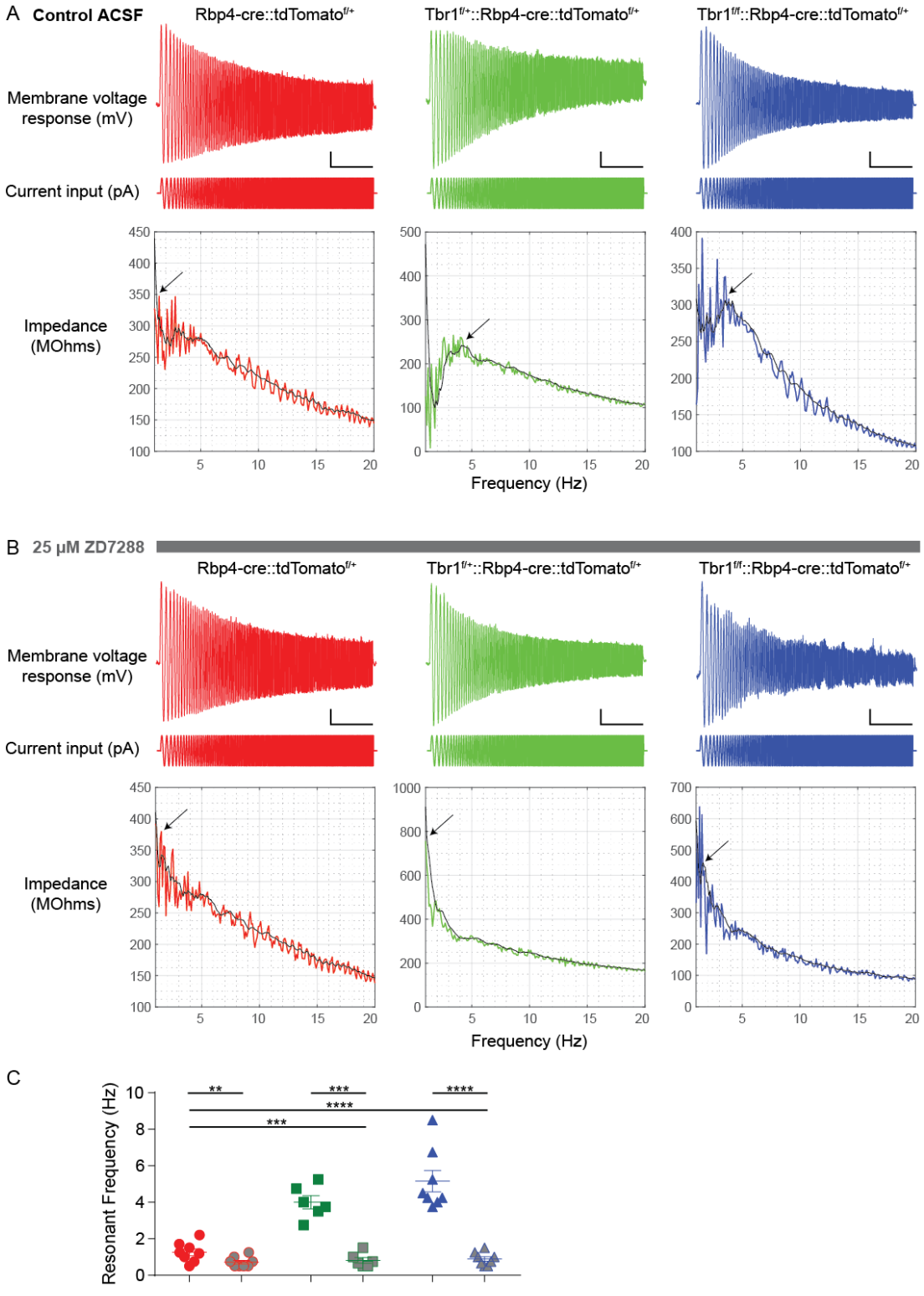

Figure 11. Loss of *Tbr1* increases layer 5 *Rbp4-cre* positive pyramidal neurons' resonant frequency within somatosensory cortex.

(**A**) Neurons were held in current clamp at -70mV. We provided a sinusoidal current of constant amplitude (100 pA peak-to-peak) with its frequency linearly increasing from 0 to 20 Hz over 20 seconds. We used the ratio of the fast Fourier transform of the voltage response (top) to the fast Fourier transform of the sinusoidal current stimulus (middle) to calculate the impedance amplitude profile (bottom). We estimated the resonant frequency to be the frequency at which the impedance profile reached its peak (arrows). Scale bar = 5 mV, 5 s. (**B**) Addition of ZD7288, an HCN channel blocker, did not significantly decrease the resonant frequency of *Tbr1*$^{\text{wildtype}}$ (red) but did decrease it by over 50% in *Tbr1*^{layer5} heterozygote mutants (green), and *Tbr1*^{layer5} homozygous mutants (blue). (**C**) Loss of *Tbr1* increased resonant frequency in both *Tbr1*^{layer5} heterozygote mutants (green), and *Tbr1*^{layer5} homozygous mutants (blue) which was blocked ZD7288. (***p<0.001).

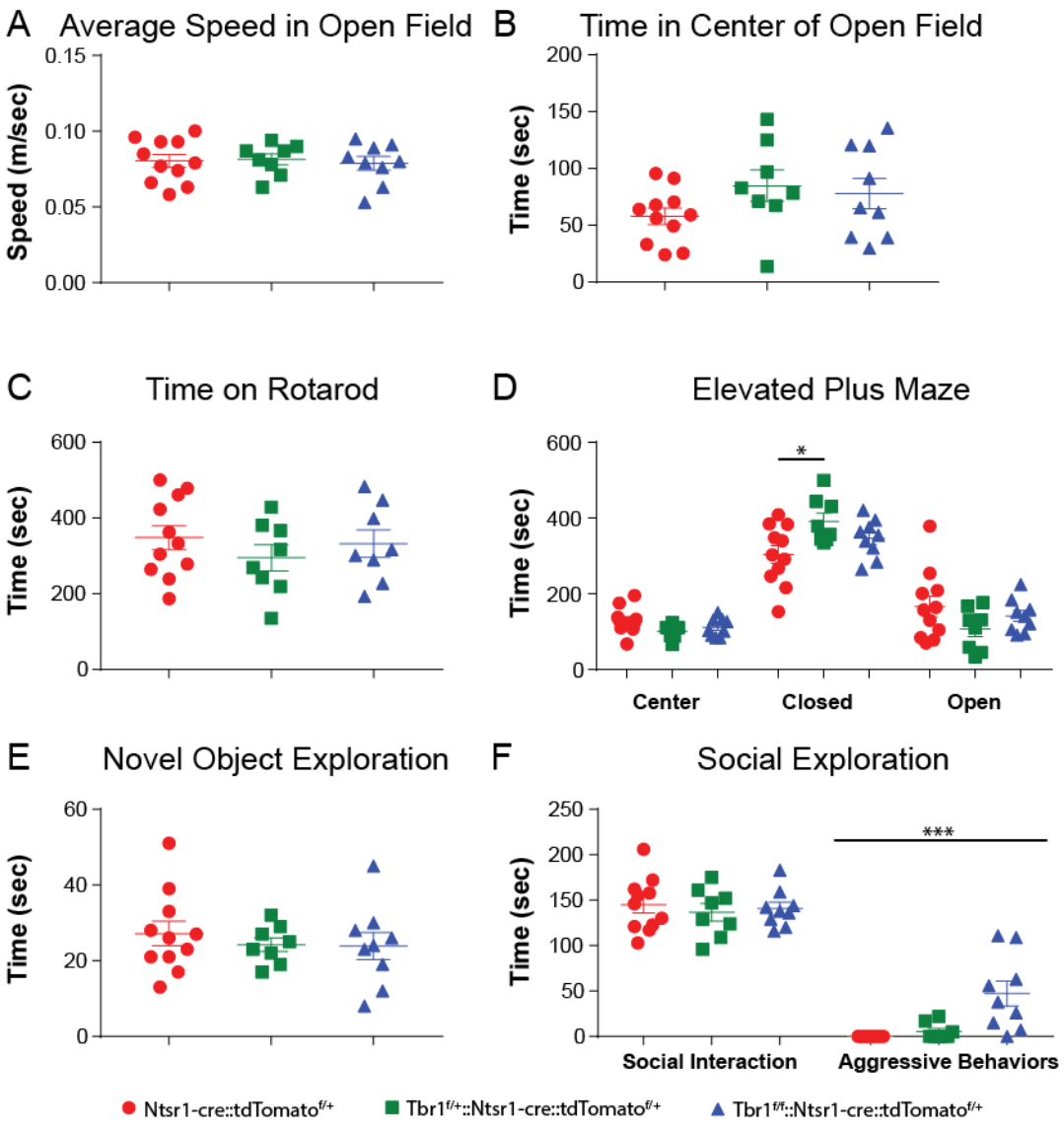

Figure 12. Loss of *Tbr1*in layer 6 Ntsr1cre positive neurons is associated with an increase in aggressive behaviors

All behavioral assays were performed on adult mice age p56-p80 with *Tbr1* ^{wildtype} shown in red, *Tbr1*^{layer6} heterozygous mutants in green, and *Tbr1*^{layer6} homozygous mutants in blue. Loss of *Tbr1* did not impair movement (**A**) or motor coordination (**C**) nor did it affect the time spent exploring the center of an open field arena (**B**). (**D**) *Tbr1*^{layer6} heterozygous mutants (green) and *Tbr1*^{layer6} homozygous mutants (blue) spent more time in the closed arms of an elevated plus maze than their *Tbr1*^{wildtype} littermates. Interestingly, loss of *Tbr1* did not affect the time spent engaged in social interaction (**F)** or novel object exploration (**E**). *Tbr1*^{layer6} homozygous mutants (blue) of both genders displayed an increase in aggressive behaviors when interacting with a novel juvenile mouse (**F**). (*p<0.05) (***p<0.001).

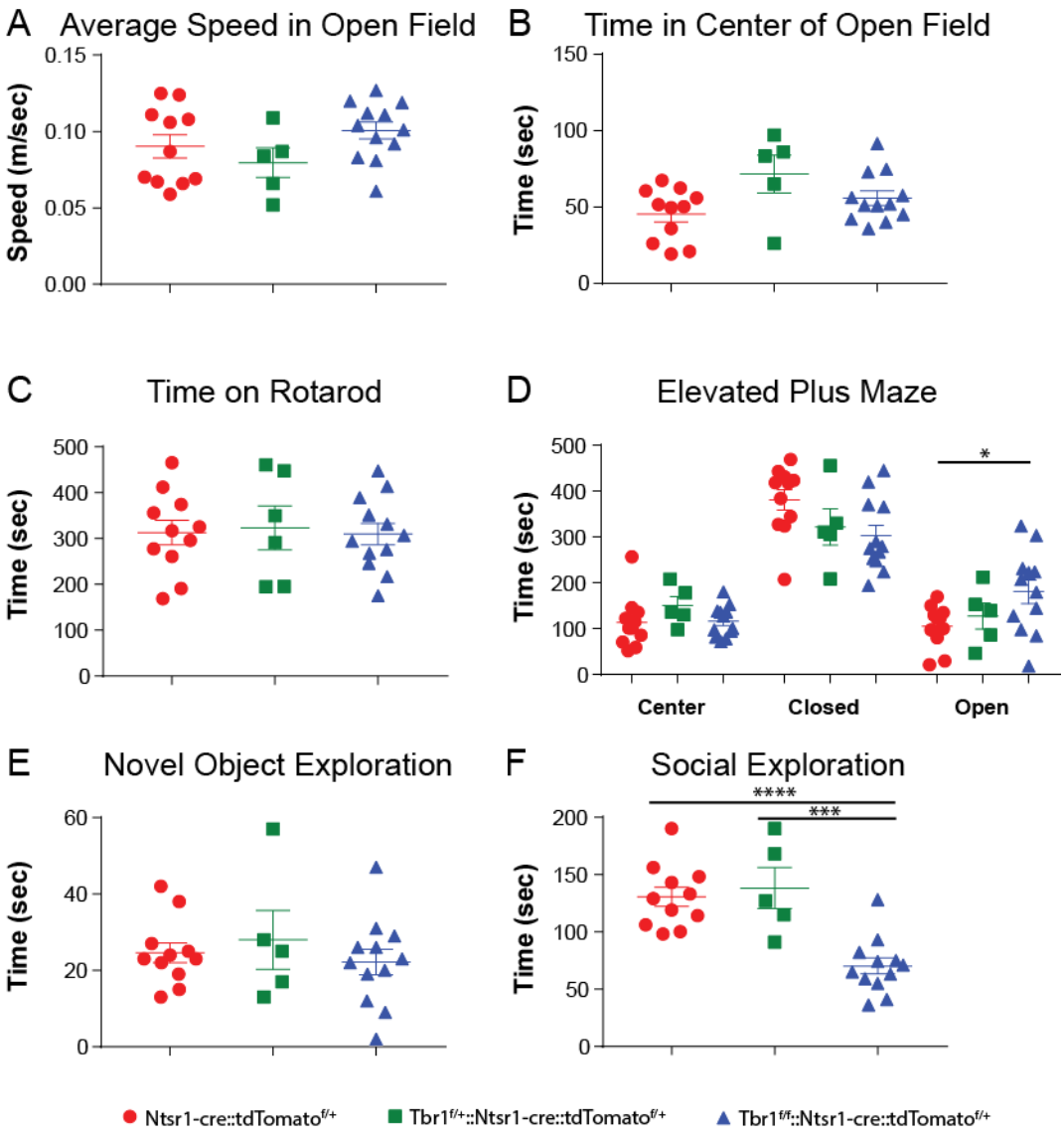

Figure 13. Loss of *Tbr1*in layer 5 *Rbp4-cre* positive neurons is associated with an increase in open arm exploration and decreased social interaction

All behavioral assays were performed on adult mice age p56-p80 with *Tbr1* ^{wildtype} shown in red, *Tbr1*^{layer5} heterozygous mutants in green, and *Tbr1*^{layer5} homozygous mutants in blue. Loss of *Tbr1* did not impair movement (**A**) or motor coordination (**C**) nor did it affect the time spent exploring the center of an open field arena (**A**). (**D**) *Tbr1*^{layer5} heterozygous mutants (green) and *Tbr1*^{layer5} homozygous mutants (blue) spent more time in the open arms of an elevated plus maze than their *Tbr1*^{wildtype} littermates. Loss of *Tbr1* did not affect the time spent engaged novel object exploration (**E**). *Tbr1*^{layer6} heterozygous (green) and *Tbr1*^{layer6} homozygous mutants (blue) of both genders displayed an decrease in social interaction (**F**). (*p<0.05) (***p<0.001) (****p<0.0001) .

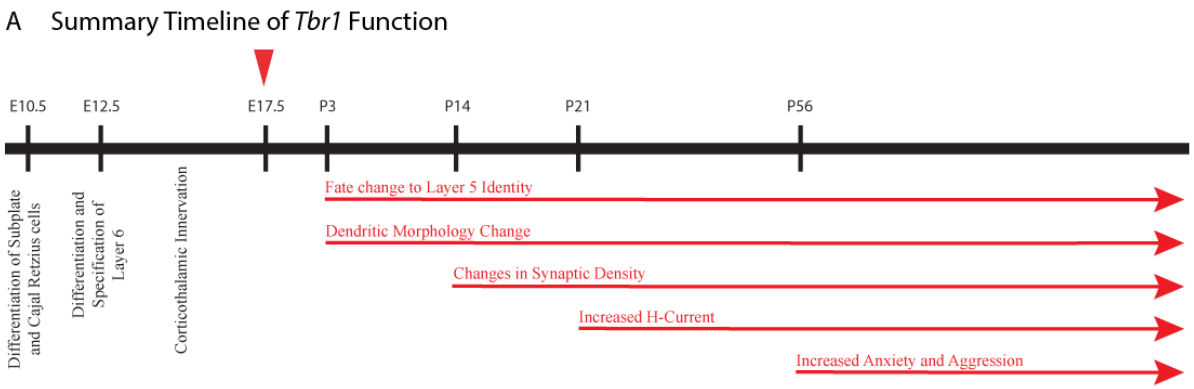

Figure 14. Summary timeline for *Tbr1* function.

Schematic representation of a timeline of *Tbr1* function prenatally into adulthood in mouse. The red arrowhead at E17.5 corresponds to the timing of knocking out *Tbr1* in layer 6 conditional mutant mice.

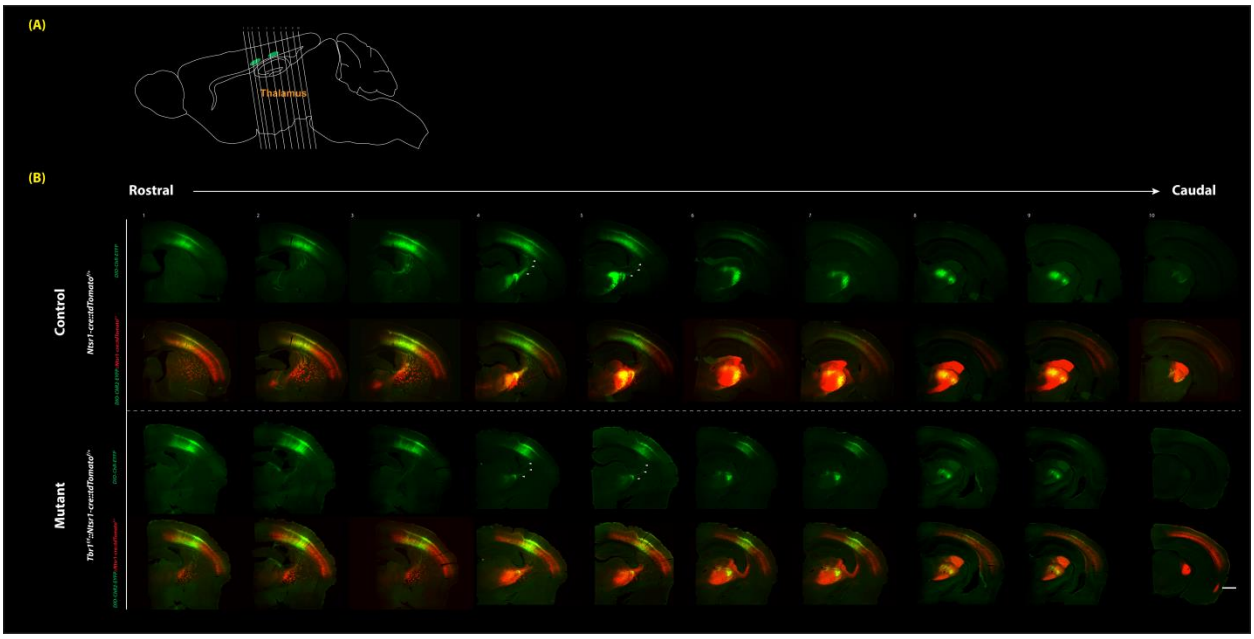

Supplementary Figure 1. Reduced corticothalamic innervation of the thalamus at P60 in *Tbr1* layer 6 CKO.

(A) Injection sites of the anterograde tracer DIO-ChR2-EYFP (green ovals) in the somatosensory cortex of *Tbr1*$^{\text{wildtype}}$ and *Tbr1*^{layer6} mutants. These lines had the *Ntsr1-cre::tdTomato*$^{f/+}$ alleles to label the layer 6 neurons and their axons by tdTomato's endogenous fluorescence (red). Numbered lines correspond to the location of each section plane presented in (B). The approximate location of the thalamus is written in orange letters. **(B)** Rostro-caudal coronal section series shows of anterograde tracer (green) and tdTomato (from recombined Ai14 allele; red) in *Tbr1*$^{\text{wildtype}}$ and *Tbr1*^{layer6} mutants. In both genotypes, tdTomato^{+} corticothalamic axons (white arrowheads) innervate thalamus, although the cKO shows reduced corticothalamic innervation in the medial structures of the *Tbr1*^{layer6} mutant thalamus. Scale: 100 μm.

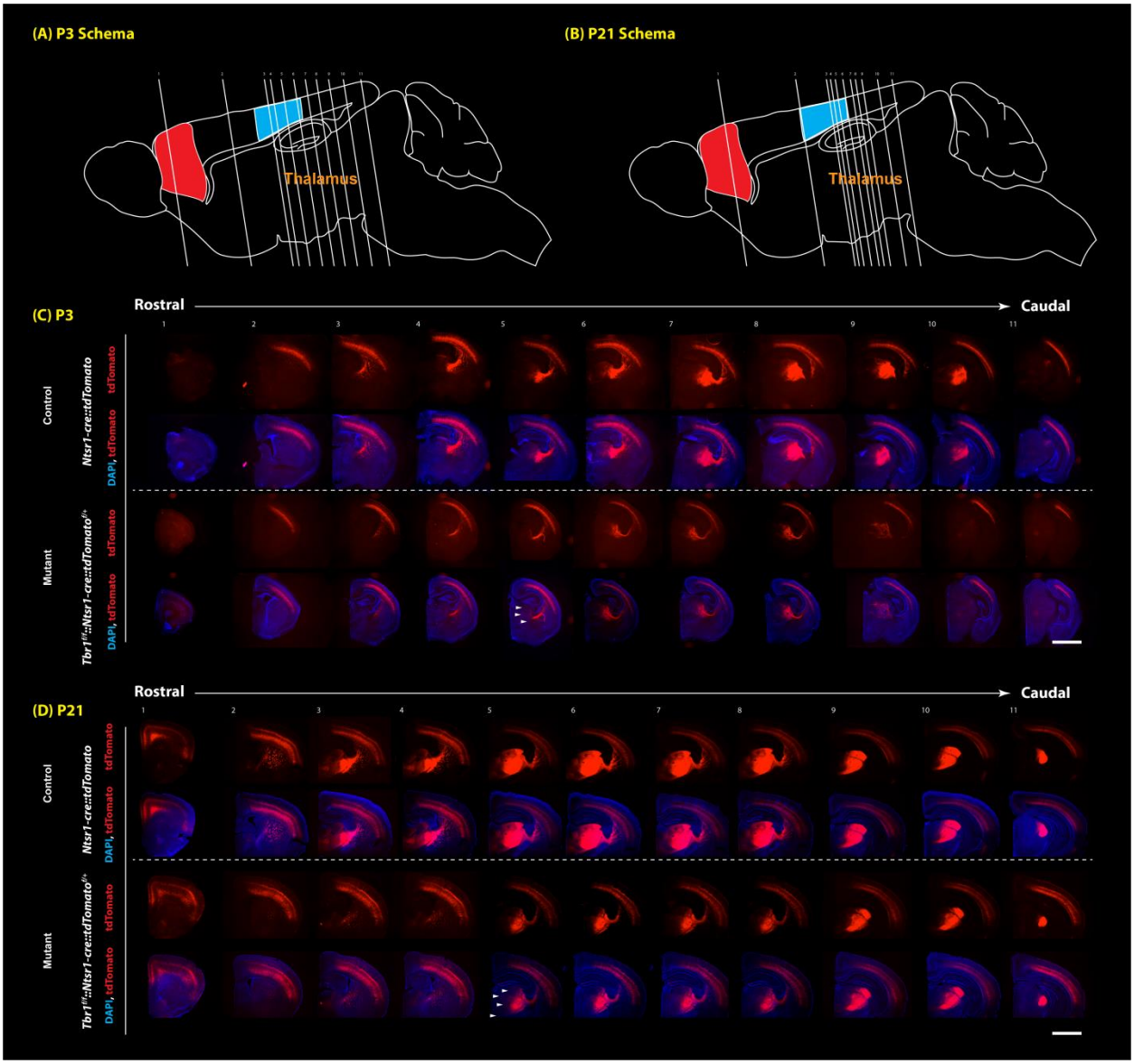

Supplementary Figure 2. tdTomato expression in layer 6 neurons and axons shows reduced corticothalamic innervation in *Tbr1*^{layer6} mutants at P3 and P21.

(A, B) Schematic representation of rostro-caudal coronal section planes (numbered lines) of *Tbr1*$^{\text{wildtype}}$ and *Tbr1*^{layer6} mutants that were used to investigate the thalamic innervation of layer 6 axons. Prefrontal and somatosensory cortex are indicated in red and blue respectively. The approximate location of the thalamus is written in orange letters. **(C, D)** Rostro-caudal coronal section series shows tdTomato in *Tbr1*$^{\text{wildtype}}$ and *Tbr1*^{layer6} mutants at P3 **(C)** and P21 **(D)**. These lines had the *Ntsr1-cre::tdTomato*$^{f/+}$ alleles to label the layer 6 neurons and their axons by tdTomato's endogenous fluorescence (red). The overlap between DAPI (blue) and tdTomato is shown. White arrowheads in panel 5 (at P3 and P21) correspond to the medial structures in the *Tbr1*^{layer6} mutant thalamus that show reduced corticothalamic innervation. Scale: 100 μm in **(C)** and 50 μm in **(D)**.

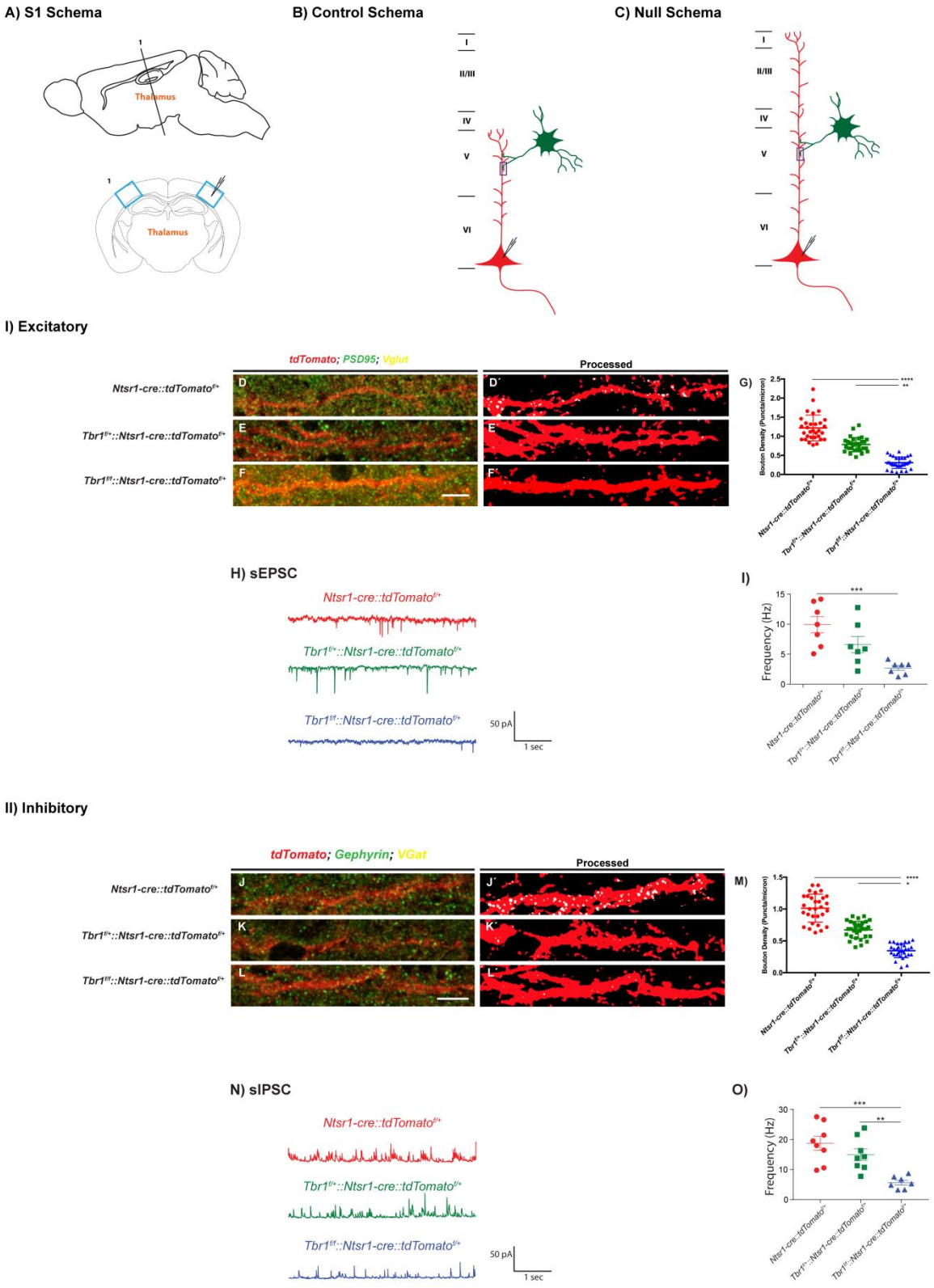

Supplementary Figure 3. Loss of *Tbr1* in layer 6 reduces excitatory(I) and inhibitory (II) synaptic input onto layer 6 pyramidal neurons in somatosensory cortex at P56.

(A) Schematic representation of somatosensory cortex (S1, blue boxes) that was used during the imaging and patching experiments. **(B, C)** Schema of layer 6 projection neuron (red) in somatosensory cortex of *Tbr1* ^{wildtype} **(B)** and *Tbr1*^{layer6} mutant **(C)**. The rectangles indicate the zone where synapses were analyzed **(B, C)** at P56. Pipette tip indicates that the soma was patched during the electrophysiology recordings **(B, C)**.

(I) Excitatory synaptic input was analyzed via synaptic bouton staining onto apical dendrites of layer 6 neurons **(D-F)** and spontaneous EPSC (sEPSC) recordings from the soma of the layer 6 pyramidal neurons **(H)** of *Tbr1* ^{wildtype} **(D)** *Tbr1*^{layer6} heterozygous mutants, and **(E)** *Tbr1*^{layer6} homozygous mutants **(F)** at P56 **(D, E, F)**. These lines had the *Ntsr1-cre::tdTomato*$^{f/+}$ alleles to label the layer 6 neurons by tdTomato's endogenous fluorescence (red). ImageJ software was used to process confocal images **(D-F)** for quantification **(D´ – F´)**. **(G)** Quantification of VGlut1^{+} boutons and PSD95^{+} clusters co-localizing onto the apical dendrites of layer 6 neurons at P56. **(H)** sEPSC recordings from the soma of layer 6 pyramidal neurons of *Tbr1* ^{wildtype}, *Tbr1*^{layer6} heterozygous mutants, and *Tbr1*^{layer6} homozygous mutants at P56. **(I)** Quantification of the sEPSC occurrence in layer 6 neurons at P56.

(II) Inhibitory synaptic input was examined through synaptic bouton staining onto apical dendrites of layer 6 neurons **(J – L)** and spontaneous IPSC (sIPSC) recordings from the soma of the layer 6 neurons **(N)** of *Tbr1* ^{wildtype} **(J)**, *Tbr1*^{layer6} heterozygote mutants **(K)**, and *Tbr1*^{layer6} homozygous mutants **(L)** at P56 **(J, K, L)**. These lines had the *Ntsr1-cre::tdTomato*$^{f/+}$ alleles to label the layer 6 neurons by tdTomato's endogenous fluorescence (red). ImageJ software was used to process confocal images **(J – L)** for quantification **(J´ – L´)**. **(M)** Quantification of VGat^{+} boutons and Gephyrin^{+} clusters co-localizing onto the apical dendrites of layer 6 neurons at P56. **(N)** sIPSC recordings from the soma of layer 6 pyramidal neurons of *Tbr1* ^{wildtype}, *Tbr1*^{layer6} heterozygous mutants, and *Tbr1*^{layer6} homozygous mutants at P56. **(O)** Quantification of the sIPSC occurrence in layer 6 neurons at P56. Two-way ANOVA was used for the statistical analysis of the control, heterozygous and null. (*p<0.05) (**p< 0.01) (***p<0.001) (****p<0.0001). Scale bar (in F and L) = 5µm.

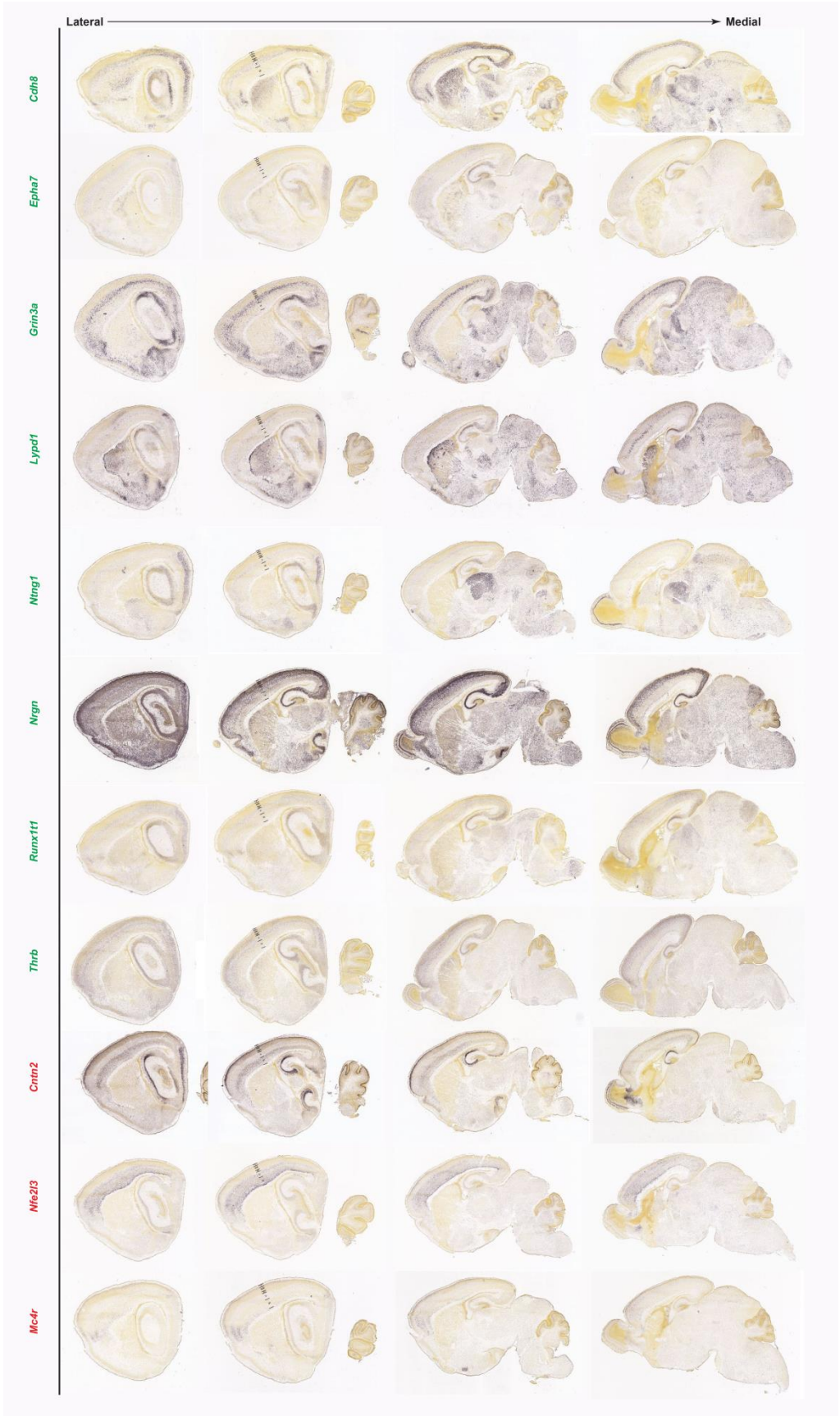
Lateral
Medial
Cdh8
Epha7
Grin3a
Lypd1
Ntng1
Nrgn
Runx1t1
Thrb
Cntn2
Nfe2l3
Mc4r

Supplementary Figure 4. *Tbr1* maintains cortical layer 6 identity through regulating the expression of layer 5 and layer 6 markers.

In situ hybridization of the latero-medial expression profile of a subset of layer 5 genes (green) and layer 6 genes (red) in the *Tbr1*^{layer6} mutants. The subset of genes was identified by utilizing FACS purified neurons of wildtype and *Tbr1*^{layer6} mutants at P5. Layer 5 markers such as *Cdh8, EphA7, Grin3a, Lypd1, Ntng1, Nrgn, Runx1l1, Thrb* are upregulated (green), whereas, layer 6 markers including *Cntn2, Nfe2l3* and *Mc4r* are downregulated (red) in the *Tbr1*^{layer6} mutants. Image credit: Allen Institute. Cortical layers are labeled. I = layer 1, II/III = layers 2/3, IV = layer 4, V = layer 5 and VI = layer 6.

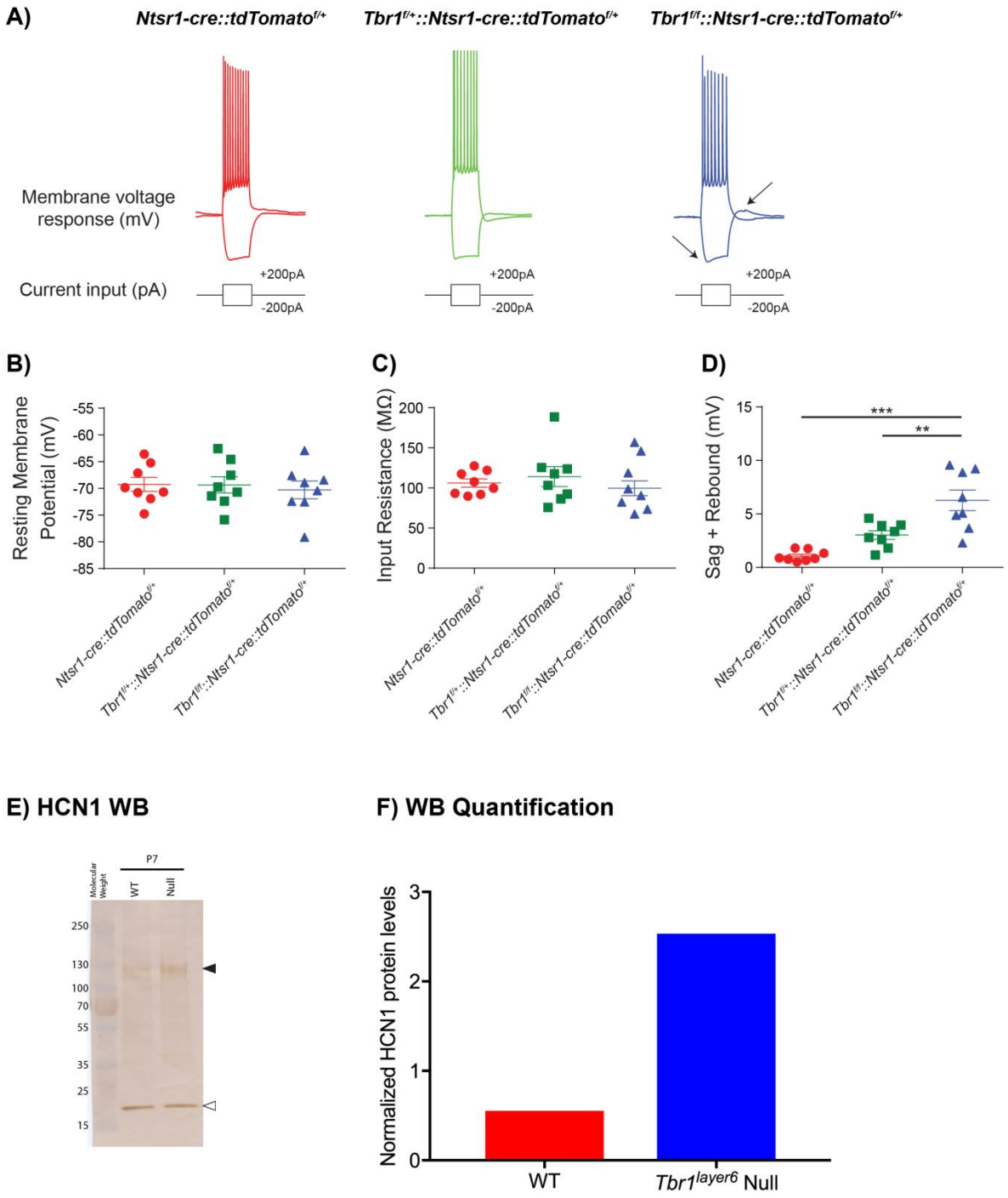

Supplementary Figure 5. Intrinsic properties of the pyramidal neurons of *Tbr1*^{layer6} mutants revealed an increase in HCN channels at P21.

(A) The layer 6 pyramidal neurons were patched at P21 and intrinsic properties were collected from whole-cell patch clamp recordings from layer 6 somatosensory cortex. Recordings from *Tbr1*^{wildtype} (red), *Tbr1*^{layer6} heterozygous mutant (green) and *Tbr1*^{layer6} homozygous mutant (blue) show that many intrinsic electrophysiological properties were unaffected by loss of *Tbr1*, including resting membrane potential **(B)**, input resistance **(C)**, and action potential halfwidth (data not shown). We estimated Ih by measuring the membrane potential sag and rebound elicited by a –200 pA current step. **(D)** sag and rebound is increased in *Tbr1*^{layer6} mutants. (**p< 0.01) (***p<0.001).

References

Bachevalier, J. and Mishkin, M. (1986) 'Visual recognition impairment follows ventromedial but not dorsolateral prefrontal lesions in monkeys.', *Behavioural brain research*, 20(3), pp. 249–61.

Bedogni, F., Hodge, R. D., Elsen, G. E., Nelson, B. R., Daza, R. A. M., Beyer, R. P., . . . Hevner, R. F. (2010). Tbr1 regulates regional and laminar identity of postmitotic neurons in developing neocortex. *Proceedings of the National Academy of Sciences, 107*(29), 13129-13134.

Bernardinelli, Y., Nikonenko, I., & Muller, D. (2014). Structural plasticity: mechanisms and contribution to developmental psychiatric disorders. *Frontiers in Neuroanatomy, 8*, 123.

Brumback, A. C., Ellwood, I., Kjaerby, C., Iafrati, I., Robinson, S.E., Lee, A., Patel, T., Nagaraj, S., Davatolhagh, F., Sohal, V.S.,. (2017) 'Identifying specific prefrontal neurons that contribute to autism-associated abnormalities in physiology and social behavior', *Molecular Psychiatry*.

Bulfone, A., Smiga, S. M., Shimamura, K., Peterson, A., Puelles, L., & Rubenstein, J. L. R. (1995). T-Brain-1: A homolog of Brachyury whose expression defines molecularly distinct domains within the cerebral cortex. *Neuron, 15*(1), 63-78.

Bulfone, A., Wang, F., Hevner, R., Anderson, S., Cutforth, T., Chen, S., . . . Rubenstein, J. L. R. (1998). An Olfactory Sensory Map Develops in the Absence of Normal Projection Neurons or GABAergic Interneurons. *Neuron, 21*(6), 1273-1282.

Clarkson, R. L., Liptak, A. T., Gee, S. M., Sohal, V. S., & Bender, K. J. (2017). D3 receptors regulate excitability in a unique class of prefrontal pyramidal cell. *The Journal of Neuroscience*.

Cobos, I., Calcagnotto ME, Vilaythong AJ, Thwin MT, Noebels JL, SC, B., & Rubenstein, J. (2005). Mice lacking Dlx1 show subtype-specific loss of interneurons, reduced inhibition and epilepsy. *Nature Neuroscience, 8*(8), 1059-1068.

Corteen, N. L., Cole, T. M., Sarna, A., Sieghart, W., & Swinny, J. D. (2011). Localization of GABA-A receptor alpha subunits on neurochemically distinct cell types in the rat locus coeruleus. *Eur J Neurosci, 34*(2), 250-262.

Crandall, S. R., Cruikshank, S. J., & Connors, B. W. (2015). A corticothalamic switch: controlling the thalamus with dynamic synapses. *Neuron, 86*(3), 768-782.

Creyghton, M. P., Cheng, A. W., Welstead, G. G., Kooistra, T., Carey, B. W., Steine, E. J., . . . Jaenisch, R. (2010). Histone H3K27ac separates active from poised enhancers and predicts developmental state. *Proceedings of the National Academy of Sciences*.

Darbandi, S., & Franck, J. P. C. (2009). A comparative study of ryanodine receptor (RyR) gene expression levels in a basal ray-finned fish, bichir (Polypterus ornatipinnis) and

the derived euteleost zebrafish (Danio rerio). *Comparative Biochemistry and Physiology Part B: Biochemistry and Molecular Biology, 154*(4), 443-448.

Davis, E. K., Zou, Y., & Ghosh, A. (2008). Wnts acting through canonical and noncanonical signaling pathways exert opposite effects on hippocampal synapse formation. *Neural Development, 3*, 32-32.

De Rubeis, S., He, X., Goldberg, A. P., Poultney, C. S., Samocha, K., Ercument Cicek, A., . . . Buxbaum, J. D. (2014). Synaptic, transcriptional and chromatin genes disrupted in autism. *Nature, 515*(7526), 209-215.

Dembrow, N. C., Chitwood, R. A., & Johnston, D. (2010). Projection-Specific Neuromodulation of Medial Prefrontal Cortex Neurons. *The Journal of Neuroscience, 30*(50), 16922.

Deriziotis, P., O'Roak, B. J., Graham, S. A., Estruch, S. B., Dimitropoulou, D., Bernier, R. A., . . . Fisher, S. E. (2014). De novo TBR1 mutations in sporadic autism disrupt protein functions. *Nat Commun, 5*.

Gadow, K. D. *et al.* (2004) 'Psychiatric symptoms in preschool children with PDD and clinic and comparison samples.', *Journal of autism and developmental disorders*, 34(4), pp. 379–93.

Gee, S., Ellwood, I., Patel, T., Luongo, F., Deisseroth, K., & Sohal, V. S. (2012). Synaptic Activity Unmasks Dopamine D2 Receptor Modulation of a Specific Class of Layer V Pyramidal Neurons in Prefrontal Cortex. *The Journal of Neuroscience, 32*(14), 4959.

Gong, X., Jia, M., Ruan, Y., Shuang, M., Liu, J., Wu, S., . . . Zhang, D. (2004). Association between the FOXP2 gene and autistic disorder in Chinese population. *American Journal of Medical Genetics Part B: Neuropsychiatric Genetics, 127B*(1), 113-116.

Harris, K. D. and Shepherd, G. M. G. (2015) 'The neocortical circuit: themes and variations.', *Nature neuroscience*. NIH Public Access, 18(2), pp. 170–81.

Hevner, R. F., Miyashita-Lin, E., & Rubenstein, J. L. R. (2002). Cortical and thalamic axon pathfinding defects in Tbr1, Gbx2, and Pax6 mutant mice: Evidence that cortical and thalamic axons interact and guide each other. *The Journal of Comparative Neurology, 447*(1), 8-17.

Hevner, R. F., Neogi, T., Englund, C., Daza, R. A. M., & Fink, A. (2003). Cajal–Retzius cells in the mouse: transcription factors, neurotransmitters, and birthdays suggest a pallial origin. *Developmental Brain Research, 141*(1), 39-53.

Hevner, R. F., Shi, L., Justice, N., Hsueh, Y.-P., Sheng, M., Smiga, S., . . . Rubenstein, J. L. R. (2001). Tbr1 Regulates Differentiation of the Preplate and Layer 6. *Neuron, 29*(2), 353-366.

Huang, T.-N., Chuang, H.-C., Chou, W.-H., Chen, C.-Y., Wang, H.-F., Chou, S.-J., & Hsueh, Y.-P. (2014). *Tbr1* haploinsufficiency impairs amygdalar axonal projections and results in cognitive abnormality. *Nat Neurosci, 17*(2), 240-247.

Huang, T.-N., & Hsueh, Y.-P. (2017). Calcium/calmodulin-dependent serine protein kinase (CASK), a protein implicated in mental retardation and autism-spectrum disorders, interacts with T-Brain-1 (TBR1) to control extinction of associative memory in male mice. *Journal of Psychiatry & Neuroscience : JPN, 42*(1), 37-47.

Iossifov, I., O'Roak, B. J., Sanders, S. J., Ronemus, M., Krumm, N., Levy, D., . . . Wigler, M. (2014). The contribution of de novo coding mutations to autism spectrum disorder. *Nature, 515*(7526), 216-221.

Krishnan, A., & Schiöth, H. B. (2015). The role of G protein-coupled receptors in the early evolution of neurotransmission and the nervous system. *The Journal of Experimental Biology, 218*(4), 562.

Lee, Anthony T., Gee, Steven M., Vogt, D., Patel, T., Rubenstein, John L., & Sohal, Vikaas S. (2014). Pyramidal Neurons in Prefrontal Cortex Receive Subtype-Specific Forms of Excitation and Inhibition. *Neuron, 81*(1), 61-68.

Ledergerber, D., & Larkum, M. E. (2010). Properties of Layer 6 Pyramidal Neuron Apical Dendrites. *The Journal of Neuroscience, 30*(39), 13031.

Lefebvre, J. L., Sanes, J. R., & Kay, J. N. (2015). Development of Dendritic Form and Function. *Annual Review of Cell and Developmental Biology, 31*(1), 741-777.

Leung, C. C., & Wong, H. Y. (2017). Role of G Protein-Coupled Receptors in the Regulation of Structural Plasticity and Cognitive Function. *Molecules, 22*(7).

Li, H., Yamagata, T., Mori, M., & Momoi, M. Y. (2005). Absence of causative mutations and presence of autism-related allele in FOXP2 in Japanese autistic patients. *Brain and Development, 27*(3), 207-210.

Liebl, F. L. W., McKeown, C., Yao, Y., & Hing, H. K. (2010). Mutations in Wnt2 Alter Presynaptic Motor Neuron Morphology and Presynaptic Protein Localization at the Drosophila Neuromuscular Junction. *PLoS ONE, 5*(9), e12778.

Lim, S. H., Kwon, S. K., Lee, M. K., Moon, J., Jeong, D. G., Park, E., . . . Lee, J. R. (2009). Synapse formation regulated by protein tyrosine phosphatase receptor T through interaction with cell adhesion molecules and Fyn. *The EMBO Journal, 28*(22), 3564.

Lodato, S., Rouaux, C., Quast, K. B., Jantrachotechatchawan, C., Studer, M., Hensch, T. K., & Arlotta, P. (2011). Excitatory Projection Neuron Subtypes Differentially Control the Distribution of Local Inhibitory Interneurons in the Cerebral Cortex. *Neuron, 69*(4), 763-779.

Long, J. E., Garel, S., Depew, M. J., Tobet, S., & Rubenstein, J. (2003). DLX5 Regulates Development of Peripheral and Central Components of the Olfactory System. *The Journal of Neuroscience, 23*(2), 568-578.

Madisen, L., Zwingman, T. A., Sunkin, S. M., Oh, S. W., Zariwala, H. A., Gu, H., . . . Zeng, H. (2010). A robust and high-throughput Cre reporting and characterization system for the whole mouse brain. *Nature Neuroscience, 13*(1), 133-140.

McCarthy, J. D., Chen, Yunshun, and Smyth, K. G., . (2012). Differential expression analysis of multifactor RNA-Seq experiments with respect to biological variation. *Nucleic Acids Research, 40*(10), 9.

McClintock, K., Hall, S. and Oliver, C. (2003) 'Risk markers associated with challenging behaviours in people with intellectual disabilities: a meta-analytic study.', *Journal of intellectual disability research : JIDR*, 47(Pt 6), pp. 405–16.

McKenna, W. L., Betancourt, J., Larkin, K. A., Abrams, B., Guo, C., Rubenstein, J. L. R., & Chen, B. (2011). *Tbr1* and *Fezf2* Regulate Alternate Corticofugal Neuronal Identities during Neocortical Development. *The Journal of Neuroscience, 31*(2), 549-564.

Morgan, M. A., Romanski, L. M. and LeDoux, J. E. (1993) 'Extinction of emotional learning: contribution of medial prefrontal cortex.', *Neuroscience letters*, 163(1), pp. 109–13.

Morishima, M. and Kawaguchi, Y. (2006) 'Recurrent Connection Patterns of Corticostriatal Pyramidal Cells in Frontal Cortex', *Journal of Neuroscience*, 26(16), pp. 4394–4405.

Muram, S., Rowe, T. M., & Hirasawa, M. (2016). Presynaptic G Protein-Coupled Receptors Differentially Modulate Spontaneous Glutamate Release in the Supraoptic Nucleus. *Journal of Neuroendocrinology, 28*(4).

Pfaffl, M. W. (2001). A new mathematical model for relative quantification in real-time RT–PCR. *Nucleic Acids Research, 29*(9), e45.

Robinson, M. D., McCarthy, D.J. and Smyth, G.K., . (2010). edgeR: a Bioconductor package for differential expression analysis of digital gene expression data. *Bioinformatics, 26*.

Rodriguez, C. I., Buchholz, F., Galloway, J., Sequerra, R., Kasper, J., Ayala, R., . . . Dymecki, S. M. (2000). High-efficiency deleter mice show that FLPe is an alternative to Cre-loxP. *Nat Genet, 25*(2), 139-140.

Rozen, S., & Skaletsky, H. (1999). Primer3 on the WWW for General Users and for Biologist Programmers. In S. Misener & S. Krawetz (Eds.), *Bioinformatics Methods and Protocols* (Vol. 132, pp. 365-386): Humana Press.

Rubenstein, J. L. R., & Merzenich, M. M. (2003). Model of autism: increased ratio of excitation/inhibition in key neural systems. *Genes, Brain and Behavior, 2*(5), 13.

Russ, J. B., & Kaltschmidt, J. A. (2014). From induction to conduction: how intrinsic transcriptional priming of extrinsic neuronal connectivity shapes neuronal identity. *Open Biology, 4*(10), 140144.

Sandberg, M., Flandin, P., Silberberg, S., Su-Feher, L., Price, James D., Hu, Jia S., . . . Rubenstein, John L. R. (2016). Transcriptional Networks Controlled by NKX2-1 in the Development of Forebrain GABAergic Neurons. *Neuron, 91*(6), 1260-1275.

Sanders, S. J., He, X., Willsey, A. J., Ercan-Sencicek, A. G., Samocha, Kaitlin E., Cicek, A. E., . . . State, Matthew W. (2015). Insights into Autism Spectrum Disorder Genomic Architecture and Biology from 71 Risk Loci. *Neuron, 87*(6), 1215-1233.

Sanders, S. J., Murtha, M. T., Gupta, A. R., Murdoch, J. D., Raubeson, M. J., Willsey, A. J., . . . State, M. W. (2012). De novo mutations revealed by whole-exome sequencing are strongly associated with autism. *Nature, 485*(7397), 237-241.

Seong, H. J., & Carter, A. G. (2012). D1 Receptor Modulation of Action Potential Firing in a Subpopulation of Layer 5 Pyramidal Neurons in the Prefrontal Cortex. *The Journal of neuroscience : the official journal of the Society for Neuroscience, 32*(31), 10516-10521.

Vokes, S. A., Ji, H., McCuine, S., Tenzen, T., Giles, S., Zhong, S., . . . McMahon, A. P. (2007). Genomic characterization of Gli-activator targets in sonic hedgehog-mediated neural patterning. *Development, 134*(10), 1977-1989.

Walsh, C. A., Morrow, E. M., & Rubenstein, J. L. R. (2008). Autism and Brain Development. *Cell, 135*(3), 396-400.

Wang, T.-F., Ding, C.-N., Wang, G.-S., Luo, S.-C., Lin, Y.-L., Ruan, Y., . . . Hsueh, Y.-P. (2004). Identification of Tbr-1/CASK complex target genes in neurons. *Journal of Neurochemistry, 91*(6), 1483-1492.

Willsey, A. J., Sanders, Stephan J., Li, M., Dong, S., Tebbenkamp, Andrew T., Muhle, Rebecca A., . . . State, Matthew W. (2013). Coexpression Networks Implicate Human Midfetal Deep Cortical Projection Neurons in the Pathogenesis of Autism. *Cell, 155*(5), 997-1007.

Yee, A., & Chen, L. (2016). Differential regulation of spontaneous and evoked inhibitory synaptic transmission in somatosensory cortex by retinoic acid. *Synapse (New York, N.Y.), 70*(11), 445-452.

Zerucha, T., Stuhmer, T., Gambarotta, A., Hatch, G., Schultz, J., Park, B., . . . Ekker, M. (2000). A Highly Conserved Enhancer in the Dlx5/Dlx6 Intergenic Region is the Site of Cross-Regulatory Interactions between Dlx Genes in the Embryonic Forebrain. *The Journal of Neuroscience, 20*(2), 709-721.

CHAPTER V

Concluding Remarks and Remaining Questions

The studies presented here reveal a novel mechanism of dopamine D2 receptor (D2R) signaling unique to a subpopulation of pyramidal neurons within layer 5 (L5) of the prefrontal cortex (PFC). I find this novel phenomenon, specifically an afterdepolarization (ADP), whereby D2R activation enhances cellular excitability in a manner dependent on synaptic inputs, to be mediated by the recruitment of G_s-associated signaling pathways rather than the classically described $G_{i/o}$-coupled mechanisms. The phenomenon studied here is one whereby even subthreshold synaptic activity can enhance neuronal excitability for a period of several hundreds of milliseconds or even up to 10 seconds later. Furthermore, I find that this phenomenon is absent in disrupted-in-schizophrenia 1 (DISC1) mouse model of schizophrenia, suggesting behavioral and clinical importance for this novel D2R signaling pathway. Additionally, and for the first time we investigated the role of *Tbr1*, an Autism Spectrum Disorder (ASD) risk gene, in these deep layer cortical neurons within adult mice. We found distinct molecular, physiological, and behavioral deficits specific to loss of *Tbr1* function in layer 5 versus layer 6 suggesting that *Tbr1* has diverse functions within different subpopulation of cortical circuits.

Many of the implications and caveats of the results presented here have been discussed individually in Chapters II, III, and IV. Therefore, in this chapter, I will discuss remaining questions, with a focus on larger implications and future directions.

Layer 5 neurons exhibiting this novel D2R-dependent afterdepolarization are well poised to affect the cognitive domains disrupted in schizophrenia and other psychiatric disorders. It is hypothesized that dopamine modulates PFC-dependent cognitive function by transitioning the cortical circuits between a state of stable active neural representations which facilitates maintenance of previously learned behavioral strategies and a destabilized state which promotes flexible behavioral responses important for successful adaptation

(Durstewitz and Seamans, 2008). The D2R-mediated phenomenon studied here could alter neuronal integration of their inputs over relatively long durations or switch neurons into a "high gain" mode whereby responses to subsequent inputs are potentiated and thereby promote flexibility within the network.

As presented in Chapter III, a dominant negative mutation in *human disrupted-in-schizophrenia 1 (DISC1)* completely abolished this D2R-mediated phenomena. Should future studies confirm that the D2R-mediated ADP is important for dopaminergic modulation of neuronal modulation in this subpopulation of deep cortical neurons, my findings suggest that the disruption of the D2R-Gs signaling mechanism may disrupt network ability to switch into a flexible state and thereby play a critical role in cognitive deficits associated with schizophrenia.

Many questions do remain regarding the specific molecular mechanisms underlying this phenomenon and its role in normal cognitive function and implications in dysfunction associated with psychiatric disorders. How is the dopamine D2 receptor (D2R) coupled to G_s? Is DISC1, a scaffolding protein, necessary to facilitate this D2R/G_s-associated signaling pathway? D2Rs have been shown to be able to form heteroreceptors, might D2R act via G_s by forming heteroreceptor with another G_s-coupled GPCR in this subpopulation of L5 pyramidal neurons? Current studies have not conclusively ruled out coexpression of dopamine D1 receptors (D1Rs) and D2Rs, nor have the expression patterns of dopamine D4 receptors (D4Rs) and dopamine D5 receptors (D5Rs) been closely examined(Clarkson *et al.*, 2017). There is controversy over whether D2Rs and D1Rs form heteroreceptors in the cortex (Beaulieu and Gainetdinov, 2011; Zhang *et al.*, 2011). It will be interesting for future studies to investigate whether knocking out D1Rs in D2R+ neurons with L5 mPFC would abolish this D2R/G_s mediated phenomenon.

Work from our lab has also shown that the quinpirole-induced ADP is absent in mice younger than 8 weeks. As discussed in Chapter II, activity at the NMDARs is necessary to unmask the quinpirole-induced ADP. It is also known that NMDA receptor (NMDAR) subunit expression shifts over the course of development, at time points similar with the appearance of the quinpirole-induced ADP (Pian *et al.*, 2010; Paoletti *et al.*, 2013). How does the NMDAR facilitate this D2R/G_s-mediated phenomenon? Are these NMDAR subunits important for the unmasking of this D2R-mediated phenomenon? Interestingly, this developmental time point in mice corresponds to the onset of adolescence/young adulthood, similar to the age of onset in schizophrenia (Häfner *et al.*, 1993).

The study presented in Chapter IV, shows that layer specific loss of function of *T-brain-1* (*Tbr1)* leads to upregulation of both D2Rs and hyperpolarization-activated cyclic nucleotide-gated (HCN) channels also resulting in increased in hyperpolarization-activated cation current (I_h) mediated by these HCN channels in deep layer cortical neurons. I_h can strongly modulate a neurons spike firing and synaptic potential integration (Shah, 2014). Future behavior experiments investigating the effect of loss of *Tbr1* function within these specific cortical layer populations in prefrontal-dependent task such as set-shifting could further elucidate the roles and function of *Tbr1* in the adult mouse cortex. Furthermore, it would be interesting to study the activity of these separate neuronal subpopulations during these PFC-dependent tasks.

Interestingly, both of the psychiatric disease models studied in this dissertation, a dominant negative mutation in *human disrupted-in-schizophrenia 1 (DISC1)* and layer specific loss of function of *T-brain-1* (*Tbr1)*, exhibited physiological perturbations impacting neuronal integration. The discovery of this D2R/G_s mediated mechanism provides a new framework in which to investigate the molecular functions of currently-prescribed

antipsychotics, as well as to explore the impact of perturbations in D2R-mediated neuromodulation on prefrontal cells and circuits. An improved understanding of how mechanisms of dopaminergic modulation are perturbed in psychiatric disease may thus aid in the development of safer and more efficient drug therapies.

Final thoughts

This work establishes a new understanding of D2R signaling within the prefrontal cortex, complicating but potentially resolving years of discrepancy in the field. It will be important to identify specific details of the molecular pathway underlying this effect and its impact on cortical circuit function and behavior. Elucidating these mechanisms has potential implications for psychiatric disease and could illuminate novel drug therapies or circuit-based approaches for understanding and treating prefrontal-related cognitive dysfunctions in psychiatric disease.

References

Beaulieu, J.-M. and Gainetdinov, R. R. (2011) 'The physiology, signaling, and pharmacology of dopamine receptors.', *Pharmacological reviews*. American Society for Pharmacology and Experimental Therapeutics, 63(1), pp. 182–217.

Clarkson, R. L. *et al.* (2017) 'D3 Receptors Regulate Excitability in a Unique Class of Prefrontal Pyramidal Cells.', *The Journal of neuroscience : the official journal of the Society for Neuroscience*, 37(24), pp. 5846–5860.

Durstewitz, D. and Seamans, J. K. (2008) 'The Dual-State Theory of Prefrontal Cortex Dopamine Function with Relevance to Catechol-O-Methyltransferase Genotypes and Schizophrenia', *Biological Psychiatry*, 64(9), pp. 739–749.

Häfner, H. *et al.* (1993) 'The influence of age and sex on the onset and early course of schizophrenia.', *The British journal of psychiatry : the journal of mental science*. The Royal College of Psychiatrists, 162(1), pp. 80–6.

Paoletti, P., Bellone, C. and Zhou, Q. (2013) 'NMDA receptor subunit diversity: impact on receptor properties, synaptic plasticity and disease', *Nature Reviews Neuroscience*. Nature Publishing Group, 14(6), pp. 383–400.

Pian, J. P. *et al.* (2010) 'N-methyl-D-aspartate receptor subunit expression in adult and adolescent brain following chronic ethanol exposure.', *Neuroscience*. NIH Public Access, 170(2), pp. 645–54.

Shah, M. M. (2014) 'Cortical HCN channels: function, trafficking and plasticity.', *The Journal of physiology*, 592(13), pp. 2711–9.

Zhang, L. *et al.* (2011) 'Calcium-related signaling pathways contributed to dopamine-induced cortical neuron apoptosis', *Neurochemistry International*, 58(3), pp. 281–294.

Publishing Agreement

It is the policy of the University to encourage the distribution of all theses, dissertations, and manuscripts. Copies of all UCSF theses, dissertations, and manuscripts will be routed to the library via the Graduate Division. The library will make all theses, dissertations, and manuscripts accessible to the public and will preserve these to the best of their abilities, in perpetuity.

I hereby grant permission to the Graduate Division of the University of California, San Francisco to release copies of my thesis, dissertation, or manuscript to the Campus Library to provide access and preservation, in whole or in part, in perpetuity.

Author Signature  Date 12/20/2017